POLITECNICO DI MILANO

School of Industrial and Information Engineering

Master Degree in Materials Engineering and Nanotechnology

Department of Chemistry, Materials and Chemical Engineering

Properties of steel surfaces coated

with organic molecules

Supervisor: Prof. Paolo GRONCHI

Co-supervisor: Ing. Sara OTTOBONI

Master Degree Thesis of:

Amani Ponzoni   783250

Academic Year 2013-2014

CONTENTS

LIST OF FIGURES

LIST OF TABLES

"Non aspettare di finire l'università, di innamorarti, di trovare lavoro, di sposarti, di avere figli, di vederli sistemati, di perdere quei dieci chili, che arrivi il venerdì sera o la domenica mattina, la primavera, l'estate, l'autunno o l'inverno. Non c'è momento migliore di questo per essere felice. La felicità è un percorso, non una destinazione. Lavora come se non avessi bisogno di denaro, ama come se non ti avessero mai ferito e balla, come se non ti vedesse nessuno. Ricordati che la pelle avvizzisce, i capelli diventano bianchi e i giorni diventano anni. Ma l'importante non cambia: la tua forza e la tua convinzione non hanno età. Il tuo spirito è il piumino che tira via qualsiasi ragnatela. Dietro ogni traguardo c'è una nuova partenza. Dietro ogni risultato c'è un'altra sfida. Finché sei vivo, sentiti vivo. Vai avanti, anche quando tutti si aspettano che lasci perdere."

Madre Teresa di Calcutta

ABSTRACT

Superhydrophobic state is one of the most interesting and attractive topic in this years due to the wide application possibilities. Roughness and surface tension are the main parameters to be controlled to obtain a surface with hydrophobic properties. The topic of this thesis is to investigate how substrate roughness and coating deposition parameters influence wettability properties. It was performed selecting two types of substrate with different roughness, applying different kinds of coatings (some of which have been synthesized in laboratory) optimizing the deposition procedure. As substrate has been chosen mild carbon steel, use both as received and after sandblasting treatment. Over these substrates a thin organic film coating has been applied. The employed coatings were purchased, carboxylic acids SAMs and butyl phosphonic acid SAM, or were synthesized and characterized in laboratory, dodecyl and octadecyl phosphonic acids SAMs and partially esterified polyacrylates. Their deposition procedure was made of three main steps: cleaning, etching and post thermal treatment. Etching time and the presence of the post thermal treatment has been widely surveyed: etching time role is to create active sites, on the substrate surface, available for the anchorage of organic molecules, while the thermal treatment stabilize bonds between film coating and substrate. For each kind of coating, three different alkyl chain length have been studied to understand their role in the wettability.

The samples have been analyzed at optical contact angle to establish the wettability grade, at atomic force microscope to discover roughness and film adhesion force, at glow discharge optical emission spectroscope to survey thickness and chemical composition of the coating, at scanning electron microscope to see the surface morphology and at electrochemical impedance to investigate their electrical behaviour.

ESTRATTO IN LINGUA ITALIANA

Lo studio della bagnabilità delle superfici è un argomento di ricerca che ha subito un grande impulso negli ultimi anni dovuto alle sue numerose possibili applicazioni. Modificando superficialmente un materiale si possono variare le sue proprietà di interfaccia con l'ambiente esterno senza cambiare il bulk. Elevata bagnabilità significa che quando un liquido viene a contatto con la superficie si espande su di essa, al contrario bassa bagnabilità superficiale garantisce che quest'ultima rimanga parzialmente asciutta se non addirittura del tutto. Il parametro principale per definire il grado di bagnabilità è l'angolo di contatto ϑ tra la goccia del liquido e la superficie presente nella relazione di Young tra le tensioni superficiali in un sistema a tre fasi solido-liquido-gas. Maggiore è l'angolo di contatto, minore sarà la bagnabilità superficiale. Una superficie è definita idrofila per $\vartheta < 90°$, idrofoba se $\vartheta > 90°$, superidrofobica quando $\vartheta > 150°$. I parametri superficiali che caratterizzano la bagnabilità sono rugosità e tensione superficiale.

Questo lavoro di tesi verte sullo studio delle proprietà dei rivestimenti organici applicati a superfici metalliche, in particolar modo si indagherà come cambia la bagnabilità superficiale al variare di rugosità e tensione superficiale. Per quanto riguarda la rugosità si è deciso di selezionare due tipi di substrato costituiti entrambi dal medesimo acciaio al carbonio basso legato, con la differenza che uno è stato utilizzato tal quale, l'altro ha subito un processo di sabbiatura prima di depositare il rivestimento. La tensione superficiale è stata invece indagata depositando sul substrato differenti tipi di coatings, costituiti da film sottili di molecole organiche, alcune delle quali acquistate commercialmente, altre sintetizzate e caratterizzate in laboratorio. Tre gruppi di rivestimenti sono stati analizzati: acidi fosfonici, acidi carbossilici e acidi poliacrilici parzialmente esterificati con catene lineari alchiliche. Per ogni gruppo, sono stati selezionate tre molecole con lunghezza della catena alchilica a 4, 12 e 18 carboni. Ciò per poter osservare come cambia la bagnabilità a seconda della lunghezza della catena e l'adesione del film al substrato variando il gruppo chimico di ancoraggio, dato che attualmente la sfida più grande a livello di rivestimenti idrofobici riguarda la loro durabilità.

Le molecole sintetizzate sono due acidi fosfonici e i tre acidi poliacrilici. Questi ultimi, senza riferimenti di letteratura, hanno presentato diverse difficoltà di sintesi nel controllo del grado di esterificazione, molto importante ai fini dell'adesione della molecola al substrato e delle proprietà di bagnabilità.

Si è osservato che il trattamento di sabbiatura aumenta la rugosità di partenza del nostro substrato d'acciaio e crea una morfologia superficiale più uniforme. Il substrato, indipendentemente che fosse sabbiato o meno, subisce un pretrattamento prima della deposizione del rivestimento: dopo una breve pulizia in diclorometano (DCM) per sgrassare, viene immerso in una soluzione di acido solforico ed un agente ossidante al fine di creare dei siti attivi per il successivo ancoraggio delle molecole organiche. In questa fase sono stati indagati tre diversi tempi di etching (1, 3 e 6 min) per capire che influenza potesse avere sulle proprietà finali del coating. È stato dimostrato che aumentando il tempo di etching si ha una migliore attivazione della superficie e la qualità del rivestimento risulta essere superiore. Inoltre per gli acidi fosfonici è stato studiato l'effetto del trattamento termico post deposizione: si è riscontrato avere un effetto benefico soprattutto nei casi in cui la catena era maggiormente lunga. Ottimizzata la procedura di deposizione per gli acidi fosfonici, è stata così applicata alla deposizione degli acidi carbossilici e acidi poliacrilici parzialmente esterificati. In entrambi i casi il gruppo di ancoraggio è un carbossile. Gli acidi carbossilici hanno avuto difficoltà nel rivestimento omogeneo della superficie, molto probabilmente dovuto ad un tempo non adeguato di deposizione, mentre per i poliacrilici è stato trovato un risultato sorprendente nel caso dell'esterificazione con catena a C12: lo stato di superidrofobicità è stato raggiunto con buone caratteristiche generali.

I campioni, oltre all'angolo di contatto, sono stati analizzati all'AFM per indagare rugosità e forza di adesione del coating, GDOES per determinare spessore e composizione del rivestimento, SEM per visualizzarne la morfologia superficiale ed EIS per le proprietà elettrochimiche.

1 INTRODUCTION

Surface science is a topic of particular interest in recent years due to the possibility to modify material surface properties without changing bulk properties.

Surface science can be defined as the study of physical-chemical phenomena that occur at interface, and so it includes two fields: surface chemistry and surface physics.

Surface chemistry, even called surface engineering, aims at modifying surface chemical composition by incorporation of selected elements or functional groups that produce various desired effects or improvements in surface properties.

Surface physics studies physical changes that occur at interface and investigates for instance surface states, surface diffusion, surface self-healing and self-assembly of nanostructures on the surface.

These two fields are linked because surface modification can be done directly during the production process of the material or with a post treatment: in the first case a possible technique is the lithography, both with bottom-up or top-down steps; while in this last case a possible way of work is the application of a coating.

Analysing the two main approaches to produce a surface modification, surface coating is an easy and economic way to achieve the desired goal, that depends on the final application of the object.

The properties that can be controlled are several, for instance wettability, roughness, hardness, reactivity, biocompatibility, thermal and/or electric conductivity, wear and corrosion resistance.

This study focuses its attention on the modification of surface wettability through a coating process. The final aim is the superhydrophobicity.

A superhydrophobic surface is a non-wettable surface with high water contact angles (WCAs>150°) where drops easily slide, that can be obtained acting on two parameters: surface roughness or surface tension.

This topic has received a strong attention in recent year because of its wide range of application, from self-cleaning surfaces to anti-bacterial and anti-icing.

The following thesis work has the target of achieve superhydrophobic state on common mild carbon steel, with easy and cheap techniques for industrial applications.

It surveys how roughness and surface tension influence wettability: roughness is modified by sandblasting the samples, while surface tension is lowered coating the samples with self-assembled monolayer technique or polymer deposition. Some of the used coatings are commercial, others are synthesized. Furthermore the optimization of key parameters of deposition procedure is done. The substrate is used as received or sandblasted, then cleaned with a solvent to remove dirty and other possible organic components. The etching step, which allows the creation of active sites, come first than the dipping in a solution containing molecules that coat the surface. A post thermal treatment follows, enhancing the adhesion of the coating to the substrate. The obtained samples are then analyzed at OCA (Optical Contact Angle), and characterized at AFM (Atomic Force Microscopy), SEM (Scanning Electron Microscopy), GDOES (Glow Discharge Optical Emission Spectroscopy), EIS (Electrical Impedance Spectroscopy). OCA tells us if the samples are hydrophobic, and it is possible to estimate also surface tension of the coatings. AFM gives information about the roughness and adhesion force, while GDOES shows the composition of the coatings layer-by-layer. Images of the coated surfaces are obtained at SEM, while EIS survey the insulating properties.

2   STATE OF ART

2.1   Superhydrophobicity

Many surfaces in nature are highly hydrophobic and self-cleaning. Examples include lotus leaves and the wings of butterflies. Numerous studies have confirmed that this combination of micrometer-scale and nanometer-scale roughness, along with a low surface energy material leads to apparent WCAs>150°, a low sliding angle and the self-cleaning effect. Surfaces with these properties are called superhydrophobic.

The wetting property of a surface is defined according to the angle ϑ, which forms a liquid droplet on the three phase contact line(interface of substrate, water and air). A surface is regarded as wetting when the contact angle, which forms a drop with this one, is lower than 90°. In the opposite case, when the contact angle is higher than 90°, the surface is non-wetting. For water, the terms hydrophilic and hydrophobic are commonly used for wetting and non-wetting surfaces, respectively.

Controlling the wetting of surfaces is an important problem relevant to many areas of technology. The interest in self-cleaning surfaces is being driven by the desire to fabricate such surfaces for satellite dishes, solar energy panels, photovoltaic, exterior architectural glass and green houses, and heat transfer surfaces in air conditioning equipment. Non-wettable surfaces may also impart the ability to prevent frost from forming or adhering to the surface. The fact that liquid in contact with such a surface slides with lowered friction suggests applications such as microfluidics, piping, boat hulls and blood vessel.

In order to mimic the properties of lotus leaves, artificial superhydrophobic surfaces have been prepared by several means, including the generation of rough surfaces coated with low surface energy molecules, roughening the surface of hydrophobic materials and creating well-ordered structures using micromachining and etching methods.

2.2 Models

A model that can describe the contact angle of a liquid on a surface according to the surface tension is given by different relations depending on surface roughness, but in general is always true that when the surface energy is lowered, the hydrophobicity is enhanced.

2.2.1 Ideal surface

Young's equation

An ideal surface is flat, smooth and has homogeneous chemical composition. For a drop on ideal surface *Young's relation* is valid:

$$\cos\vartheta = \frac{\gamma_{sv} - \gamma_{sl}}{\gamma_{lv}}$$

where γ is the surface tension existing at the interface of two systems, solid-liquid (sl), solid-vapour (sv) and liquid-vapour (lv).
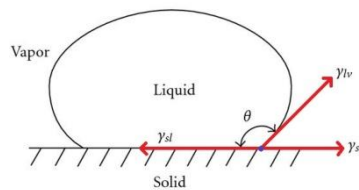
Fig. 1: Schematic diagram of the contact angle and its surface tension components.

2.2.2 Rough surface

Wetting on rough surfaces may assume either of two regimes: homogeneous wetting, where the liquid completely penetrates the roughness grooves, or heterogeneous wetting, where air is trapped underneath the liquid inside the roughness grooves. The transition between this two regimes has a major role in superhydrophobicity, and the fundamental difference is the hysteresis value[1].

Hysteresis (H) is the difference between advancing (ϑ_A) and receding (ϑ_R) contact angle:

$$H = \vartheta_A - \vartheta_R$$

the smaller the hysteresis is, the more it will be easy to move the liquid droplet[2].
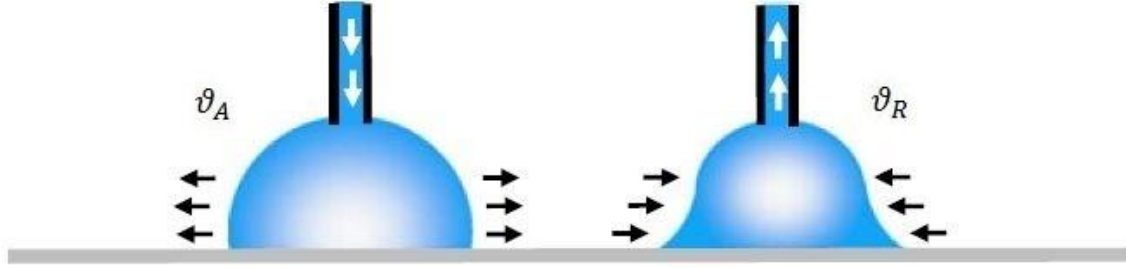
Fig. 2: Advancing and receding dynamic contact angle.

Studies have attributed contact angle hysteresis to surface roughness[3,4,5,6,7] and heterogeneity[8,9,10,11,12,13,14,15], as well as metastable energetic states[11,13,16]. Some found that the hysteresis decreases with increasing molecular volume of the liquid on the monolayers[17,18]. In more recent studies, contact angle hysteresis in found to be related to molecular mobility and packing of the surface[19,20,21], liquid penetration and surface swelling[22,23]. Previous studies showed that contact angle hysteresis is strongly dependent on the liquid molecular size and solid/liquid contact time, leading to the presumption that liquid sorption and liquid retention are causes of contact angle hysteresis[2].

The static contac angle(WCA) thus lies between ϑ_A and ϑ_R.

In these cases a new contact angle is observed, called apparent contact angle and noted ϑ'. It should be noticed that locally, the contact angle between the liquid droplet and the surface is always the angle of Young.

Wenzel state

A drop on a rough and hydrophobic surface can be in a completely wetting configuration and the model is well described by *Wenzel equation*:

$$\cos\vartheta' = r\frac{\gamma_{sv} - \gamma_{sl}}{\gamma_{lv}} = r\cos\vartheta$$

where r is the roughness, defined as the ratio of the actual area of the rough surface to the geometric projected area.
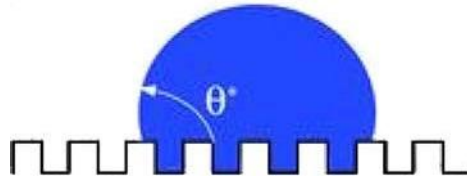
Since the condition $r \geq 1$ is always true, surface roughness enhances both the hydrophilicity of hydrophilic surfaces and hydrophobicity of hydrophobic ones.

Cassie-Baxter state

A drop that partially wets a rough and hydrophobic surface, is well modelized by *Cassie-Baxter equation* which describes a surface composed of solid and air:

$$\cos \vartheta' = f \cos \vartheta + (1 - f) \cos 180°$$

where f is the fraction of wetted solid area with a water contact angle of ϑ, and assuming a water contact angle for air of $180°$.
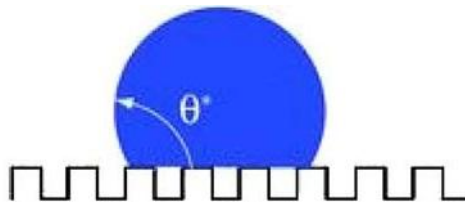
Fig. 4: Drop in Cassie-Baxter state.

A more general form of this equation can explain also the wetting behaviour in the case of a chemically inhomogeneous surface completely wetted.

It is experimentally demonstrated that during the regime where Wenzel mode is dominant, the contact angle and its hysteresis on hydrophobic rough surfaces increase as the roughness factor increases; contact angle continues to increase when the roughness factor exceeds the value 1,7 whereas the hysteresis starts to decrease. This decrease in hysteresis occurs as a consequence of the switching of the dominant hydrophobicity mode from Wenzel to Cassie due to the increase of air fraction at the interface between the solid and water.

2.3 Superhydrophobization methods and developments

Techniques to make superhydrophobic surfaces can be simply divided into two categories: making a rough surface from a low surface energy material and modifying a rough surface with a material of low surface energy.

2.3.1 Making a rough substrate

There are many ways to make rough surfaces, such as

mechanical stretching

laser/plasma chemical etching

lithography

sol-gel processing

solution casting

layer-by-layer assembling

electron discharge deposition

electrospinning deposition

chemical vapour deposition

Some of the up listed techniques are going to be described:

Etching and Lithography

Different etching methods including plasma etching, laser etching and chemical etching have all been used in the past years to fabricate superhydrophobic surfaces. Plasma treatment leads to polymer shrinkage and the generation of random roughness. Often it is necessary to hydrophobize the surface of the polymer again after treatment.
Laser treatment is less random and allows the formation of designed structures, but is less suited for large surfaces.

Lithography is a well established technique for creating large-area periodic micro-/nano-patterns.

Sol-gel

In most of the sol-gel processes investigated, no post-process hydrophobization is used for the achievement of superhydrophobicity since low surface energy materials are already included in the sol-gel process.

Layer-by-layer deposition

Layer-by-layer self-assembly in a rich process to fabricate thin film coatings with molecular level control over film thickness and chemistry using electrostatic interaction and hydrogen bonding.

Positive and negative polyions are coated onto surfaces in sequence. Roughness can develop if one of the components contain solid particles. As long as last layer is hydrophobic, or a hydrophobic capping layer is used, superhydrophobicity will appear after enough cycles.

This is a simple method suitable for covering complex objects.

Electrochemical deposition

Electrochemical reaction and deposition has been extensively used to prepare superhydrophobic surfaces.

Rough surfaces for superhydrophobicity have been electrodeposited in metals, but polymers are more interesting as they can allow single stage deposition as long as the polymer deposited becomes hydrophobic. Such surfaces can coat complex objects and can be used to post-treat conductive areas, leaving the rest of the substrate clear.

Electrospinning deposition

Electrospinning is a powerful technique to make ultrafine fibers and has been found to provide sufficient surface roughness for superhydrophobicity. Electrospinning a hydrophobic material leads to superhydrophobicity in one step.

Chemical Vapour Deposition (CVD)

CVD has been widely used for the modification of surface chemistry as well as the synthesis of nanostructured surfaces, for instance aligning carbon nanotubes.

2.3.2 Low surface tension material

There are a lot of materials of particular interest due to their extremely low surface energies, that can be classified in categories:

Fluorocarbons (Teflon)

Silicones (PDMS)

organic materials

3 MATERIALS AND METHODS

The aim of this research was the achievement of superhydrophobicity applying coating on common carbon steel for industrial application. So the starting point was to reach the goal with low cost in order to carry out the procedure on large scale.

3.1 MATERIALS

3.1.1 Substrate

Common mild carbon steel was used as substrate. Its chemical composition, analyzed with a SPECTROLAB metal analyzer/OES/fixed, is reported in Tab. 1:

Tab. 1 - Chemical composition of mild carbon steel substrate.

Elements	%
C	0.05
Si	0.01
Mn	0.23
Cr	0.03
Mo	<0.01
Ni	0.01
Cu	0.02
V	0.001

In this study carbon steel substrate was used both as received and after sandblasting treatment.

Sandblasting was performed with a Lampugnani S-SAB using corindone (chemical composition: Al_2O_3 95.8% - SiO_2 0.7% - FeO_3 0.3% - TiO_2 3%; particle size 150-210 µm; gun pressure 4-5 bar).

After sandblasting treatment, substrates were stocked in a chamber under N_2 atmosphere, including silica gel, in order to avoid oxidation of the surface and prevent from humidity corrosion, respectively.

3.1.2 Organic coatings

In this research different kind of coatings were employed, some of which were synthesized, others were purchased and used as received.

Commercial coatings applied on the sample as purchased are butyric acid (CA3, 99+% Alfa Aesar), tridecanoic acid (CA12, Fluka), nonadecanoic acid (CA18, 99.5% Fluka) and 1-butylphosphonic acid (C4P, 98% Alfa Aesar). 1-dodecylphosphonic acid (C12P) and 1-octadecylphosphonic acid (C18P) are synthesized using the following commercial reagents: triethyl phosphite (98% Aldrich), 1-Br-dodecane (97% Sigma Aldrich), 1-Br-octadecane (97% Sigma Aldrich), hydrobromidric acid (HBr, 48% Fluka), n-pentane (98% Alfa Aesar), n-hexane (95+% Alfa Aesar). Partially esterified polyacrylate with alkyl chain of several lengths C4 (PA4), C12 (PA12) and C18 (PA18) were obtained employing polyacrylic acid(PAA, m.w.=1515), 1-butanol (99.5% Fluka), 1-dodecanol (98% Alfa Aesar), 1-octadecanol (97% Alfa Aesar), sulfuric acid (96% Sigma Aldrich) and diethyl ether (99% Sigma Aldrich). Further solvents were used in the deposition process: dichloromethane (DCM, 99.9% Sigma Aldrich), tetrahydrofuran (THF, 99.9% Sigma Aldrich) and an oxidizing powder called NoChromix® (GODAX Laboratories Inc.).

3.1.2.1 Butyric acid - CA3
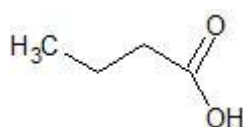
Fig. 5: CA3 molecular structure.

Butyric acid has the following specifications: m.w.= 88.11 ; m.p.= -8°C ; b.p.= 163°C.

3.1.2.2 Tridecanoic acid - CA12
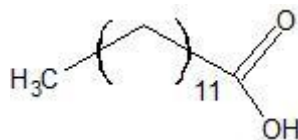
Fig. 6: CA12 molecular structure.

Tridecanoic acid has the following specifications: m.w.= 214.34 ; m.p.= 41 °C ; b.p.= 236 °C.

3.1.2.3 Nonadecanoic acid - CA18
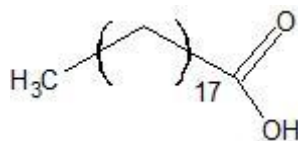
Fig. 7: CA18 molecular structure.

Nonadecanoic acid has the following specifications: m.w.= 298.5 ; m.p.= 69 °C.

3.1.2.4 Butyl phosphonic acid - C4P
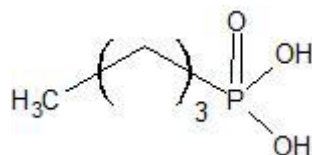
Fig. 8: C4P molecular structure.

Butyl phosphonic acid has the following specifications: m.w.= 138.1 ; m.p.= 100 °C.

3.1.2.5 Dodecyl Phosphonic Acid - C12P
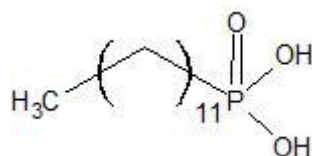
Fig. 9: C12P molecular structure.

Synthesis

Phosphonic acids have been synthesized from their brominated precursors via the Michaelis-Arbuzov reaction.[24] A mixture of 1-Br-dodecane (5.2 g) and triethyl phosphite (3.78 g) was stirred and heated at 120-150 °C for 4 h in a flask. Then HBr 48% (17.5 ml) was added to the flask, going on with the stirring and heating at reflux T (70-80 °C) for 3 h. After cooling at room temperature, distillation of water and bromoethane (BrEt) was performed rising T till 160 °C. The product was washed with n-pentane, recrystallized from n-hexane and again washed in n-hexane. The cleaned product was dried for 12 h at 70 °C to remove any solvent.[25]

Fig. 10: C12P synthesis reactions.

Characterization
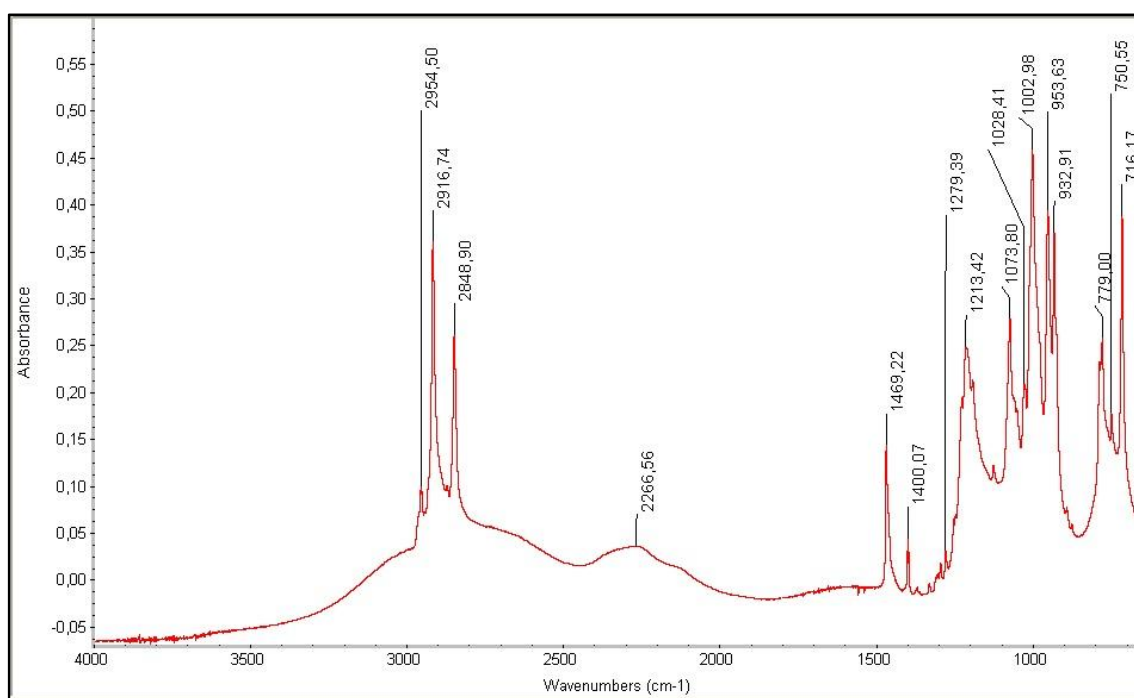
- FTIR

Fig. 11: C12P - FTIR spectrum.

This spectrum shows several well defined peaks: the three peaks at 2954-2916-2848 cm^{-1} are characteristic of CH_3^{as}-CH_2^{as}-CH_2^{s} stretching vibrations respectively, at 2266 cm^{-1} P-OH vibration is found, while P=O stretching is present at 1213 cm^{-1}. Peaks at low frequencies are due to P-O-C and P-C vibrations.[26,27]

All these characteristic peaks confirm that the reaction occurred and the expected functionalities are present.

- DSC

The DSC spectrum is reported in Fig. 12. The set up of the thermal analysis cycle was composed by two heating ramps with an intermediate cooling.
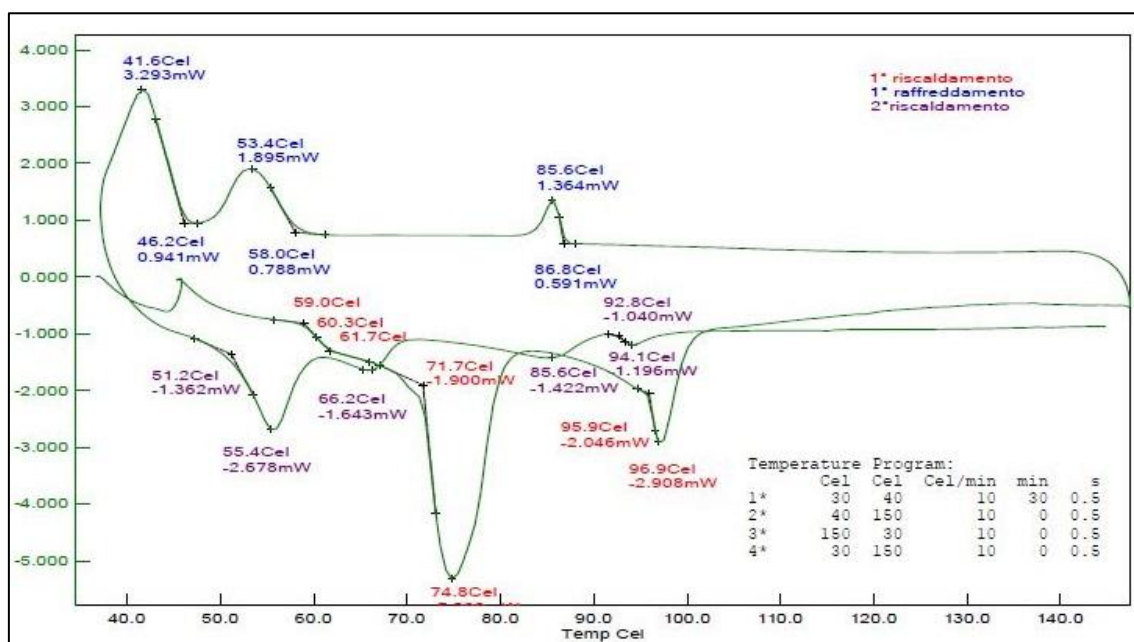
In the first heating ramp two different endothermic peaks are present at 74.8 °C and 96.9 °C, with a probable glass transition around 60.3 °C. Peak at 96.9 °C is surely related to C12P as in literature a melting point at 98°C is reported[25]. Since the main reagents 1-Br-dodecane (m.p. = -11 °C, b.p.=135 °C) and triethyl phosphite (m.p. = -70 °C, b.p. = 156 °C) have phase transition at different temperature, the most probable cause for the endothermic peak at 74.8 °C is that some volatile components may be present in the sample. BrEt may be trapped like impurities in the solid product, producing unpredicted effects during heating ramp of the analysis. This can be supposed as there is no corresponding exothermic peak in the cooling ramp. During the second heating ramp relevant peaks are observed at 55.4 °C and 94.1 °C (peak maximum). The first peak could correspond to monoethyl or diethyl phosphonic acid, while the second very feeble peak to the C12P product. Both the peaks have a corresponding signal during the previous cooling ramp.

- DTG/TG
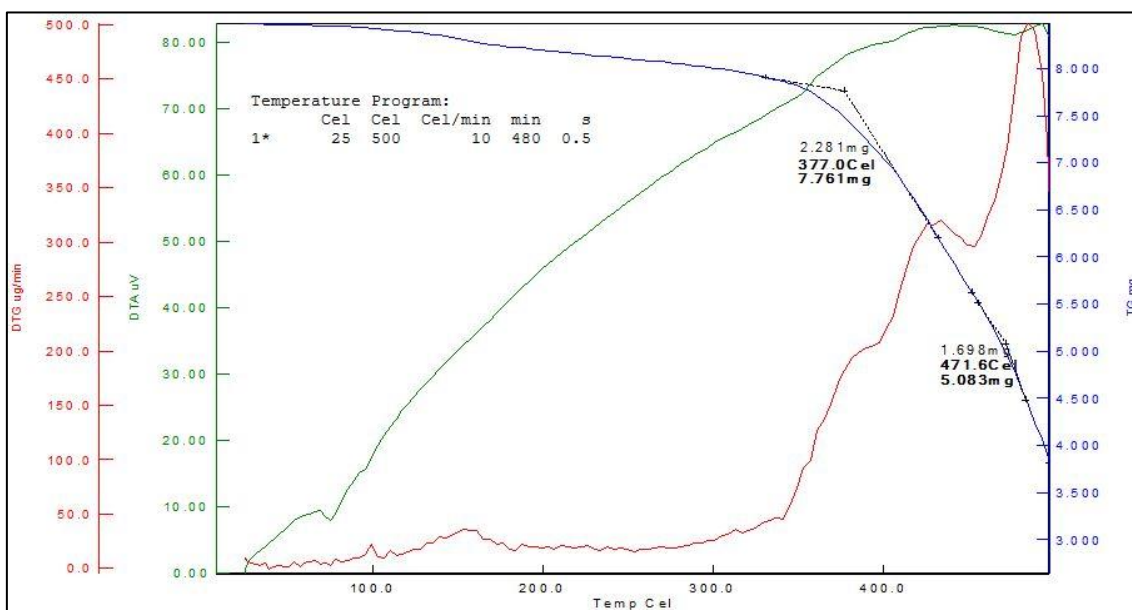
The most significant weight loss starts at 377.0 °C, in accordance with the predicted ACD/Labs boiling point b.p. = 380 °C [28], confirming the product occurrence. Furthermore no evident decrease of weight is found around 75 °C, meaning the endothermic peak in DSC analysis (Fig. 12) is related to a high vaporization enthalpy substance or to an internal transformation like cyclization, without decomposition.

- ^{1}H-NMR
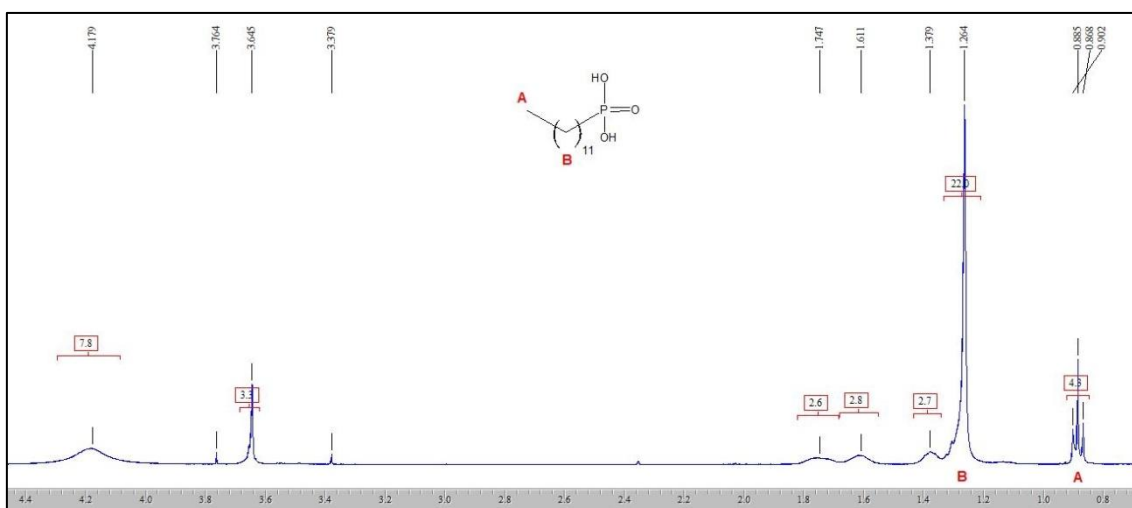
Fig. 14: C12P - ^{1}H-NMR spectrum (in CDCl$_3$).

The interpretation of ^{1}H-NMR spectra is done with the aid of ChemNMR H-1 Estimation software which suggests a possible spectrum of C12P molecule. The peak at 0.88 ppm

25

is linked to CH_3 terminal group of the chain, while the high intensity peak at 1.26 ppm is related to CH_2 of alkyl chain.[24] The presence of the other peaks means a not pure product is obtain, probably containing some unreacted reagent because peaks at 1.61 ppm and 3.38 ppm can be found in BrEt and 1-Br-dodecane spectra, while in the unsubstituted ethyl phosphite estimated spectrum the peak at 3.64 ppm is present.

3.1.2.6 Octadecyl Phosphonic Acid - C18P
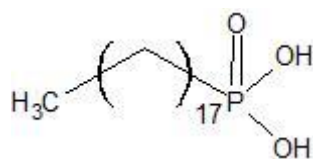
Fig. 15: C18P molecular structure.

Synthesis

A mixture of 1-Br-octadecane (6.674 g) and triethyl phosphite (3.323 g) put inside a flask was stirred and heated at 170 °C for 4 h. Then HBr 48% (35.638 g) was added to the flask, keeping on stirring and heating at reflux T (70-90 °C) for 3 h. After cooling down at room temperature, distillation of water and BrEt was performed rising T till 125 °C. The product was washed with n-pentane, recrystallized from n-hexane and again washed in n-hexane. The cleaned product was now dried for 3 h at 70 °C to remove any solvent.[26]
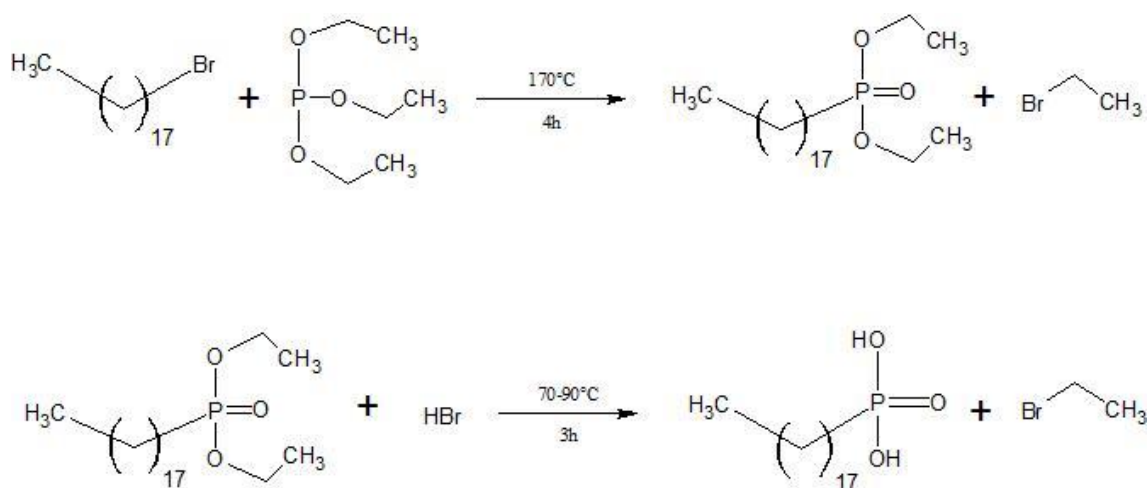
Fig. 16: C18P synthesis.

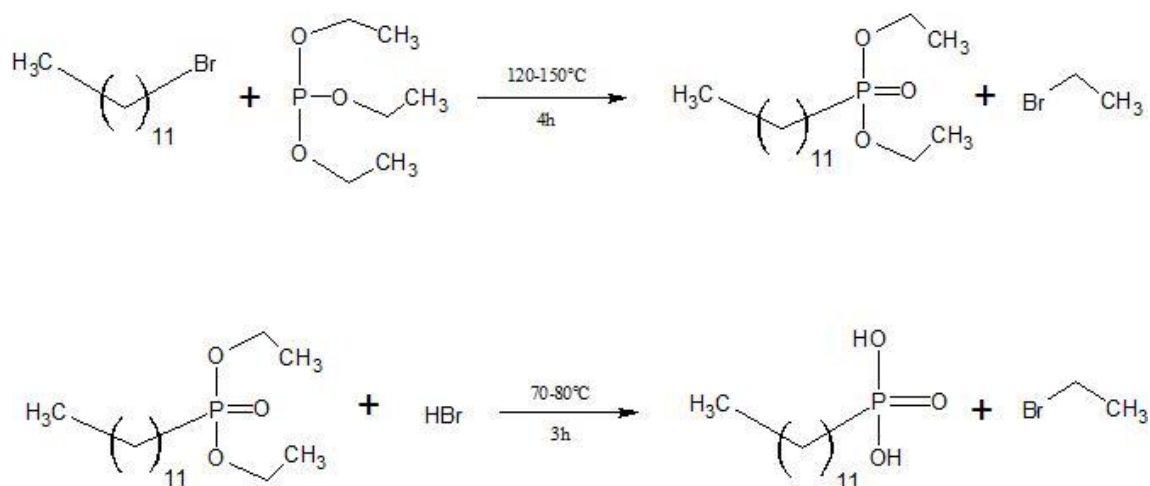**Characterization**
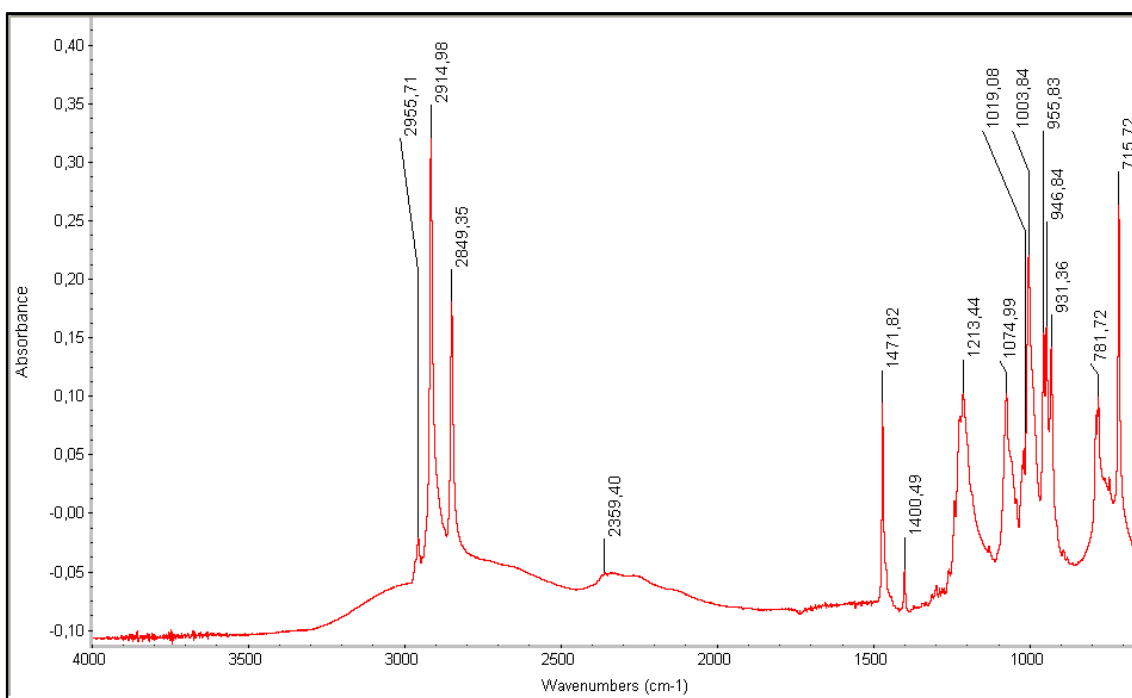
- FTIR

Fig. 17: C18P - FTIR spectrum.

As in the case of C12P, this spectrum shows several well defined peaks: the three peaks at 2955-2914-2849 cm^{-1} are characteristic of CH_3^{as}-CH_2^{as}-CH_2^s stretching vibrations respectively, at 2359 cm^{-1} P-OH vibration, while P=O stretching is present at 1213 cm^{-1}. Peaks at low frequencies are due to P-O-C and P-C vibrations.[26,27]

All this characteristic peaks confirm that the reaction occurred and the expected functionalities were present. Furthermore "C18P - FTIR spectrum." overlaps very well "C12P - FTIR spectrum.", with the only difference in the intensity of CH_3^{as}-CH_2^{as}-CH_2^s stretching vibrations peaks. This was a confirmation about the success of C12P synthesis.

- DSC
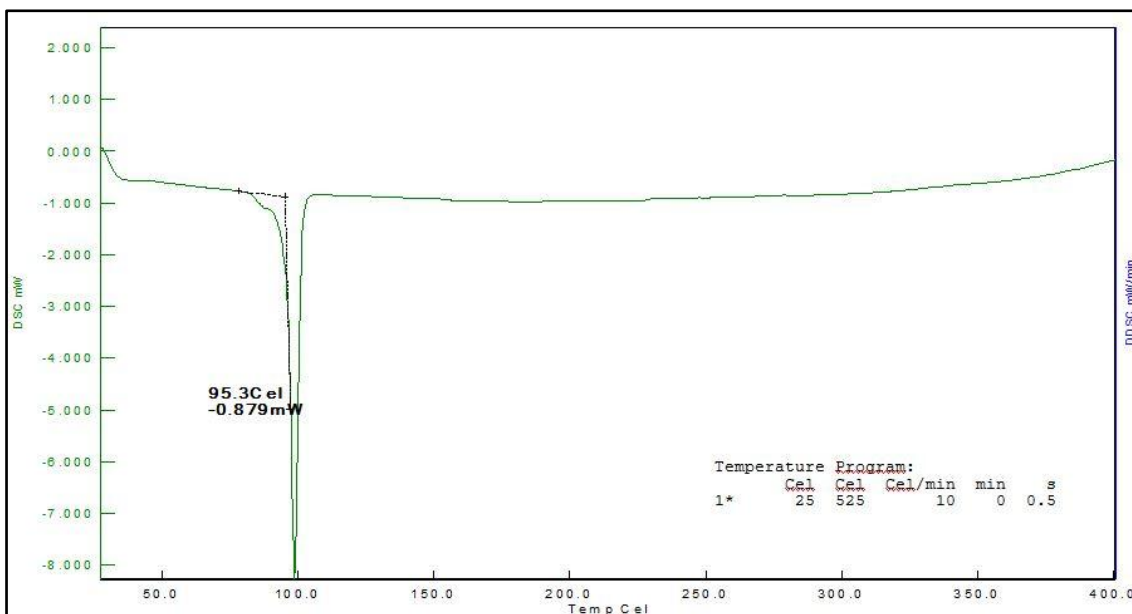
Fig. 18: C18P - DSC analysis (in N_2).

The plot shows an endothermic peak at 95.3 °C, corresponding to the melting point of C18P.[29] The obtained product seems very pure since that is the only well defined peak presents in the spectrum.

- DTG/TG
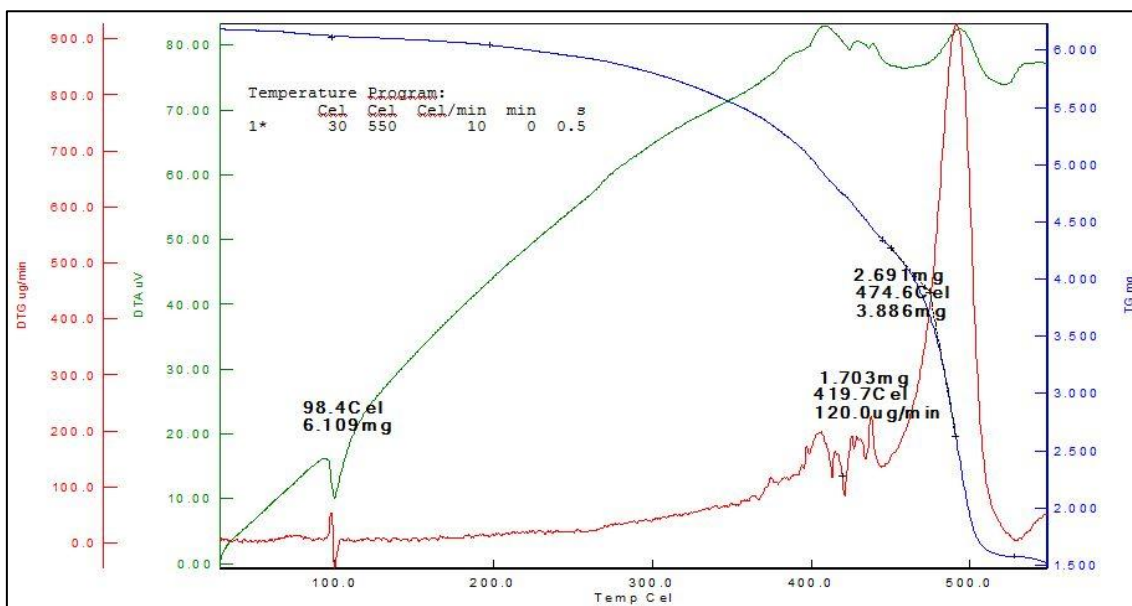
Fig. 19: C18P - DTG/TG analysis (in air).

In this graph it can be seen a phase transition at 98.4 °C, corresponding to the melting temperature of C18P as suggested by DSC analysis (see Fig. 18), and thermal degradation begins over 350 °C with the most significant weight loss sets at 474.6 °C.

28

3.1.2.7 Butyl Polyacrylic Acid PA4
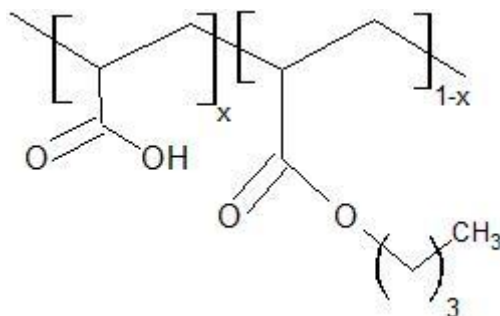
Fig. 20: PA4 molecular structure.

Synthesis

A classical Fischer esterification between PAA and 1-butanol using sulfuric acid as catalyst was used to synthesize PA4. The acid-catalyzed esterification of carboxylic acids with alcohols to give esters is a typical reaction in which the products and reactants are at equilibrium. The equilibrium may be influenced by either removing one product from the reaction mixture (for example, removal of the water by azeotropic distillation or absorption by molecular sieves) or by employing an excess of one reactant.[30]

The trouble was the presence of water: it kept PAA in solution allowing the reaction with the alcohol but since this was an equilibrium reaction it hindered the product formation.

A blend of PAA 50wt% (40 g), 1-butanol (76 ml) and sulfuric acid (0.2 ml) was placed inside a flask. 1-butanol is present in excess, over the quantity required to obtain a complete esterification of the polymer, in order to stabilize the solution and allow the formation of azeotropic compound with PAA.[31] This mixture was mechanically stirred and heated at reflux T (96 °C due to the azeotropic compound) using a Marcusson glassware to manage the presence of water inside the flask. The reaction was stopped after 20 h when a defined peak at 1730 cm^{-1} in the FTIR spectrum was found (see Fig. 22). In order to remove any solvent, the obtained product was put in the rotavapor. After this passage, the unpurified product was dissolved in n-pentane with the aid of a magnetic stirrer, then the addition of water allowed cleaned PA4 precipitation (stirring going on overnight). Centrifuge (30 min at 5000 rpm) separates the two phases and n-

pentane was more easily mechanically removed. Finally PA4 was dried in a vacuum oven at 105 °C for 4 h.
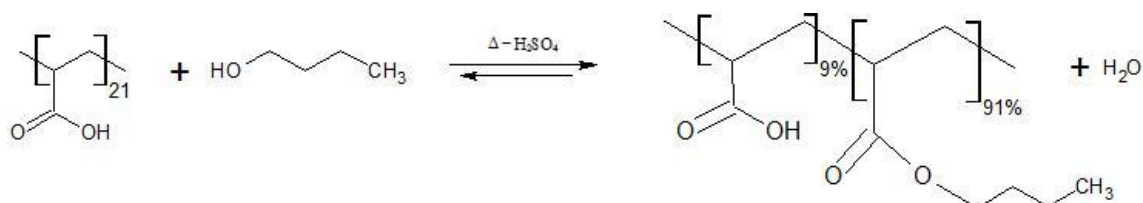
Fig. 21: PA4 esterification reaction.

Characterization
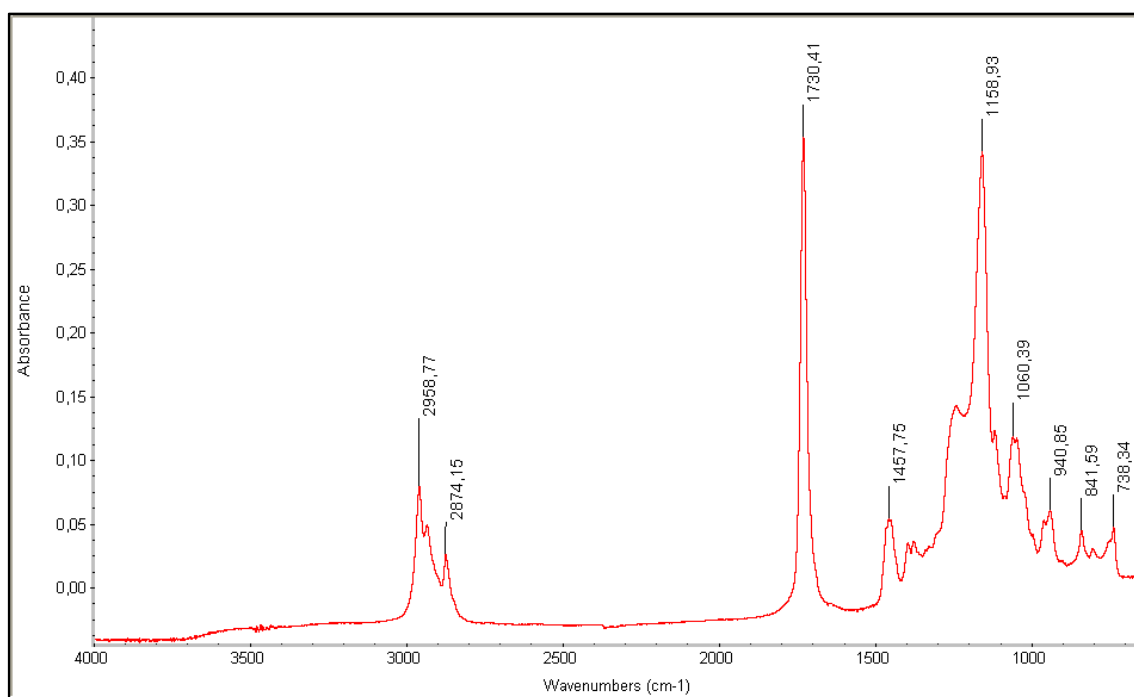
- FTIR

Fig. 22: PA4 - FTIR spectrum.

The reference peak in this spectrum is the one referred to the carbonyl group C=O. In the case of unesterified carboxyl group, it is set at 1700 cm^{-1}, but when it is esterified this peak shifts at higher values of vibrations(>1725 cm^{-1}). Here the peak moves to 1730 cm^{-1}, meaning a partial esterification of PAA occurred.[27]

- DSC
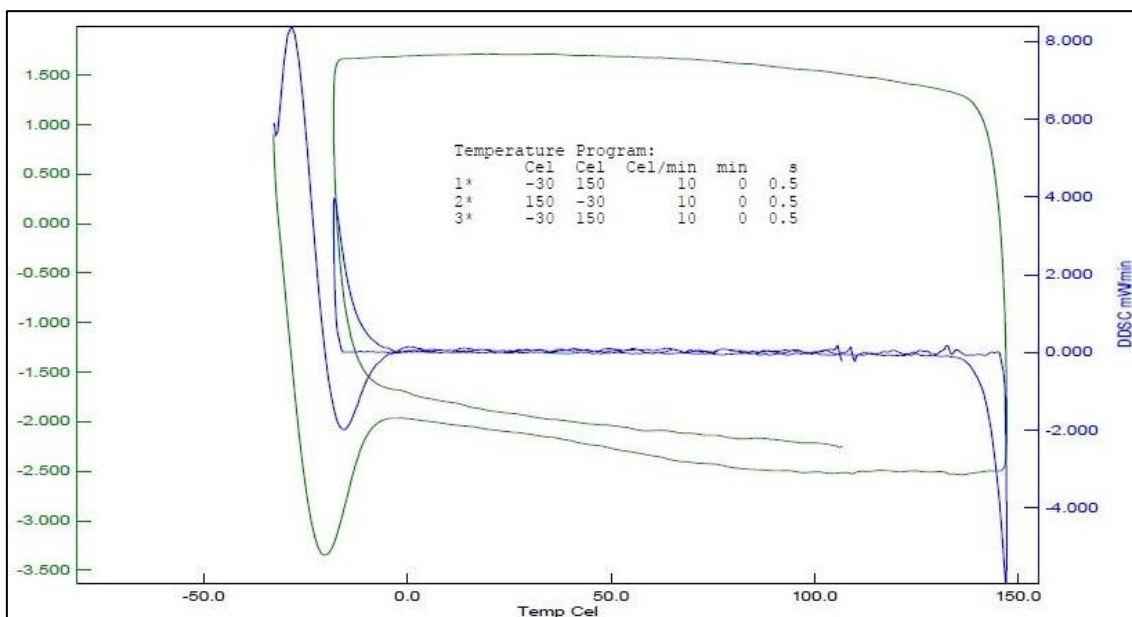
Fig. 23: PA4 - DSC analysis (in N_2).

This analysis does not show any interesting information about the molecule, because neither endothermic nor exothermic peaks are present in this range of temperature.

- DTG/TG
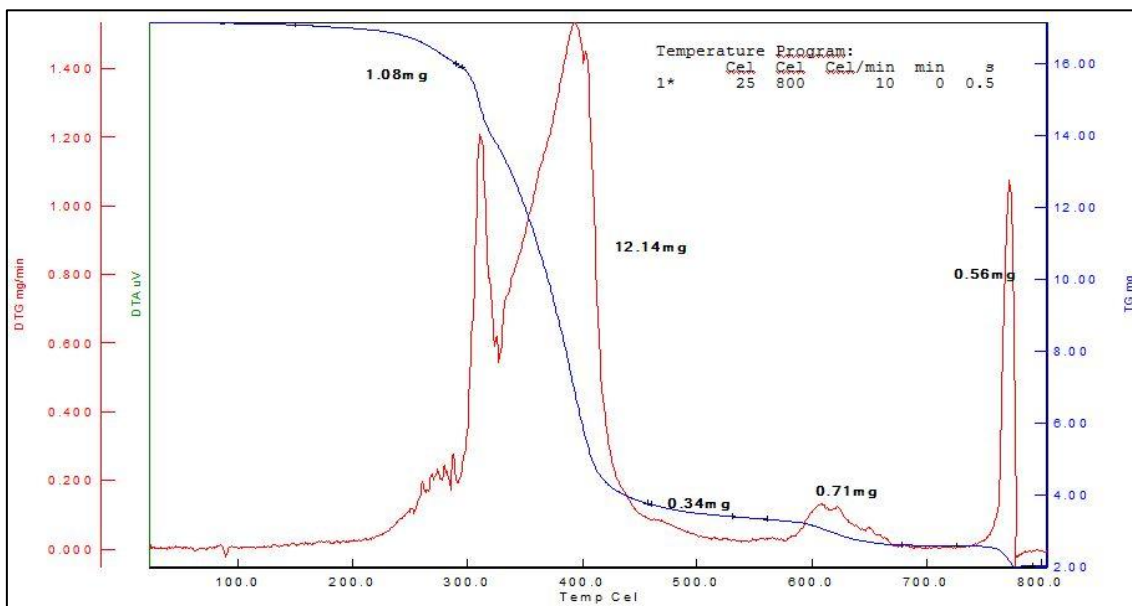
Fig. 24: PA4 - DTG/TG analysis (in air).

Analysis started at room temperature and till 200 °C no thermal degradation was found. Then there was a first weight loss at 300 °C but the most significant was set at 350-400 °C.

- ^{1}H-NMR
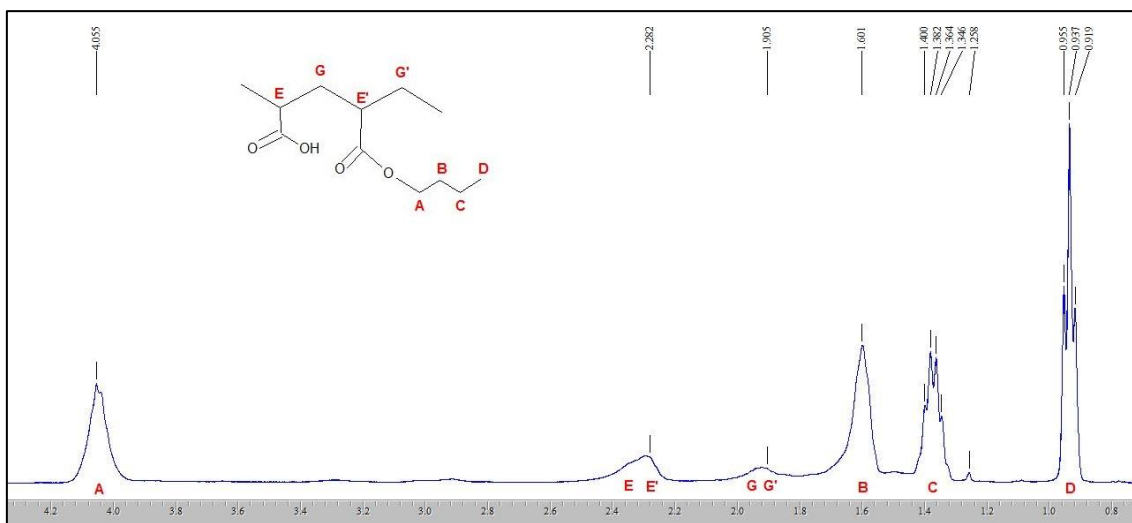
Fig. 25: PA4 - ^{1}H-NMR spectrum (in CDCl$_3$).

Peak at 0.93 ppm is referred to CH$_3$ terminal group of alkyl chain, while the ones at 1.37 ppm and 1.60 ppm are due to the central CH$_2$ of alkyl chain. CH$_2$ on alkyl chain near the oxygen of the ester produces the peak at 4.05 ppm. Peak at 1.90 ppm is linked to CH$_2$ of PA4 backbone, while the one at 2.28 ppm contains CH of the backbone bound to carboxyl groups.

- TITRATION

Titration was required in order to know the esterification degree obtained in the synthesis.

The standard ISO 2114:2000(E) was followed: 0.3787 g of PA4 were dissolved in 50 ml of toluene:ethanol (2:1 vol.) solution previously neutralized with KOH 0.01 M solution, then 27.3 ml of KOH 0.01 M in ethanol solution were used to titrate the PA4. After some computations, it was obtained an esterification degree of 91%.

3.1.2.8 Dodecyl Polyacrylic Acid PA12
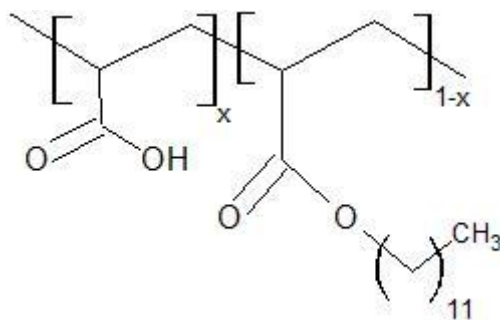
Fig. 26: PA12 molecular structure.

Synthesis

A classical Fischer esterification between PAA and 1-dodecanol using sulfuric acid as catalyst was used to synthesize PA12. The trouble was the presence of water: it kept PAA in solution allowing the reaction with the alcohol but since this was an equilibrium reaction it hindered the product formation.

PAA 50wt% (40 g), 1-dodecanol (26 g) and sulfuric acid (0,3 ml) were put in a flask. This mixture was mechanically stirred and heated at reflux T using a Marcusson glassware to manage the presence of water inside the flask (96 °C at the beginning due to the azeotropic compound [31], but when water recirculation was blocked, T was risen up to 200 °C). After 10 h a peak at 1734 cm^{-1} with a right-hand shoulder in FTIR spectrum was found (see Fig. 28), meaning a partial esterification occurred, so the reaction was stopped. The dirty product was dissolved in n-pentane with the aid of a magnetic stirrer. When dissolution was completed, stirring was stopped to allow the precipitation of PAA while PA12 remains in solution. The solution composed by PA12 dissolved in n-pentane was put in the rotavapor to remove any solvent, n-pentane included, purifying PA12.
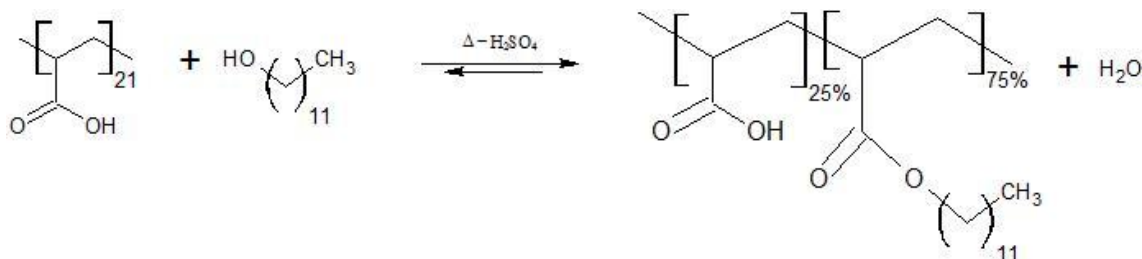
Fig. 27: PA12 esterification reaction.

Characterization
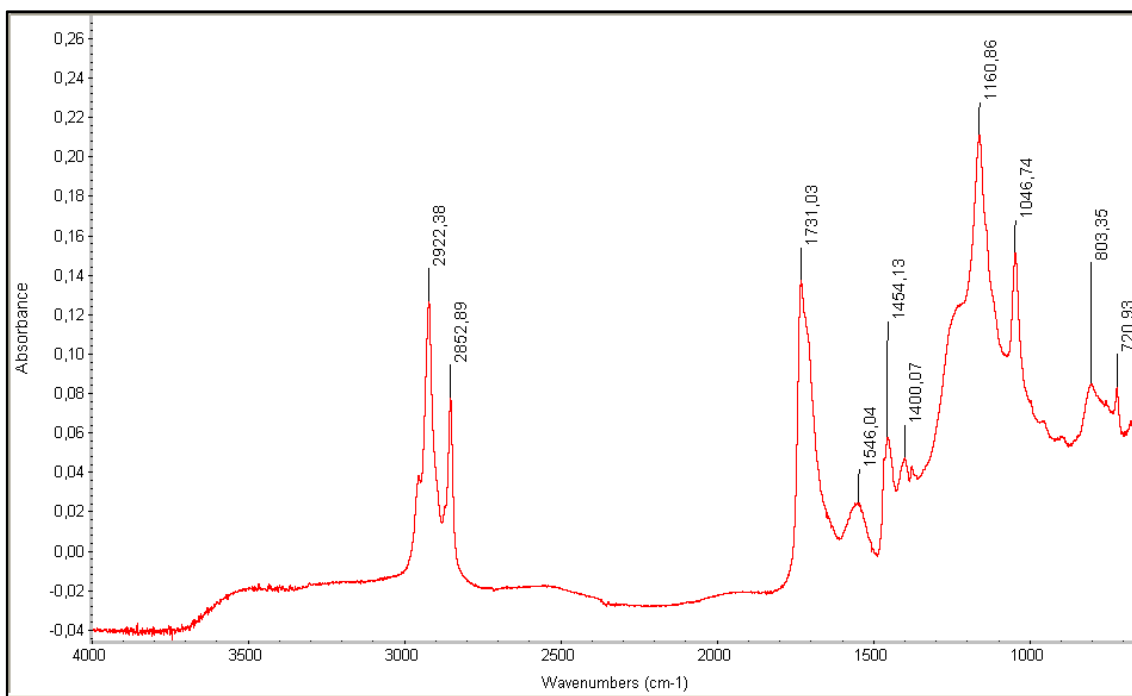
- FTIR

Fig. 28: PA12 - FTIR spectrum.

All the considerations done in the case of PA4 are valid also here. The reference peak is the one referred to the carbonyl group C=O. In the case of unesterified carboxyl group, it is set at 1700 cm^{-1}, but when it is esterified this peak shifts at higher values of vibrations. Here the peak moves at 1731 cm^{-1}, meaning a partial esterification of PAA occurred.[27] It has to be noted a very important thing: this peak shows a right-shoulder, so the presence in the PAA of both esterified and not esterified carboxyl group can be easily supposed.

- DSC
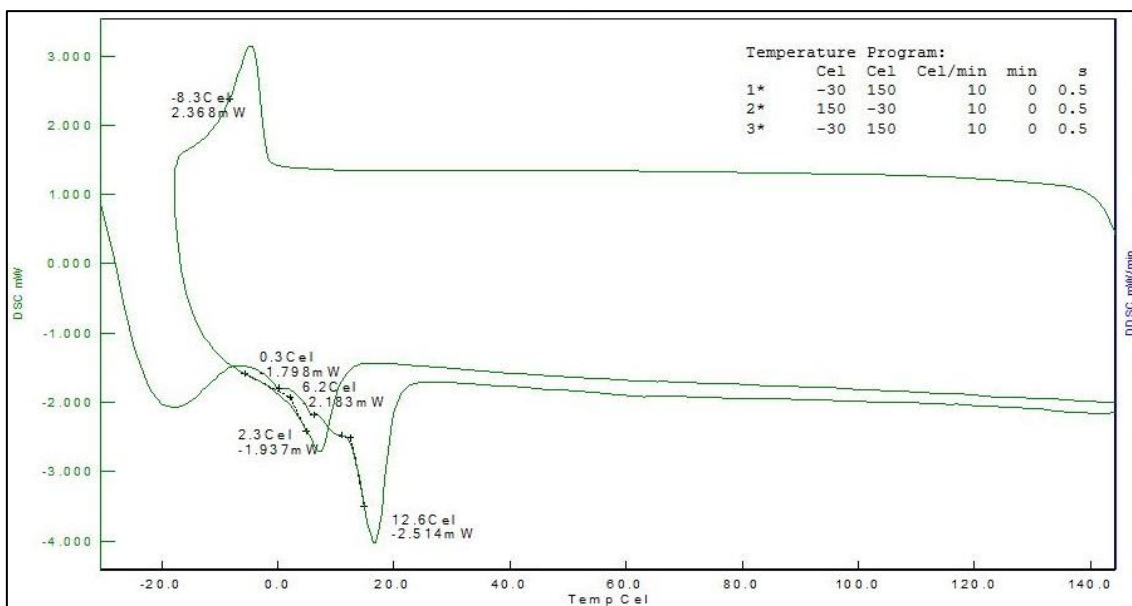
Fig. 29: PA12 - DSC analysis (in N₂).

Looking at the plot a softening is set at 0.3 °C and 6.2 °C while the melting point of this molecule is around 12.6 °C, but after one thermal cycle it shifts at lower T (2.3 °C). There are no reference in literature about this molecule.

- DTG/TG
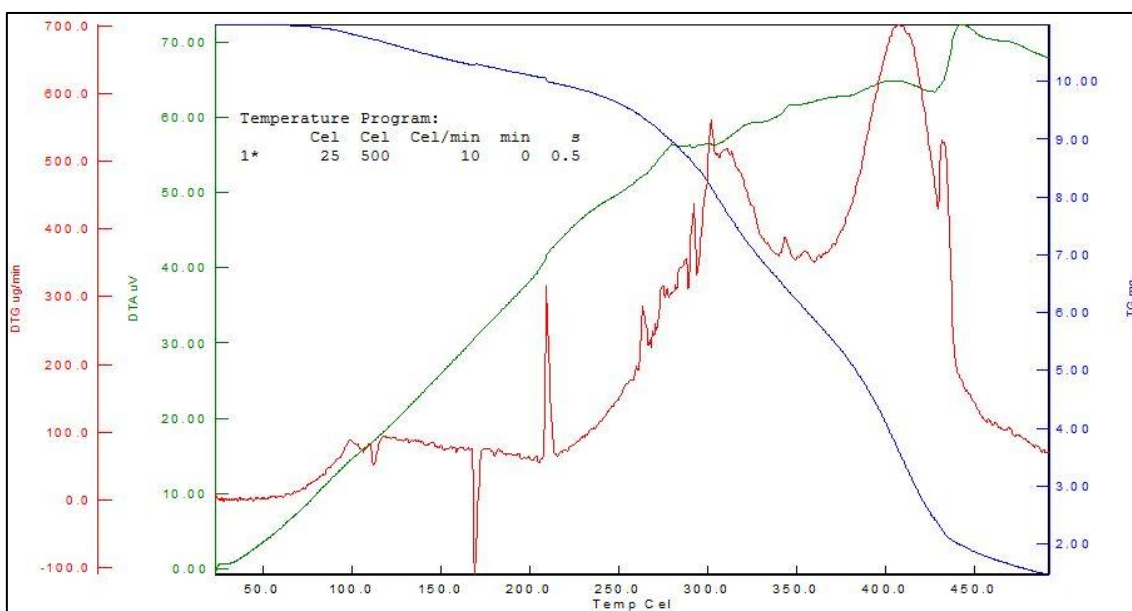
Fig. 30: PA12 - DTG/TG analysis (in air).

This analysis started at 25 °C so the melting point can't be seen, but it shows that the molecule begins to deteriorate at 100 °C and its larger weight loss begins at T higher

than 250 °C. The peaks in DTG plot (red line) at 170 °C and 210 °C are instrumental errors.

- ^{1}H-NMR
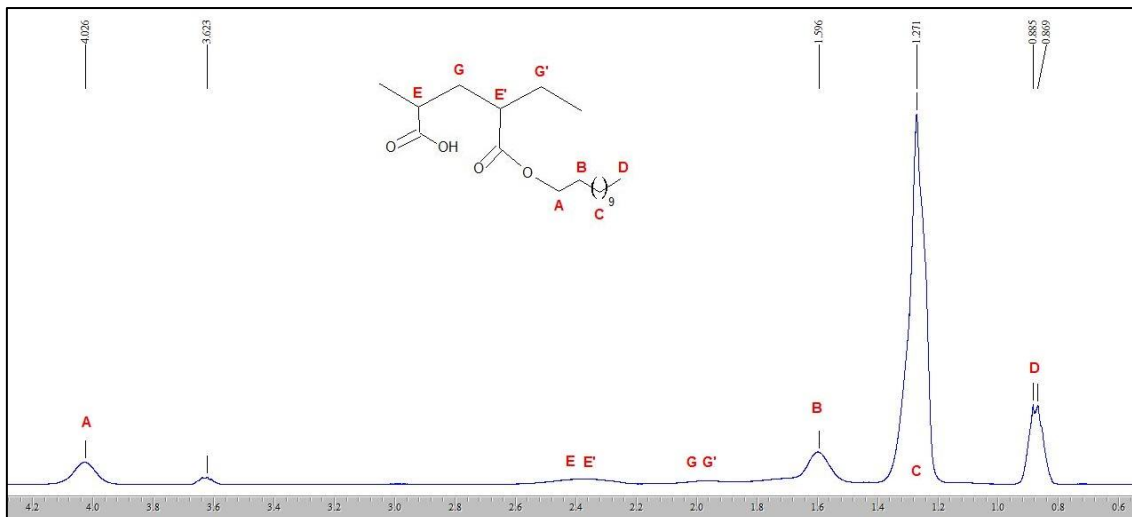
Fig. 31: PA12 - ^{1}H-NMR spectrum (in CDCl$_3$).

Peak at 0.88 ppm is referred to CH$_3$ terminal group of alkyl chain, while the ones at 1.27 ppm and 1.59 ppm are due to the central CH$_2$ of alkyl chain. CH$_2$ on alkyl chain near the oxygen of the ester causes the peak at 4.02 ppm. Because of the length of alkyl chain, the previously described peaks have high intensity, so the others seems very broad peaks. Peak around 1.9 ppm is linked to CH$_2$ of the backbone of PA12, while the one at 2.4 ppm contains CH of the backbone bound to carboxyl groups.

- TITRATION

Titration was required in order to know the esterification degree obtained in the synthesis.

The standard ISO 2114:2000(E) was followed: 0.2190 g of PA12 were dissolved in 50 ml of toluene:ethanol (2:1 vol.) solution previously neutralized with KOH 0.01 M solution, then 27.7 ml of KOH 0.01 M in ethanol solution were used to titrate the PA12. After some computations, it was obtained an esterification degree of 75%.

3.1.2.9 Octadecyl Polyacrylic Acid - PA18
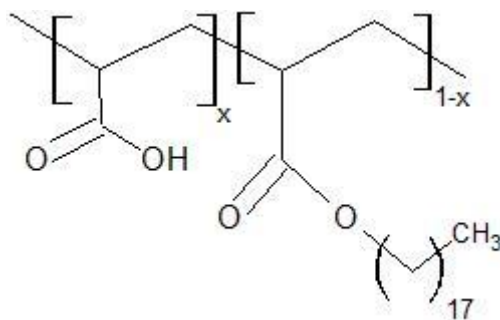
Fig. 32: PA18 molecular structure.

Synthesis

A classical Fischer esterification between PAA and 1-octadecanol using sulfuric acid as catalyst was used to synthesize PA18. The trouble was the presence of water: it kept PAA in solution allowing the reaction with the alcohol but since this was an equilibrium reaction it obstructed the product formation.

In order to obtain a theoretical 50% esterification degree, PAA 50wt% (40 g), 1-octadecanol (38 g) and sulfuric acid (0.3 ml) were blended in a flask at T = 70 °C so also the alcohol was at liquid state. This mixture was mechanically stirred and heated at reflux T, using a Marcusson glassware to manage the presence of water inside the flask for 2 days, periodically re-adding small quantities of sulfuric acid to improve the reaction rate. After this time a low intensity peak at 1731 cm^{-1} showing a shoulder at lower frequencies in FTIR spectrum was found (see Fig. 34), so the reaction was stopped. The dirty product was washed in diethyl ether grinding with the aid of a magnetic stirrer in order to allow the dissolution of unreacted 1-octadecanol while PA18 precipitates. Then the content of the flask was filtered, noting a whitening of the final product.
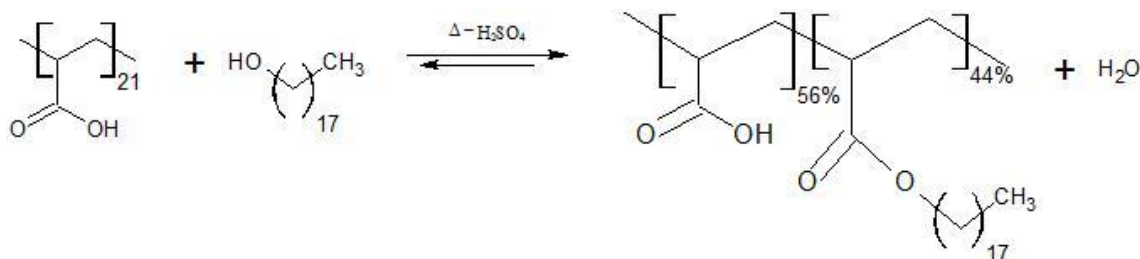
Fig. 33: PA18 esterification reaction.

Characterization

37
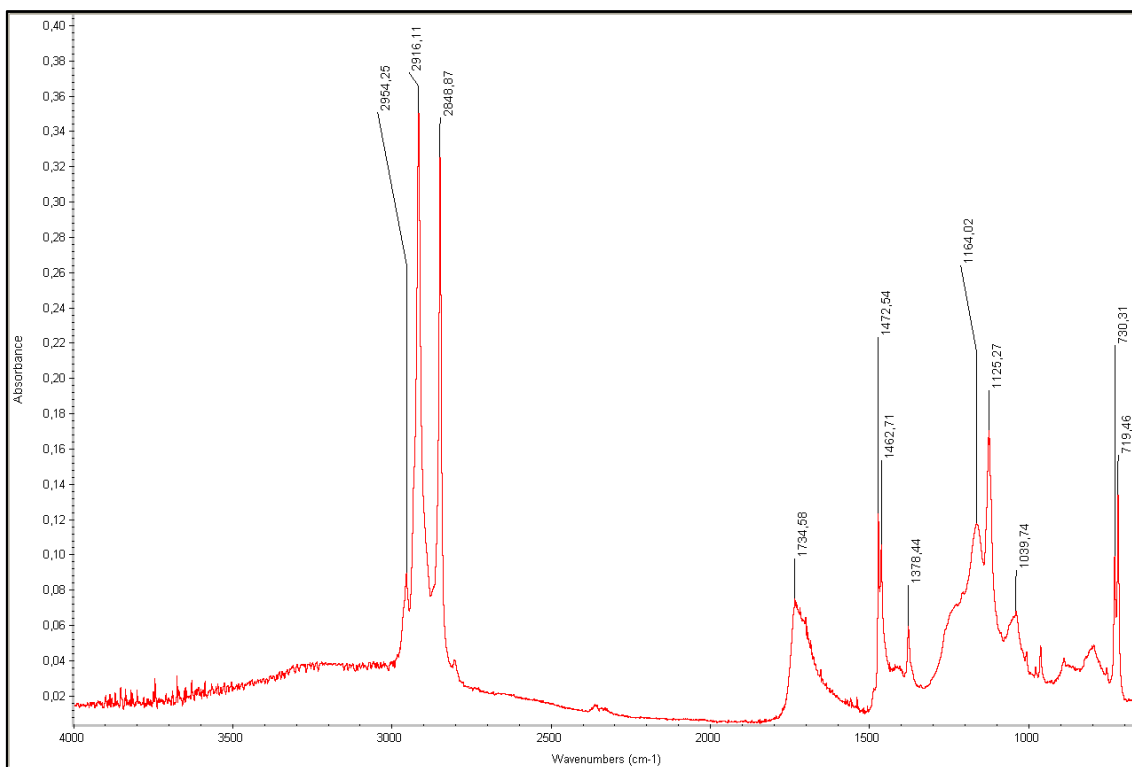
- FTIR

All the considerations done in the case of PA12 are valid also here. The reference peak is the one referred to the carbonyl group C=O. In the case of not esterified carboxyl group, it is set at 1700 cm^{-1}, that shifts at higher values of frequencies when carboxyl belongs to an ester group. Here the peak moves to 1734 cm^{-1}, meaning a partial esterification of PAA occurred.[27] It has to be noted that this peak has lower intensity with respect the others spectra (see "Fig. 22: PA4 - FTIR spectrum." and "Fig. 28: PA12 - FTIR spectrum.") due to the longer alkyl chain, and it showed a very important right-shoulder, meaning a non-negligible presence in the product of unesterified carboxyl group.

- DSC
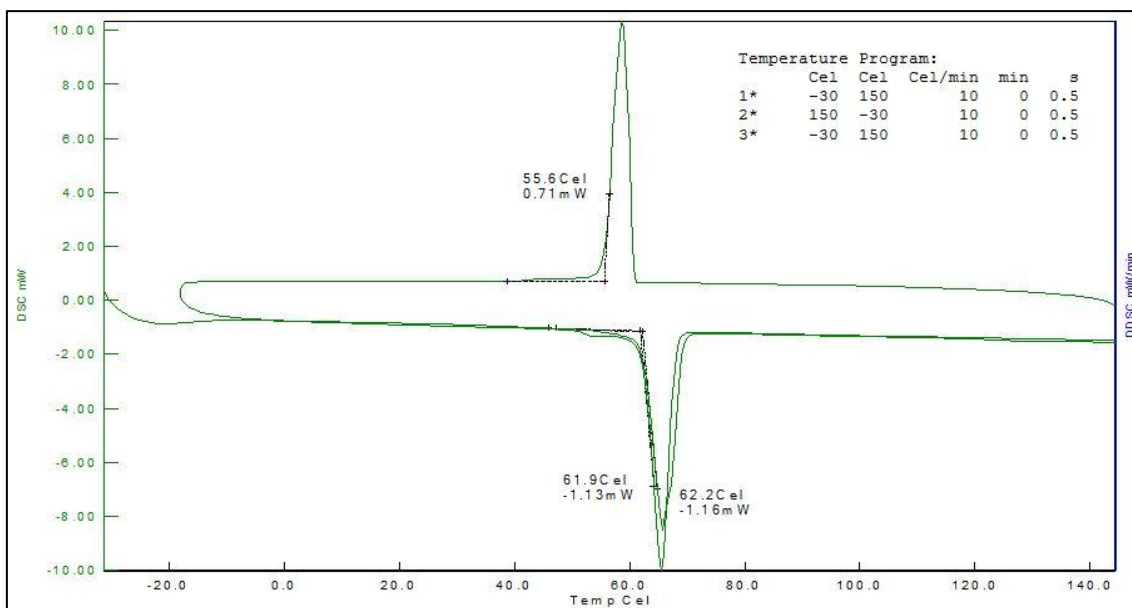
The two cycles showed a melting point in the range 61.9-62.2 °C. the temperature range is near to the m.p. of 1-octadecanol. The peak was asymmetric probably meaning that a mixture of esterified/unesterified polymer was obtained.

- ^{1}H-NMR
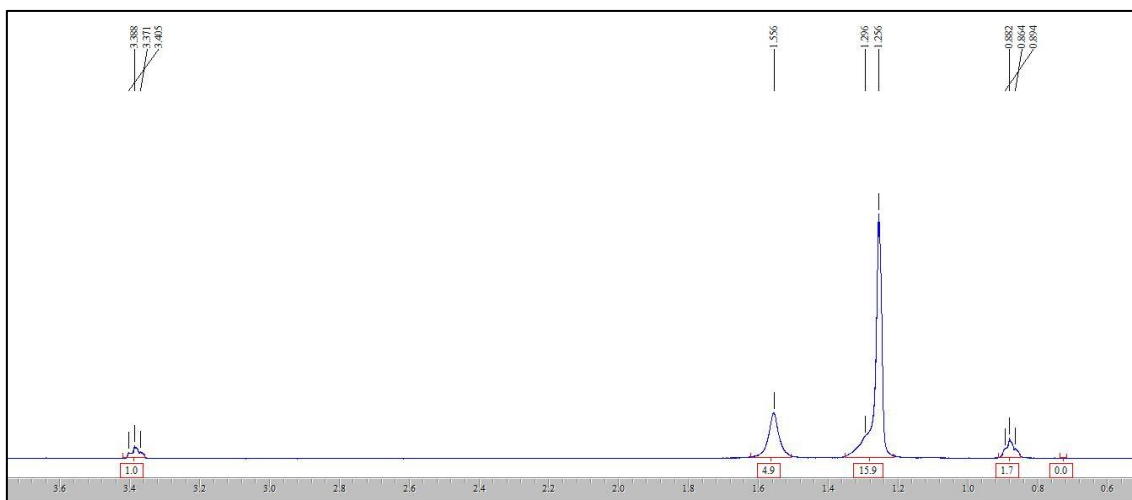
The ^{1}H-NMR spectrum (Fig. 36) interpretation has been very troublesome due to the low product solubility. The obtained signal was too feeble for a right interpretation.

- TITRATION

Titration was required in order to know the esterification degree obtained in the synthesis.

The standard ISO 2114:2000(E) was followed: 0.2014 g of PA18 were dissolved in 50 ml of toluene:ethanol (2:1 vol.) solution previously neutralized with KOH 0.01 M solution, then 61.0 ml of KOH 0.01 M in ethanol solution was used to titrate the PA18. After some computations, it was obtained an esterification degree of 44%.

3.2 METHODS

3.2.1 Fourier Transform Infrared Spectroscopy (FTIR)

Infrared spectroscopy is a technique based on the vibrations of the atoms of a molecule. An infrared spectrum is commonly obtained by passing infrared radiation through a sample and determining what fraction of the incident radiation is absorbed at a particular energy. The energy at which any peak in an absorption spectrum appears corresponds to the frequency of a vibration of a part of a sample molecule. For a molecule to show infrared absorptions it must possess a specific feature, i.e. an electric dipole moment of the molecule must change during the vibration. This is a description of stretching and bending movements that are collectively referred to as vibrations. Infrared radiation is absorbed by organic molecules and converted into energy of molecular vibration. In IR spectroscopy, an organic molecule is exposed to infrared radiation. When the radiant energy matches the energy of a specific molecular vibration, absorption occurs. In a typical IR spectrum the wavenumber, plotted on the X-axis, is proportional to energy; therefore, the highest energy vibrations are on the left. The absorbance is plotted on the Y-axis. Even simple organic molecules give rise to complex IR spectra. Both the complexity and the wavenumbers of the peaks in the spectra give the chemist information about the molecule. The complexity is useful to match an experimental spectrum with that of a known compound with a peak-by-peak correlation. To facilitate this analysis, compilations of IR spectra are available. The wavenumbers (sometimes referred to as

frequencies) at which an organic molecule absorbs radiation give information on functional groups present in the molecule. Certain groups of atoms absorb energy and therefore, give rise to bands at approximately the same frequencies. There are two types of molecular vibrations, stretching and bending. In order to be IR active, a vibration must cause a change in the dipole moment of the molecule.

In this work a Thermo scientific mod. Nicolet iS10 was employed.

3.2.2 Nuclear Magnetic Resonance Spectroscopy (^{1}H-NMR)

Nuclear magnetic resonance spectroscopy (NMR) is an analytical technique that gives detailed information about molecular structure of the sample observing particular atomic nuclei having a magnetic moment.

NMR measures radiofrequency electromagnetic radiation absorption of molecules dipped in a strong magnetic field. These radiations cause nuclear spin transitions of ^{1}H atom which provides molecular structure details. NMR is based on the fact that when a population of magnetic nuclei is placed in an external magnetic field, the nuclei become aligned in a predictable and finite number of orientations. For ^{1}H there are two orientations. In one orientation the protons are aligned with the external magnetic field and in the other where the nuclei are aligned against the field.

In this work a Bruker AV 400 (400MHz) equipped with a 5 mm multinuclear probe with reverse detection was employed. The sample was dissolved in deuterated chloroform($CDCl_3$).

3.2.3 Differential Scanning Calorimetry (DSC)

Differential Scanning Calorimetry, or DSC, is a thermal analysis technique that looks at how a material's heat capacity is changed by temperature. A sample of known mass is heated or cooled and the changes in its heat capacity are tracked as changes in the heat flow. This allows the detection of transitions such as melts, glass transitions, phase changes, and curing. Differential Scanning Calorimetry is a technique used to measure thermal properties of polymers based on the rate at which they absorb heat energy compared to a reference material. The technique takes advantage of the energy changes involved in the various phase transitions of certain polymer molecules. This allows several properties of the material to be ascertained: melting points, enthalpies of melting, crystallization temperatures, glass transition temperatures and degradation temperatures.
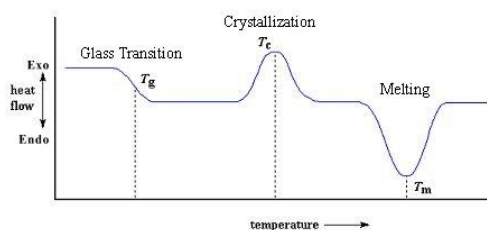
Fig. 37: DSC interpretation.

42

Glass transition temperature (T_g): this is the point at which, on heating, an amorphous polymer changes from being hard, brittle and glass like to being a soft rubber like substance. This point may be identified as a dip on a graph of heat flux versus increasing temperature, this is due to the molecule having a greater degree of freedom and absorbing energy to maintain the same rate of heating as the reference. It can then be concluded that glass transition is an endothermic process.

Melting temperature (T_m): this is the point at which the polymer molecules have gained enough vibrational freedom to break free from the solid binding forces and form a liquid. Due to the increased freedom of these molecules, the DSC graph should take a sudden dip at this temperature to indicate the endothermic nature of the process, which is a first order transition.

In this work a Seiko instruments SII Exstar 6000 DSC 6200 was employed.

3.2.4 Thermal Gravimetric Analysis (DTG/TG)

Thermogravimetric analysis is a technique in which the mass of a substance is monitored as a function of temperature or time as the sample specimen is subjected to a controlled temperature program in a controlled atmosphere. A TGA consists of a sample pan that is supported by a precision balance. That pan resides in a furnace and is heated or cooled during the experiment. The mass of the sample is monitored during the experiment. A sample purge gas controls the sample environment. This gas may be inert or a reactive gas that flows over the sample and exits through an exhaust. Phenomena causing mass changes can be physical(gas adsorption, gas desorption, phase transitions, vaporization, sublimation) or chemical(decomposition, break down reactions, gas reactions, chemisorption).

In this work a Seiko instruments SII Exstar 6000 TG/DTA 6300 was employed.

3.2.5 Atomic Force Microscopy (AFM)

The AFM allows the imaging of the topography of conducting and insulating surfaces.

In the AFM the sample is scanned by a tip, which is mounted to a cantilever spring. While scanning, the force between the tip and the sample is measured by monitoring the deflection of the cantilever. A topographic image of the sample is obtained by plotting the deflection of the cantilever versus its position on the sample. Alternatively, it is possible to plot the height position of the translation stage. This height is

controlled by a feedback loop, which maintains a constant force between tip and sample. Image contrast arises because the force between the tip and sample is a function of both tip–sample separation and the material properties of tip and sample. To date, in most applications image contrast is obtained from the very short range repulsion, which occurs when the electron orbitals of tip and sample overlap (Born repulsion). However, further interactions between tip and sample can be used to investigate properties of the sample, the tip, or the medium in between. These measurements are usually known as "force measurements". In an AFM force measurement the tip attached to a cantilever spring is moved towards the sample in normal direction. Vertical position of the tip and deflection of the cantilever are recorded and converted to force-versus-distance curves, briefly called "force curves".

In this work a NT-MDT Solver Pro was employed. Measurements were performed in contact mode, area 50x50µm, tip CSG10 (constant force 0.01-0.5N/m), scanning frequency 0.8Hz.

3.2.6 Optical Contact Angle (OCA)

Contact angles were in general measured using a commercial instrument (described below). For a selected sample, they were also analyzed by home-made setup and software to compare the results obtained by the two methods.

Fig. 38: OCA set up.

The optical contact angle (OCA) measurement tool provides analytical values by estimation of static and dynamic contact angles and solid surface tension.

For static contact angle measurements, the sessile drop technique is employed, by using a high resolution camera and a software implementing the algorithm. An image of a side view of a drop gently deposed onto the surface sample is acquired and analyzed to get the contact angle ϑ, formed between the liquid/solid interface and the liquid/air interface. Photos of the drops are taken in backlight mode, and their profile is automatically fitted by the software applying the circular fitting method. The operator

has to adjust the baseline (*i.e.* the position of the line representing the base surface) position only.

The dynamic sessile drop analysis is similar to the static version, but it requires the drop to be modified. A common type of dynamic sessile drop study determines the largest contact angle possible without increasing its solid/liquid interfacial area by adding volume dynamically. This maximum angle is called the advancing angle ϑ_A. Volume is then removed to produce the smallest possible angle, named the receding angle ϑ_R. The difference between the advancing and receding angles is the contact angle hysteresis H.

In this work a Dataphysics mod. OCA 15 plus device was employed.

3.2.7 Scanning Electron Microscopy (SEM)

In a typical SEM, an electron beam is thermionically emitted from an electron gun fitted with a tungsten filament cathode. Tungsten is normally used in thermionic electron guns because it has the highest melting point and lowest vapour pressure of all metals, thereby allowing it to be heated for electron emission, and because of its low cost. The electron beam, which typically has an energy ranging from 0.2 keV to 40keV, is focused by one or two condenser lenses to a spot about 0.4 nm to 5 nm in diameter. The beam passes through pairs of scanning coils or pairs of deflector plates in the electron column, typically in the final lens, which deflect the beam in the x and y axes so that it scans in a raster fashion over a rectangular area of the sample surface. SEM can produce very high-resolution images of a sample surface topography and composition, revealing details less than 1 nm in size. Due to the very narrow electron beam, SEM micrographs have a large depth of field yielding a characteristic three-dimensional appearance useful for understanding the surface structure of a sample. When the electron beam hits the sample surface, several kind of electrons are emitted: backscattered electrons are beam electrons that are reflected from the sample by elastic scattering; secondary electrons have low-energy (<50 eV) and are ejected from the k-shell of the specimen atoms by inelastic scattering interactions with beam electrons. Due to their low energy, these electrons originate within a few nanometers from the sample surface. The last type of emitted

signal is Auger electrons in the energy range of 50 eV - 3k eV, due to Auger intra-atomic electron transition.

In this work a Tescan Mira3 LM was employed.

3.2.8 Electrochemical Impedance Spectroscopy (EIS)

EIS measures the dielectric properties of a medium as a function of frequency. It is based on the interaction of an external field with the electric dipole moment of the sample, often expressed by permittivity. It is also an experimental method of characterizing electrochemical systems. This technique measures the impedance of a system over a range of frequencies, and therefore the frequency response of the system, including the energy storage and dissipation properties, is revealed. Often, data obtained by EIS is expressed graphically in a Bode plot or a Nyquist plot. Impedance is the opposition to the flow of alternating current (AC) in a complex system.

In this work a Potentiostatic galvanic Solartron analytical modulab model 2100A was employed.

3.2.9 Glow Discharge Optical Emission Microscopy (GDOES)

Glow Discharge Optical Emission Spectrometry (GDOES) is used to perform chemical analysis and surface profiles on solid conductive materials. A GDOES is made up of a discharge lamp, an optical spectrometer, and a data acquisition and processing system. The sample is put on a copper electrode (so the sample is the cathode, the copper the anode). The discharge is applied between the anode and the cathode, that triggers off a sample surface erosion. Atoms ejected are then excited by an Argon plasma, and finally come back to their fundamental energy level, emitting a characteristic X-photon. Emitted photons, whose energy is characteristic of a chemical element energy level, are then collected by photomultipliers, that allows to quantify elemental composition of a material.

In this work a Spectruma Analytik GmbH, GDA750 HR was employed.

3.2.10 Optical Emission Spectroscopy (OES)

In the OES technique, atoms in a sample are excited by energy that comes from a spark formed between sample and electrode. The energy of the spark causes the electrons in

the sample to emit light which is converted into a spectral pattern. By measuring the intensity of the peaks in this spectrum, OES analyzer can produce qualitative and quantitative metal analysis of the material composition. This technique is utilized to determine elemental composition of the steel as substrate.

In this work a SPECTROLAB metal analyzer/OES/fixed was employed.

3.2.11 Titration

Titration was performed following the specification of ISO 2114:2000(E). Acid groups quantity present in the test portion was measured titrating by potassium hydroxide KOH 0.01M in ethanol solution. A weighted test portion was dissolved in a previously neutralized toluene:ethanol=2:1 (in volume) solution.

Salting reaction was the following:

$$KOH + COOH \rightarrow COO^{-}K^{+} + H_2O$$
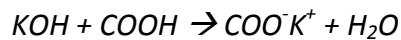
The quantity of KOH solution required to salt carboxyl groups was measured using phenolphthalein pH indicator and a burette. Knowing the volume of KOH (V_{KOH}) used to neutralize all acid groups and the solution molarity (M_{KOH}), it was possible to get the number of mole of KOH:

$$mol_{KOH} = M_{KOH} \, [mol/l] * V_{KOH} \, [l]$$

looking at the above salting reaction, one mole of KOH was required to neutralized one mole of COOH present in the polymer, so:

$$mol_{KOH} = mol_{COOH}$$

3.2.12 Deposition Procedure

The formation of a thin film on a metallic surface is highly influenced by the oxidizing agent, its concentration and treatment time. Optimization of these three parameters was necessary depending on the selected substrate. Hereafter a typical deposition procedure is reported.

3.2.12.1 Substrate pretreatment

Substrate pretreatment was the same for both untreated and sandblasted substrate and it was formed by three steps in a row:

➢ CLEANING: substrate is soaked in DCM[a] for 2 min under a gently agitation

DCM removes all organic residues, like grease, present on the substrate.

➢ ETCHING: substrate is dipped in a solution of sulfuric acid and NoChromix® for 1/3/6 min

This step allows the formation of active sites for the anchorage of polar head groups. The right amount of NoChromix®, as indicated in the leaflet, was added to sulfuric acid to enhance etching strength on the metallic substrate.[32] NoChromix® is the trade name of a metal free oxidizer agent. Changing etching time it was evaluated if this parameter influences the deposition, *e.g.* on the number of available active sites or on their strength.

➢ RINSING: substrate is dipped in de-ionized water for 15 s

Rinsing step with de-ionized water removes NoChromix® residues from the substrate that can hinder a correct deposition of the coating molecules.

3.2.12.2 Coating deposition

This step was differently performed depending on the anchoring group:

1. in the case of SAMs with phosphonic head the substrate was dipped in a 1 mM solution of alkyl phosphonic acid dissolved in THF[b] for 22 h[33] at room temperature (23 °C), then it underwent a post thermal treatment (1 h at 110 °C)[34] or directly rinsed in fresh THF for 15 s.

---

[a] dichloromethane
[b] tetrahydrofuran
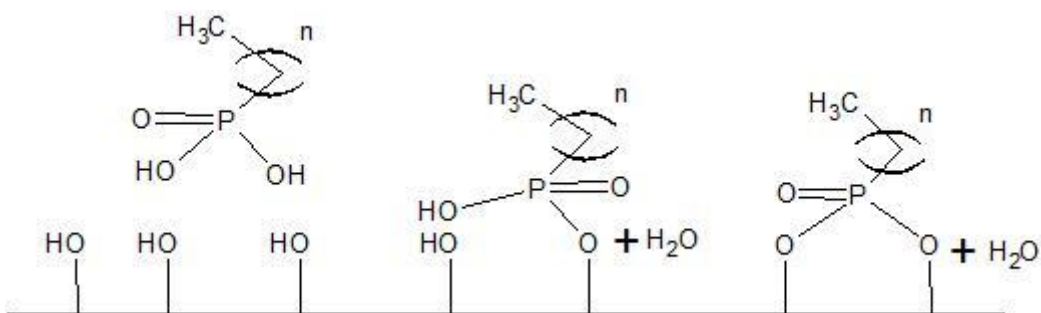
Fig. 39: Alkyl Phosphonic Acid(CnP) anchoring mechanism in bidentate mode.

2. for carboxylic acids and partially esterified polyacrylate with free carboxyl head the substrate was dipped in a warm(50 °C) 1 mM THF solution of the respective acid for 2 h, then stored in an oven (120 °C for 18 h)[35] and eventually rinsed in fresh THF for 15 s.
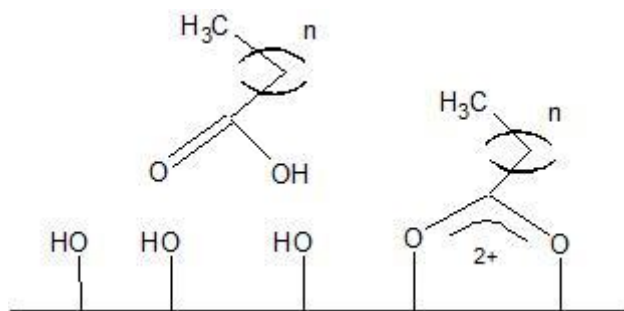
Fig. 40: Carboxylic Acid(CAn) anchoring mechanism for bridge type conformation.
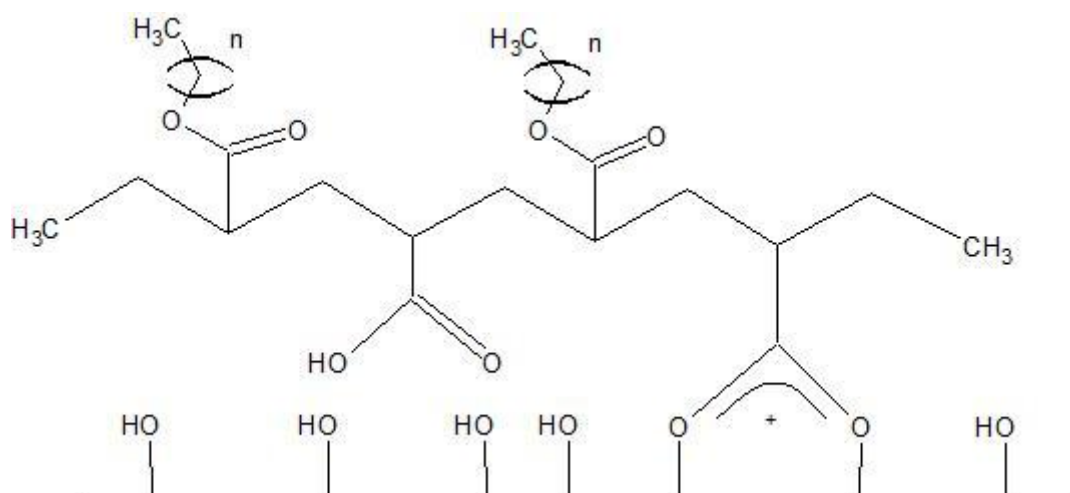
Fig. 41: Partially Esterified Polyacrylate(PAn) anchoring mechanism for bridge type conformation.

4 RESULTS

As widely known in literature, surface wettability is influenced by two main parameters: surface roughness R and surface tension γ.

In this work, the influence of the roughness was surveyed selecting the steel substrates into two groups: one as purchased, the other was sandblasted after purchasing. On the other site surface tension was kept in consideration studying 3 different coatings shown in Fig. 42: phosphonic SAMs (a), carboxylic SAMs (b) and partially esterified polyacrylate (c). Three kind for each coating were analyzed (n = 4, 12, 18).
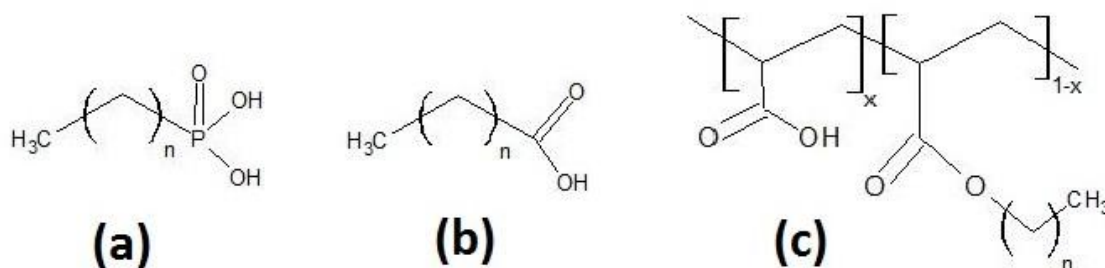
Fig. 42 - Coatings chemical structure.

The purpose was to compare each other and to understand how substrate pretreatment and deposition parameters influence the properties of the coating.

The following table is a list of labels referred to the different samples analyzed in this thesis project:

Tab. 2 - Samples name explanation.

Sample name	Experimental label	Substrate	Pretreatment (etching time)	Coating	Post Thermal Treatment
C4P_1	A.A1.A.A	untreated	1 min	C4P	No
C4P_2	B.A1.A.A	sandblasted	1 min	C4P	No
C4P_3	B.A3.A.A	sandblasted	3 min	C4P	No
C4P_4	B.A6.A.A	sandblasted	6 min	C4P	No
C4P_5	B.A1.A.B	sandblasted	1 min	C4P	1h – 110°C
C4P_6	B.A3.A.B	sandblasted	3 min	C4P	1h – 110°C
C4P_7	B.A6.A.B	sandblasted	6 min	C4P	1h – 110°C
C4P_8	A.A6.A.B	untreated	6 min	C4P	1h – 110°C

C12P_1	A.A1.B.A	untreated	1 min	C12P	No
C12P_2	B.A1.B.A	sandblasted	1 min	C12P	No
C12P_3	B.A3.B.A	sandblasted	3 min	C12P	No
C12P_4	B.A6.B.A	sandblasted	6 min	C12P	No
C12P_5	B.A1.B.B	sandblasted	1 min	C12P	1h – 110°C
C12P_6	B.A3.B.B	sandblasted	3 min	C12P	1h – 110°C
C12P_7	B.A6.B.B	sandblasted	6 min	C12P	1h – 110°C
C12P_8	A.A6.B.B	untreated	6 min	C12P	1h – 110°C
C18P_1	A.A1.C.A	untreated	1 min	C18P	No
C18P_2	A.A3.C.A	untreated	3 min	C18P	No
C18P_3	A.A6.C.A	untreated	6 min	C18P	No
C18P_4	A.A6.C.B	untreated	6 min	C18P	1h – 110°C
C18P_5	B.A1.C.A	sandblasted	1 min	C18P	No
C18P_6	B.A3.C.A	sandblasted	3 min	C18P	No
C18P_7	B.A6.C.A	sandblasted	6 min	C18P	No
C18P_8	B.A1.C.B	sandblasted	1 min	C18P	1h – 110°C
C18P_9	B.A3.C.B	sandblasted	3 min	C18P	1h – 110°C
C18P_10	B.A6.C.B	sandblasted	6 min	C18P	1h – 110°C
PA4	B.A6.D.C	sandblasted	6 min	PA4	18h – 110°C
PA12	B.A6.E.C	sandblasted	6 min	PA12	18h – 110°C
PA18	B.A6.F.C	sandblasted	6 min	PA18	18h – 110°C
PA4_0	A.A6.D.C	untreated	6 min	PA4	18h – 110°C
PA12_0	A.A6.E.C	untreated	6 min	PA12	18h – 110°C
PA18_0	A.A6.F.C	untreated	6 min	PA18	18h – 110°C
CA3	B.A6.G.C	sandblasted	6 min	CA3	18h – 110°C
CA12	B.A6.H.C	sandblasted	6 min	CA12	18h – 110°C
CA18	B.A6.I.C	sandblasted	6 min	CA18	18h – 110°C
CA3_0	A.A6.G.C	untreated	6 min	CA3	18h – 110°C
CA12_0	A.A6.H.C	untreated	6 min	CA12	18h – 110°C
CA18_0	A.A6.I.C	untreated	6 min	CA18	18h – 110°C

C4P, C12Pand C18P refer to coating type represented in Fig. 42(a); PA4, PA12 and PA18 to the type in Fig. 42(c); CA3, CA12 and CA18 to the type in Fig. 42(b).

4.1 AFM

AFM was used to discover the roughness of the surface. Four measurements on each sample were performed in contact mode, area 50x50 μm, tip CSG10 (constant force 0.01-0.5 N/m), scanning frequency 0.8 Hz. In Tab. 3 are reported the mean values of arithmetic roughness R_a, root mean square roughness R_q and the maximum height of the profile R_t.

SAMPLE	R_a (nm)	R_q (nm)	R_t (nm)
Untreated bare substrate	207.2798	284.1233	2893.575
C4P_8	169.4035	227.9190	1904.670
C12P_8	167.7090	213.6065	1803.518
C18P_4	171.4535	223.5523	1956.238
PA4_0	243.7738	317.9568	2609.063
PA12_0	213.1340	280.9650	2355.923
PA18_0	163.0153	217.0340	2209.375
CA3_0	160.8943	213.4368	1969.683
CA12_0	166.4153	212.3443	1869.843
CA18_0	195.0113	249.1940	2277.380
Sandblasted bare substrate	289.7993	366.3210	2807.055
C4P_7	284.2430	363.2153	2577.963
C12P_7	332.6383	430.2235	4495.125
C18P_10	308.4700	395.5643	3164.218
PA4	359.9103	459.8283	3520.095
PA12	361.1693	456.8580	3854.918
PA18	393.9580	496.9973	4410.135
CA4	359.4060	478.4160	4851.310
CA12	371.1920	464.5218	3080.908
CA18	261.7110	345.3908	2563.818

The order of magnitude of surface roughness was in the order of $10^{-7} \, m$ for all the samples. Looking at bare substrate, sandblasting increases both R_a and R_q, but no significant change was seen in R_t. So the untreated substrate was smoother than the sandblasted one (see Fig. 43 and Fig. 44).
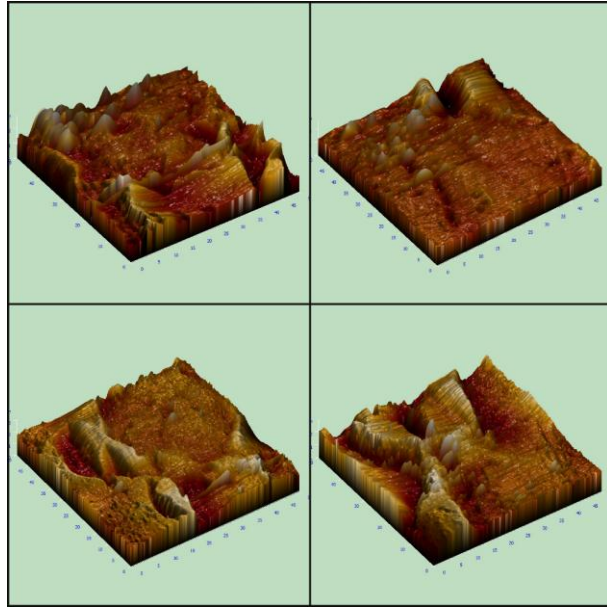
Fig. 43 - 3D AFM images of bare untreated substrate.
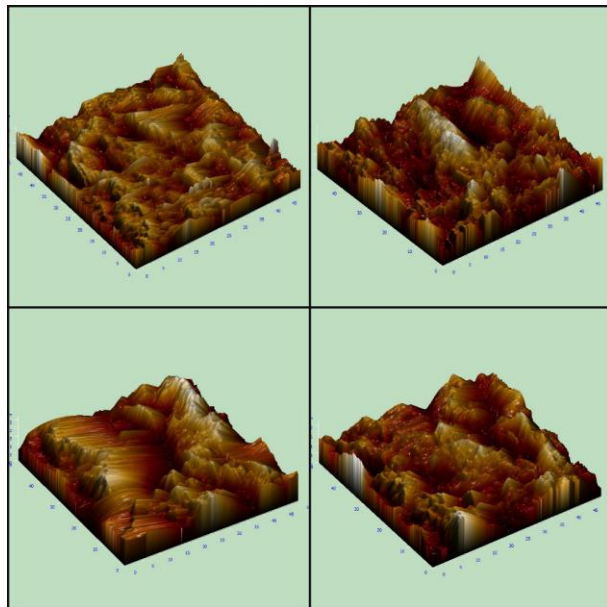
Fig. 44 - 3D AFM images of bare sandblasted substrate.

Analyzing samples on untreated substrate, it can be seen that phosphonic acid coatings had lower roughness parameters compared to bare substrate, as in the cases of carboxylic acids, while for esterified carboxyl polyacrylates these values were quite similar to the original one.

All coatings applied on sandblasted substrate, but CA18, increase the roughness.

Fig. 45 represents 3D scanned area of the sample C12_8, showing a different surface morphology with respect to bare untreated substrate seen in Fig. 43.
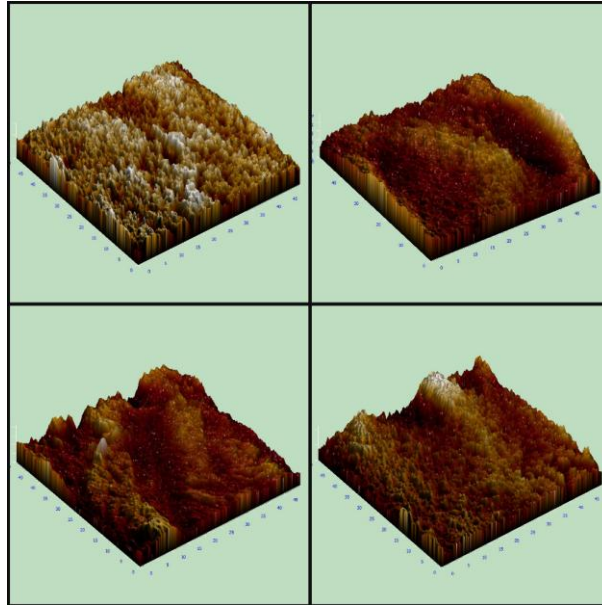
Fig. 45 - 3D AFM images of C12P_8 sample.

Fig. 46, Fig. 47 and Fig. 48 are referred to coated sandblasted substrate: C12P_7, PA12 and CA12 respectively. The surface morphology seems not uniform for all the cases, probably due to the sandblasting pretreatment.
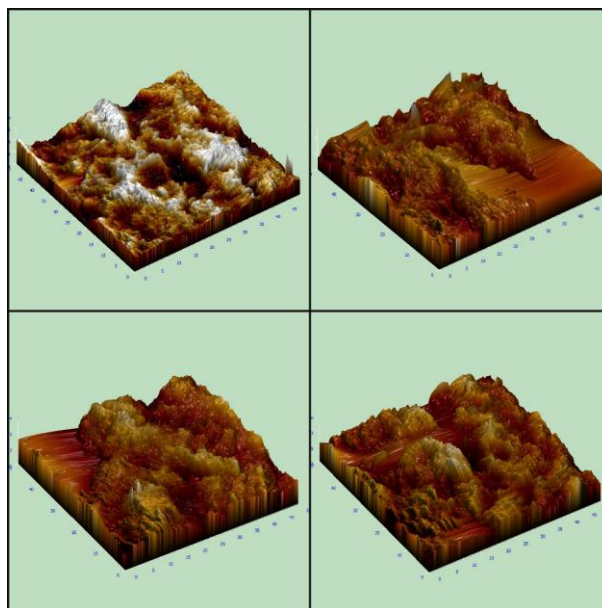
Fig. 46 - 3D AFM images of C12P_7 sample.
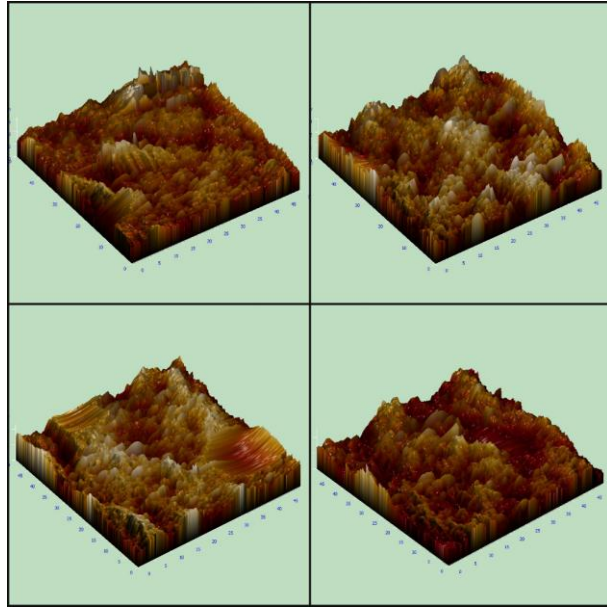
Fig. 47 - 3D AFM images of PA12 sample.
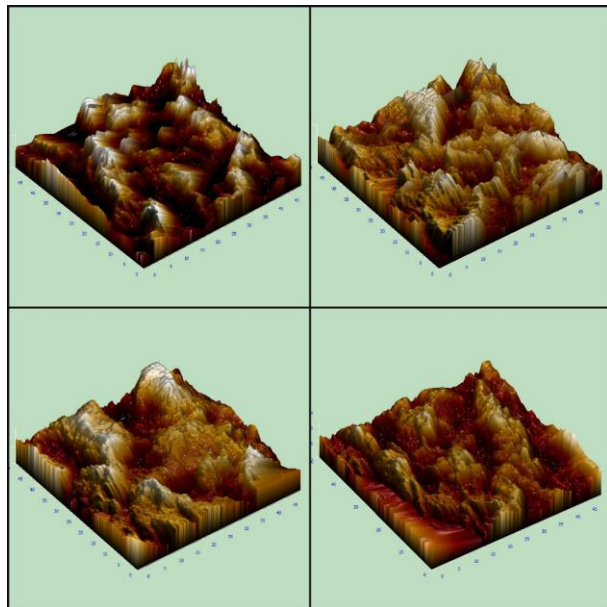
Fig. 48 - 3D AFM images of CA12 sample.

ADHESION FORCE

In contact modes adhesion forces have a significant effect on the cantilever during the probe withdrawal from the sample. These forces result in the deflection of the cantilever before it breaks contact with the surface.[36] The adhesion force can be calculated assuming the force is a linear function of the probe displacement relative to the sample surface along the Z-axis.

By Hooke's law:

$$F = k \times \Delta\, Height$$

where k = 0.25 N/m is the cantilever stiffness.

Tab. 4 reports adhesion force of phosphonic acid and carboxylic acid coatings, showing values in the range 11-31 nN. Looking at phosphonic coatings it can be said that adhesion force on untreated substrate was higher than on sandblasted substrate, but it had to be keep in consideration also standard deviation, so no particular differences between various coatings nor any trend were found. Besides in literature there are no references about coatings adhesion force calculated in this way.

Tab. 4 - Coatings adhesion force.

SAMPLE	Adhesion force (nN) [Std. Dev.]
C4P_8	24.550 [3.446]
C12P_8	28.655 [7.879]
C18P_4	31.665 [11.824]
CA3_0	14.130 [3.871]
CA12_0	12.225 [2.019]
CA18_0	15.225 [2.110]
C4P_7	20.335 [5.676]
C12P_7	16.535 [6.454]
C18P_10	20.040 [10.593]
CA4	20.745 [4.079]
CA12	28.055 [8.512]
CA18	11.325 [6.942]

4.2 Contact Angle

The contact angle analysis allowed to understand the sample wettability: if $\vartheta > 150°$ the coating is superhydrophobic, while for $90° < \vartheta < 150°$ it is considered hydrophobic.

These data were collected by a Dataphysics mod. OCA 15 plus. Typically 10 measurements of static sessile drop were performed on each sample but only average ϑ, maximum ϑ, minimum ϑ and standard deviation (Std. Dev.) are reported below.

First of all it was important to determine the wettability of bare substrate, in order to compare with the coated ones, and establish if an improvement was obtained.

Tab. 5 - Contact angle data of bare substrates.

CONTACT ANGLE	BARE UNTREATED SUBSTRATE	BARE SANDBLASTED SUBSTRATE
ϑ_{avg} (°)	60	57
ϑ_{max} (°)	78	71
ϑ_{min} (°)	39	49
Std. Dev. (°)	10	5

As it can be seen, both untreated and sandblasted substrates are hydrophilic because their contact angles are lower than 90°. But it was important to highlight the role of the sandblasting procedure: it slightly lowered average ϑ but greatly reduced standard deviation, meaning a more homogeneous morphology of the substrate surface was obtained.

4.2.1 Alkyl Phosphonic Acids

4.2.1.1 Results from static sessile drop analysis by OCA

Let's see firstly the study about phosphonic acid: three different alkyl chain lengths were compared to understand if it influences wettability grade.

Both untreated and sandblasted substrate were coated using 1 min of etching time and no post thermal treatment.

Tab. 6 - Sandblasting role on wettability.

COATING	SANDBLASTING	
	UNTREATED SUBSTRATE	SANDBLASTED SUBSTRATE
	ϑ_{avg} (°) [Std. Dev.]	ϑ_{avg} (°) [Std. Dev.]
C4P	88 [20]	139 [2]
C12P	103 [17]	157 [5]
C18P	147 [5]	164 [6]

As it can be seen, the higher the chain length the higher the hydrophobicity.

Sandblasted substrate significantly increased the contact angle ϑ and reduced the standard deviation (as already pointed out looking at Tab. 5), meaning a more homogeneous coating was obtained.

These data suggest to choose sandblasted substrate to obtain better results of hydrophobic properties.

Setting sandblasted substrate as default substrate, etching time was surveyed in order to understand if longer surface activation time gets some improvements. In literature[32] standard etching time is 1 min, it was however decided to investigate three different etching time: 1 min, 3 min and 6 min. Here below are reported the results of contact angles in the cases of phosphonic SAMs coatings.

Tab. 7 - Etching time role on wettability.

COATING	ETCHING TIME		
	1 min	3 min	6 min
	ϑ_{avg} (°) [Std. Dev.]	ϑ_{avg} (°) [Std. Dev.]	ϑ_{avg} (°) [Std. Dev.]
C4P	139 [2]	136 [5]	145 [4]
C12P	157 [5]	167 [2]	170 [4]
C18P	164 [6]	137 [18]	100 [11]

SAM with C18 alkyl chain showed an opposite trend: lower contact angles were found increasing etching time, and also the standard deviations for C18P coating are higher than in the other cases.

As suggested in literature[34] after the deposition step, the sample can be thermally treated in an oven at 110 °C for 1 h to stabilize the film self-organized on the surface.

As in the previous survey, sandblasted substrate was set as default substrate. For a complete discussion, in Tab. 8 were reported the results of contact angles in the cases of phosphonic SAMs coatings without setting a specific etching time but with the post thermal treatment.

Tab. 8 - Post thermal treatment role on wettability for sandblasted substrates.

COATING	POST THERMAL TREATMENT		
	Etching time		
	1 min	3 min	6 min
	ϑ_{avg} (°) [Std. Dev.]	ϑ_{avg} (°) [Std. Dev.]	ϑ_{avg} (°) [Std. Dev.]
C4P	152 [3]	137 [7]	145 [1]
C12P	164 [9]	171 [7]	175 [4]
C18P	176 [5]	174 [8]	172 [7]

The data put in evidence the thermally driven stabilization of phosphonic acid films self-organized on the surface. Comparing with Tab. 7 a significant increase in contact angles was present for C18P coating, with lower standard deviation values, while the decreasing trend with longer etching time seems to be confirmed. In the cases of C4P and C12P coating an improvement was obtained too, but not so important as for C18P.

DYNAMIC HYSTERESIS CONTACT ANGLE

Contact angles provide a measure of the surface repellency,[37] whereas hysteresis provides an indication of drop mobility.[38] For the best case of each alkyl phosphonic acid an additional analysis was done: the dynamic hysteresis contact angle. This analysis was performed using a motor-driven syringe to pump liquid steadily into the sessile drop at moderate rate of 1 µl/s starting from a water drop with volume 3 µl.
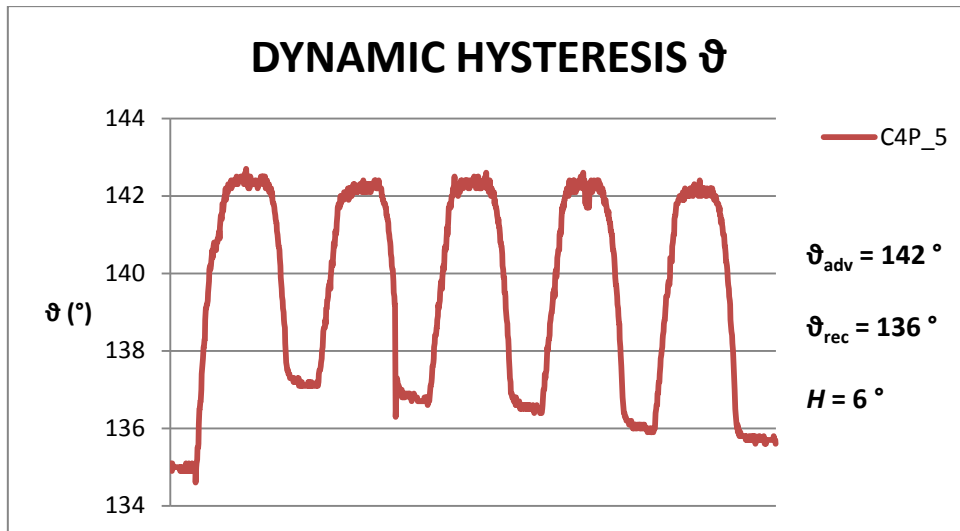
Fig. 49 - C4P_5 dynamic hysteresis contact angle.

In the Fig. 49 the first 5 cycles of dynamic contact angles for the sample C4P_5 are reported. Advancing contact angle $\vartheta_A = 142\,°$ was nearly constant, while ϑ_R shows a decreasing trend increasing the number of cycles, so enlarging the hysteresis H. It is plausible that liquid sorption and/or retention caused a decrease of both ϑ_A and ϑ_R.[2] In the static sessile drop analysis of this sample, the contact angle value was $\vartheta = 152\,°$, higher than ϑ_A.
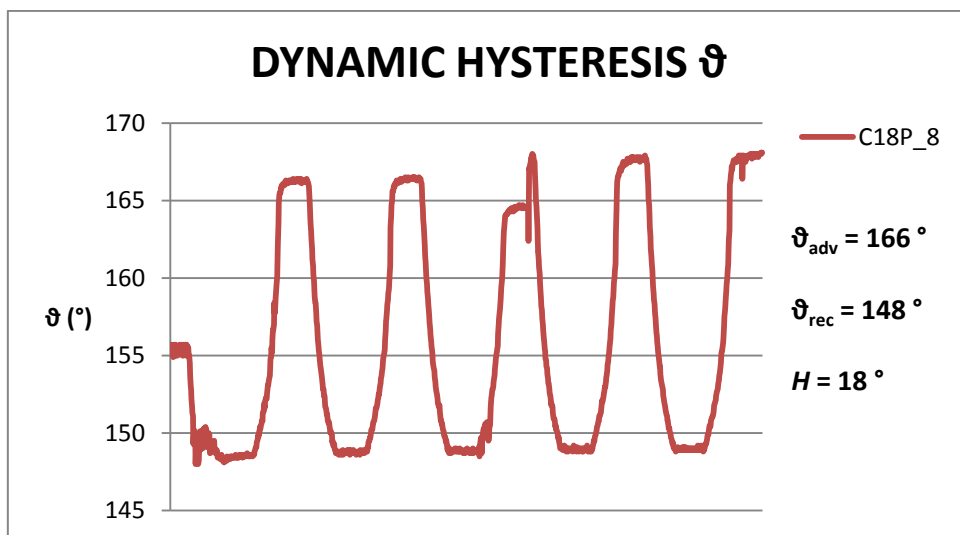
Fig. 50 - C18P_8 dynamic hysteresis contact angle.

Here above is presented the last analysis, for the sample C18P_8: both $\vartheta_A = 166\,°$ and $\vartheta_A = 148\,°$ remained constant after 5 cycles, but it differs from the others cases for the large value of hysteresis $H = 18°$. In the static sessile drop analysis of this sample, the contact angle value was $\vartheta = 176\,°$, higher than ϑ_A.

DYNAMIC HYSTERESIS ϑ
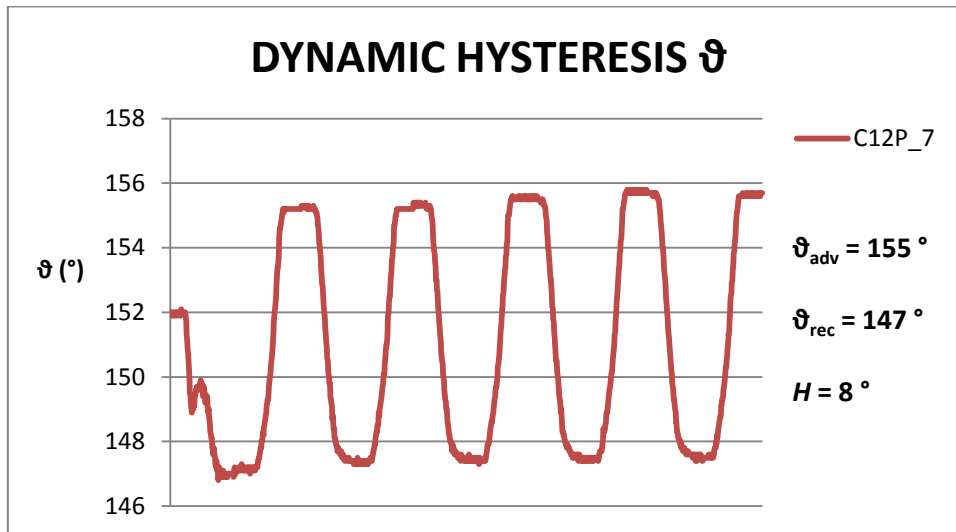
Fig. 51 - C12P_7 dynamic hysteresis contact angle.

Fig. 51 shows dynamic contact angle analysis for the sample C12P_7. Contrary to the previous sample, in this case $\vartheta_A = 155\,°$ and $\vartheta_R = 147\,°$ is kept constant after 5 cycles, with an hysteresis contact angle of $H = 8°$. In the static sessile drop analysis of this sample, the contact angle value was $\vartheta = 175\,°$, higher than ϑ_A.

4.2.1.2 Results from advanced software analysis

The contact angle of sample C12P_7 was also measured using the setup and software developed by prof. M. Guilizzoni and prof. G. Sotgia at the Department of Energy, Politecnico di Milano. This second setup also uses a photograph of the side view of the drop (acquired by a single lens reflex camera with a macro lens) as the only input for the procedure. The drop contour is extracted from the picture using the Sobel edge detection operator, after some pre-processing to increase the filter performance (particularly to reduce the disturbances due to the noise present in real images). The experimental drop profile is then fitted by the theoretical drop profile predicted by the axisymmetric Laplace-Young equation.[39] Such profile is calculated by numerical integration (by centered-form finite differences) of the equation in dimensionless arc-length form. The baseline, *i.e.* the contour of the base surface, is then extracted too. For superhydrophobic surfaces the latter step may require manual correction due to the sensitivity of the results to errors in its identification (see the following). Contact

angle can be then easily determined at the intersection between the calculated profile and baseline. Further details about the procedure can be found in ref. <mark>[REF. 2 E 3].</mark>

Looking at Fig. 52, shots were taken in backlight mode (C) or multidirectional light mode (A,B): in the first case the drop contour can be extracted more easily, but precise identification of the baseline is quite difficult; on the contrary in the second mode the baseline can be established with a higher accuracy. In Fig. 52 A) and B) the same drop is analyzed setting the baseline at different levels: in A) the baseline is correct returning a contact angle of 159.2°, while in B) the baseline is too low giving, incorrectly, a higher value of contact angle (165.3°), similar to the one obtained in C): 166.3°.

More drops were gently deposed on the sample, showing a good repeatability with average contact angle 159° and standard deviation 1°.
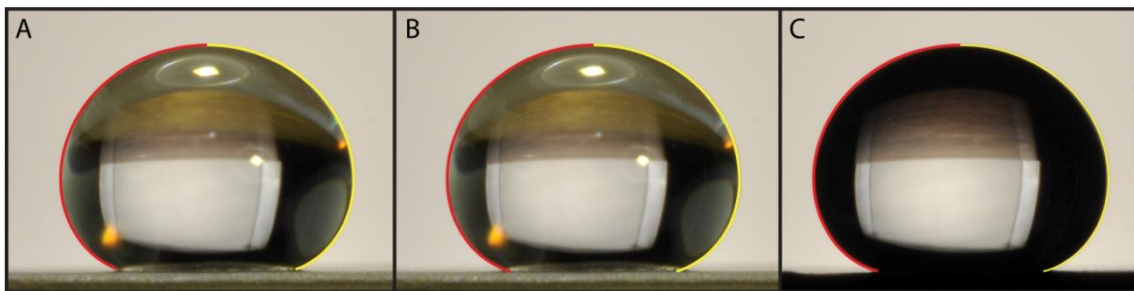
Fig. 52 - Optical image of the drop in backlight mode (C) and in multidirectional mode (A,B). Red line represents left contour of the drop profile, while the right one is highlighted in yellow. In the image contours were enlarged to 3 pixels to increase their visibility.

Deposing many drops on the same point, a degradation of the coating wettability was also observed (Fig. 53). For a correct evaluation of the latter, a standard test procedure should therefore be established. Fig. 53 evidences very well how the two depicted drops have different shapes, one of which also shows a quite peculiar shape (with a sort of cavity) because the drop lays on a deteriorated area with inhomogeneous wettability grade.

Since the fitting model is different from the one used for all the other samples investigated during the thesis work (Laplace-Young fitting here, circular fitting for the others), for a more in-depth comparison it was applied also to a photo taken and analyzed at OCA (which gave contact angle 175°), finding a much lower contact angle (166°).

Apart from the different fitting, which may already have a large influence for "big" drops,[40] the analysis of the possible causes of this discrepancy evidenced first of all that in the investigated picture the baseline has different height levels between left and right drop profile (Fig. 54). The difference, quantifiable in 5 pixel, is probably due to the not perfect planarity of the sample, the camera or the sample holder.
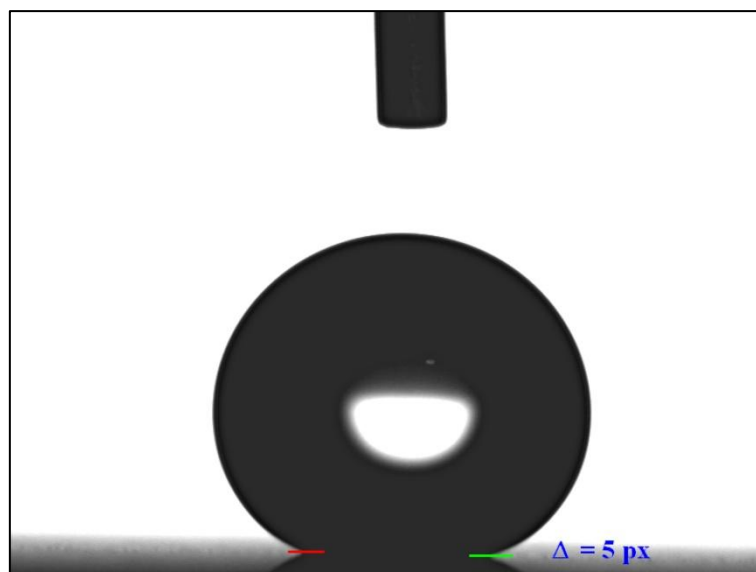
Fig. 54 - Difference of baseline height between left (red) and right (green) profile of the drop. In the image baseline levels were enlarged to 3 pixels to increase their visibility.

Moving the baseline and fitting the same drop, it has been demonstrated that for superhydrophobic states, where the drop profile becomes very "flat" near the baseline, a change of 5 pixel in height can produce up to 15° difference in the estimated contact angle. This confirms previous literature results.[40]

It can be therefore concluded that the uncertainty of this kind of measurements on superhydrophobic surfaces can be a problem for the use of contact angle information as a reliable tool to rank the surfaces.

An improvement of the sessile drop technique, particularly in the set up and baseline identification, seems therefore to be necessary to standardize measurements.

4.2.2 Alkyl Carboxylic Acids

As in the case of partially esterified polyacrylate, only sandblasted substrates 6 min etched are analyzed. The anchoring groups were again carboxyl groups, so the post thermal treatment was always present. In Tab. 9 the contact angles are reported.

Tab. 9 - Alkyl carboxylic acid coatings contact angle.

SAMPLE	ϑ_{avg} (°) [Std. Dev.]
CA3	<10 [-]
CA12	37 [6]
CA18	67 [54]

Samples exhibit hydrophilic behavior. In the case of CA3 was extremely difficult to analyze drop profile since it splashed and stuck on the surface instantaneously. Also CA12 showed bad results in terms of wettability: it was less hydrophilic than CA3 but it worsen the contact angle data with respect to the bare substrate. CA18 had higher value of contact angle, but standard deviation was large, meaning an inhomogeneous coating was obtained, showing both hydrophilic ($\vartheta = 21$ °) and hydrophobic ($\vartheta = 147$ °) area on the same surface.

4.2.3 Partially Esterified Polyacrylates

Completed the study on alkyl phosphonic acid, it was decided to survey the others type of coatings fixing pretreatment parameters: only sandblasted substrate 6 min etched. In these cases the anchoring group was again like for alkyl carboxylic acid a carboxyl group, so the post thermal treatment was always required as suggested in literature.[35] In Tab. 10 the contact angles were reported.

Tab. 10 - Partially esterified polyacrylic coatings contact angle.

SAMPLE	ϑ_{avg} (°) [Std. Dev.]	Esterification grade
PA4	93 [9]	91%
PA12	158 [17]	75%
PA18	64 [8]	44%

The goal of superhydrophobicity was reached only in the case of PA12 coating. PA4 film was homogeneous but showed just slightly hydrophobic behavior. PA18 changes surface wettability only few degrees with respect to bare surface (Tab. 5), probably the molecule did not anchor correctly on the substrate or the obtained product was not the expected one.

4.3 Surface Tension

As widely known, low wettability is correlated to low surface tension. A high solid surface tension corresponds to high wettability (hydrophilic or low hydrophobic behavior). Besides the study of surface roughness, surface tension of the coated substrate was surveyed using Owens-Wendt geometric mean approach. Surface

tension was divided into two components: dispersive and polar.[41,42] The resulting equation when combined with Young's equation is:

$$\gamma_l(1 + \cos\vartheta) = 2[(\gamma_l^p \gamma_s^p)^{1/2} + (\gamma_l^d \gamma_s^d)^{1/2}]$$

where ϑ is the contact angle, γ_l is the liquid surface tension while γ_s^p and γ_s^d are the polar and dispersive components of solid tension, respectively. The total surface tension is merely the sum of the two components:

$$\gamma_s = \gamma_s^p + \gamma_s^d$$

To obtain γ_s^p and γ_s^d the contact angle of at least two liquids with known surface tension components(γ_l^p, γ_l^d and γ_l) on the solid must be determined.[43]

The two employed liquids were water ($\gamma_w = 72.8\ mN/m$; $\gamma_w^p = 50.7\ mN/m$; $\gamma_w^d = 22.1\ mN/m$) and formamide ($\gamma_f = 58.2\ mN/m$; $\gamma_f^p = 22.2\ mN/m$; $\gamma_f^d = 36.0\ mN/m$).

In the Tab. 11 were reported the values of surface tension of the coatings.

Tab. 11 - Coatings surface tensions.

SAMPLE	WATER	FORMAMIDE	COATING		
	ϑ_w	ϑ_f	γ_s^d	γ_s^p	γ_s
	(°)	(°)	(mN/m)	(mN/m)	(mN/m)
C12P_2	157	155	0.079	0.049	0.128
C12P_3	167	153	0.782	0.205	0.987
C12P_4	170	160	0.231	0.057	0.288
C12P_5	164	158	0.168	0.005	0.173
C12P_6	171	158	0.398	0.125	0.523
C12P_7	175	153	1.136	0.468	1.604
C4P_5	152	111	30.103	9.145	39.248
C4P_6	137	129	2.232	0.150	2.382
C4P_7	145	140	0.720	0.133	0.853
C4P_4	145	123	9.478	1.228	10.706
C18P_1	147	135	2.576	0.055	2.631
C18P_2	114	142	7.900	23.897	31.797
C18P_3	104	138	13.934	40.194	54.128
C18P_4	91	112	3.581	39.340	42.921
C18P_5	164	148	1.458	0.359	1.817

C18P_6	137	153	1.304	4.525	**5.829**
C18P_7	100	155	35.347	66.417	**101.764**
C18P_8	176	159	0.421	0.173	**0.594**
C18P_9	174	156	0.681	0.267	**0.948**
C18P_10	172	156	0.624	0.222	**0.846**
PA4	93	81	14.041	5.620	**19.661**
PA12	158	157	0.037	0.060	**0.097**
PA18	64	27	49.770	7.265	**57.035**
CA4	10	10	11.862	61.978	**73.840**
CA12	37	10	24.962	34.765	**59.727**
CA18	67	69	4.357	32.849	**37.206**

The worst results were obtained in the cases of carboxylic acid coating and the sample PA18, showing high value of surface tension. Lowers surface tension values were found for coatings which showed high contact angle for both the liquids and the gap between them was close. The coating with lower surface tension was the PA12, having similar contact angle for water and formamide both higher than 150°.

4.4 GDOES

The GDOES analysis shows layer-by-layer chemical composition of the film coating enabling to understand film thickness looking at the concentration of each element.

The analyzed samples were chosen with the same alkyl chain length C12, in order to compare three different types of coating: phosphonic SAM (C12P_7), carboxylic SAM (CA12) and polyacrylate (PA12).

The spectra were reported here plotting only the significant elements.
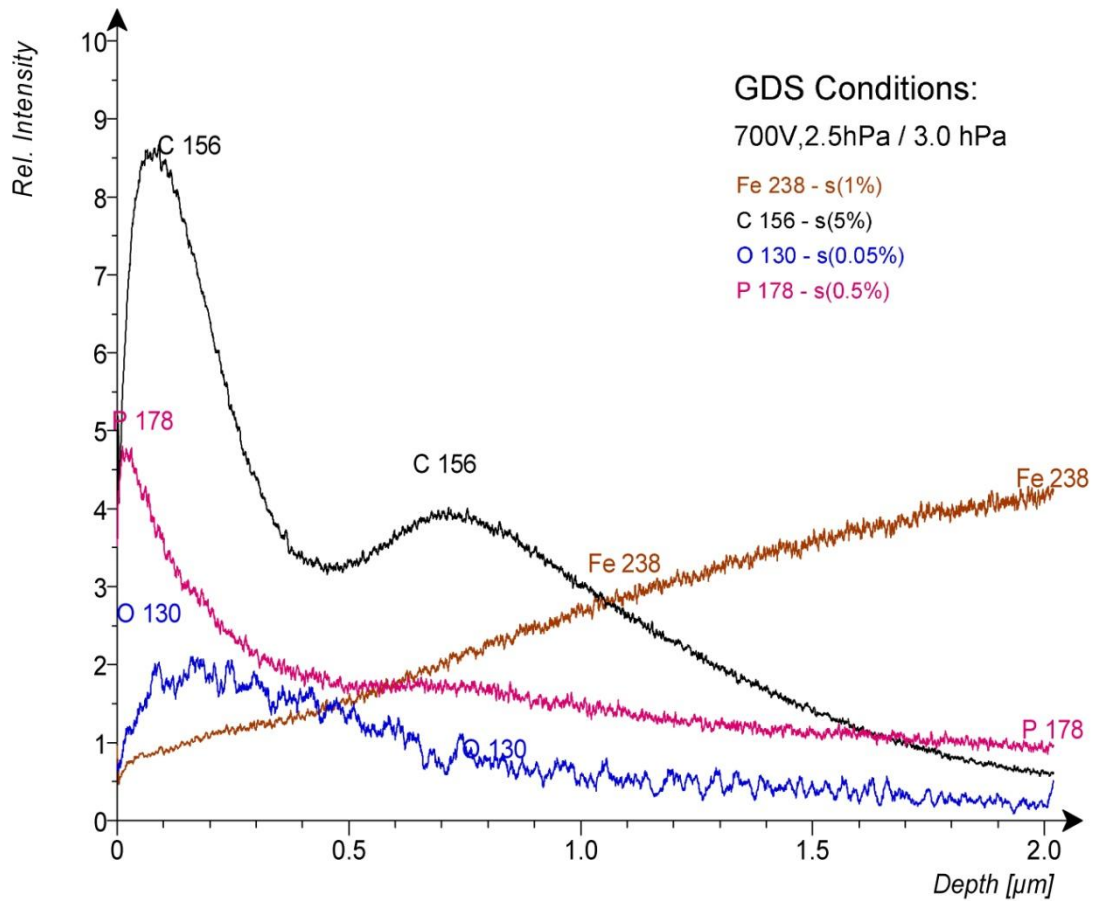
Fig. 55 - C12P_7 GDOES analysis.

The presence of phosphorus signal confirmed that film deposition successfully occurred. The main information regards coating thickness: it can be estimated in 1.5 μm because of the saturation trend of iron signal Fe 238 and the simultaneously disappearance of the other elements. This was not in accordance with the theory, since it should be found a nanometer monolayer coating due to C12P molecules size.
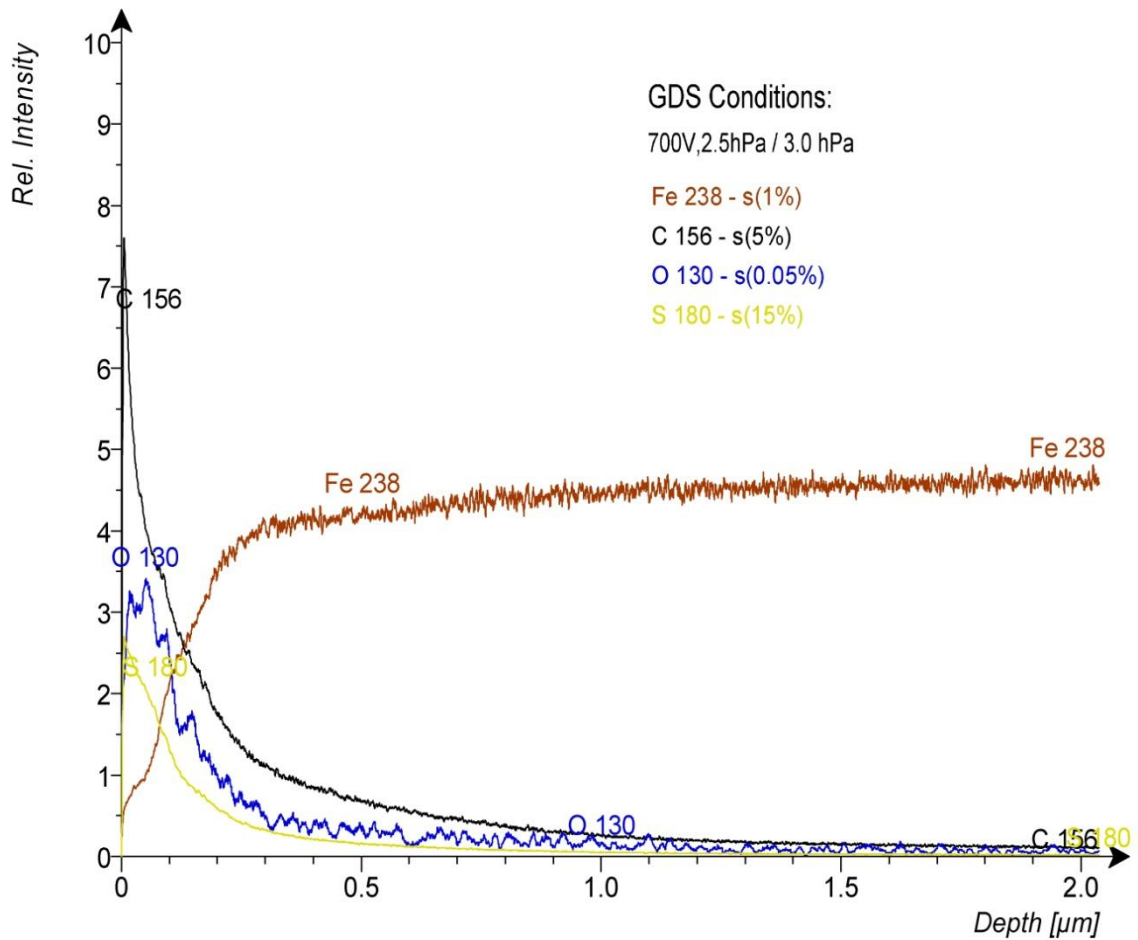
Fig. 56 - CA12 GDOES analysis.

Fig. 56 shows a coating thickness of 0.3 μm. Since coating molecules were constituted only by C, O and H elements (already present in the bulk composition), it was not easy to identify film thickness. Here was reported also sulfur signal S 180 because its concentration was not negligible: probably something had gone wrong during deposition procedure, as confirmed comparing with contact angle analysis.
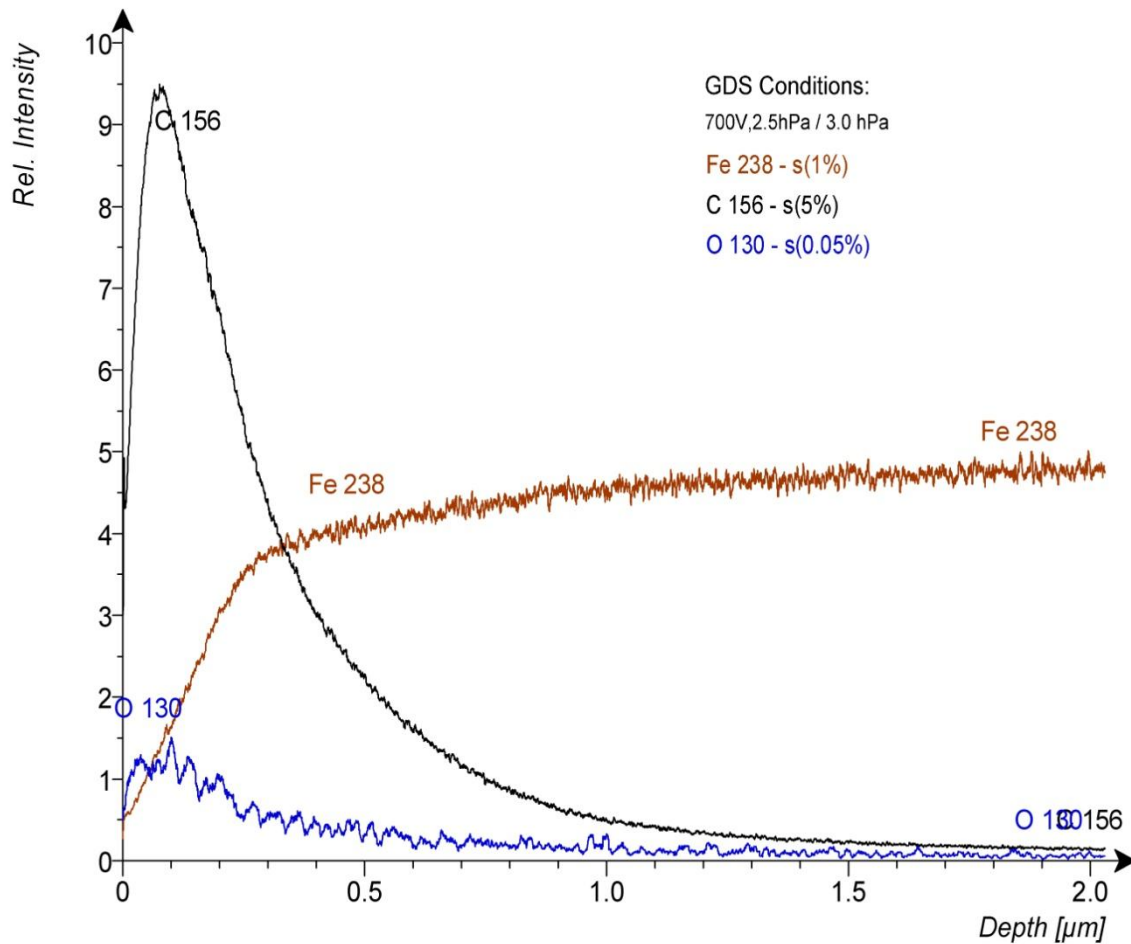
Fig. 57 - PA12 GDOES analysis.

As in the case of CA12 GDOES analysis, there was no a reference element signal to doubtless identify coating thickness, but again relying on Fe 238 signal it can be said that 0.3 µm coating thickness was obtained. Correctly C 156 signal had a very important intensity at low depths due to alkyl chain and also polymer backbone.

In order to have a good comparison between these spectra, here below overlay spectra of single elements were presented.
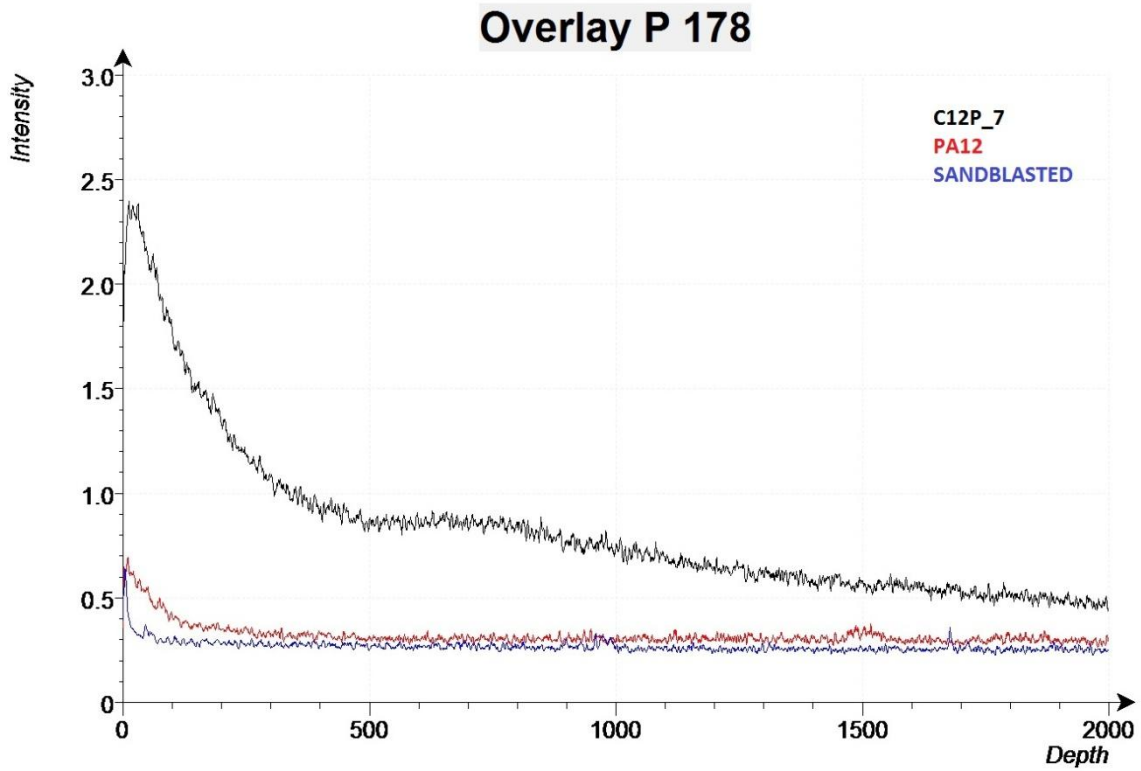
Fig. 58 - Overlay P 178 GDOES spectra.

P 178 signals of C12P_7 and PA12 samples were compared to the uncoated sandblasted substrate. This comparison proved that in C12P_7 sample a phosphonic coating was applied on the substrate, while in the case of PA12 there was no additional phosphorus content.
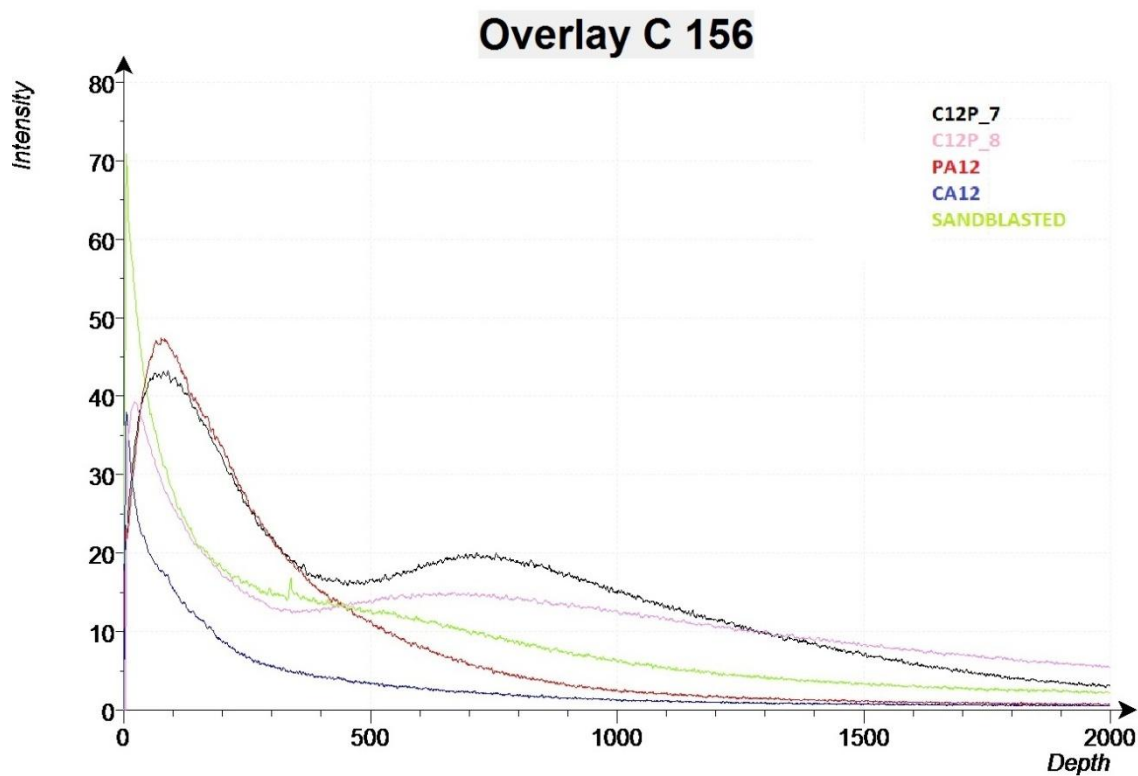
Fig. 59 - Overlay C 156 GDOES spectra.

C12P_7 and C12P_8 showed both a second peak around 700-800 μm depth. CA12 did not exhibit any peak but its trend followed the bare sandblasted substrate one, meaning that probably the anchoring of the carboxylic SAMs failed. PA12 had a low depth peak confirming a film had been deposited.
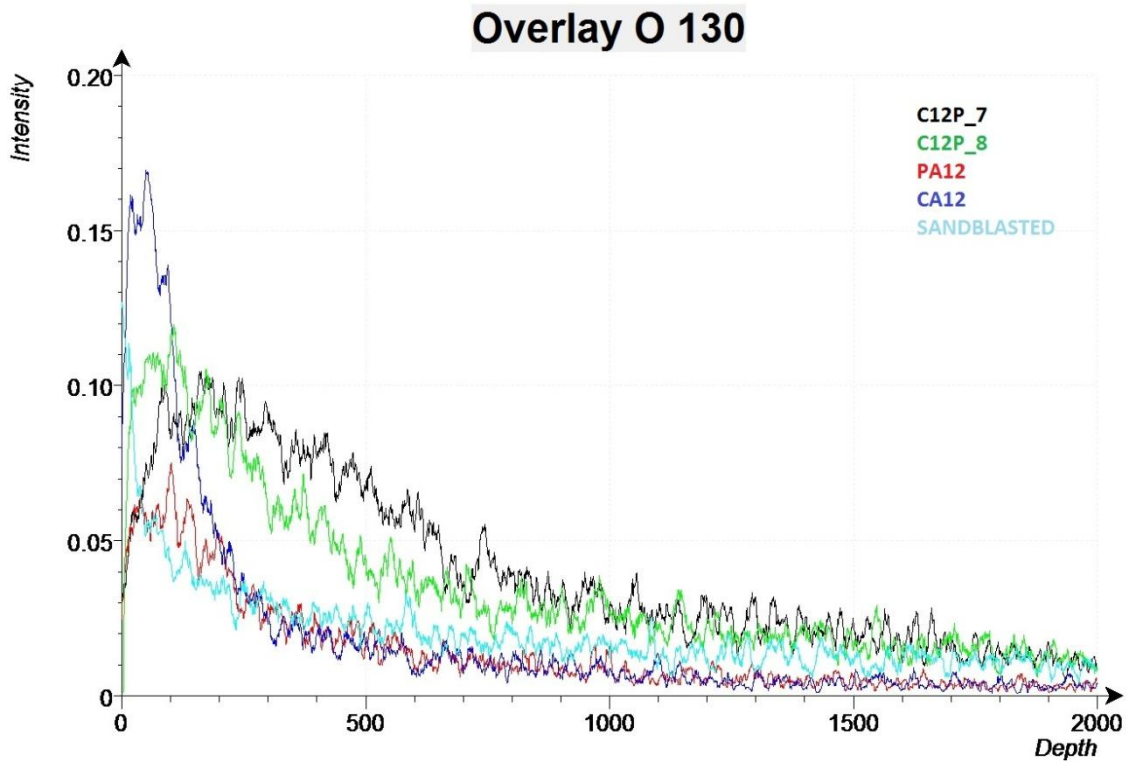
Fig. 60 - Overlay O 130 GDOES spectra.

This spectrum showed the overlay of O 130 signals, which had large noise due to their low intensities. Because of this, it was useless in order to compare the samples.

4.5 SEM

SEM images were obtained analyzing Auger electrons. Only C12P_7 and PA12 samples were analyzed, while bare substrate was surveyed after etching step besides just after sandblasting.
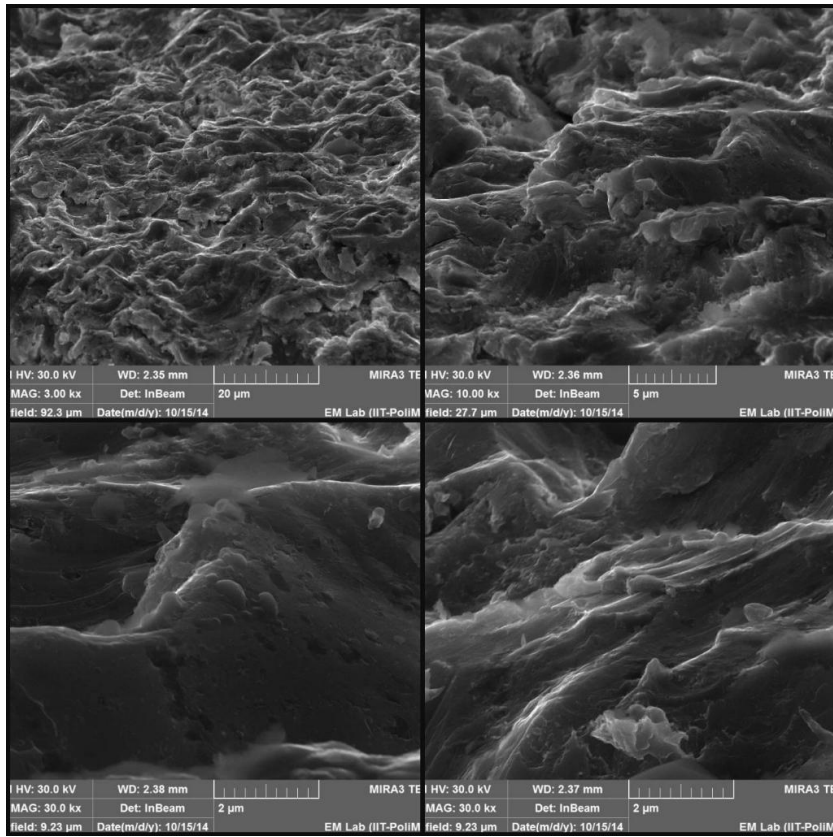
Fig. 61 - SEM images of bare sandblasted substrate with different magnification.
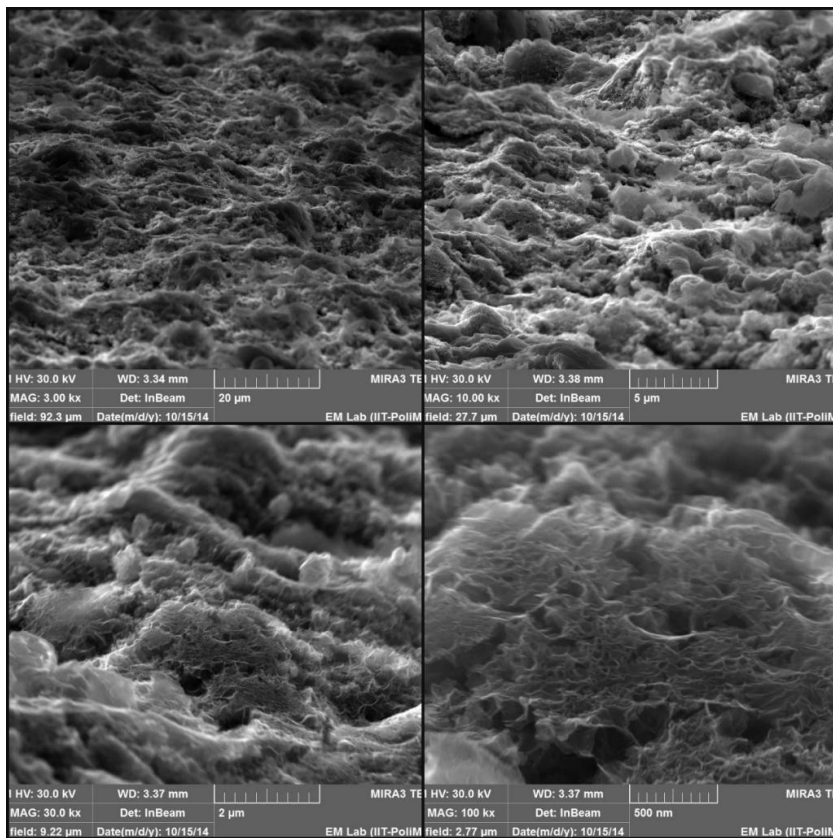
Fig. 62 - SEM images of bare sandblasted substrate 6 min etched with different magnification.
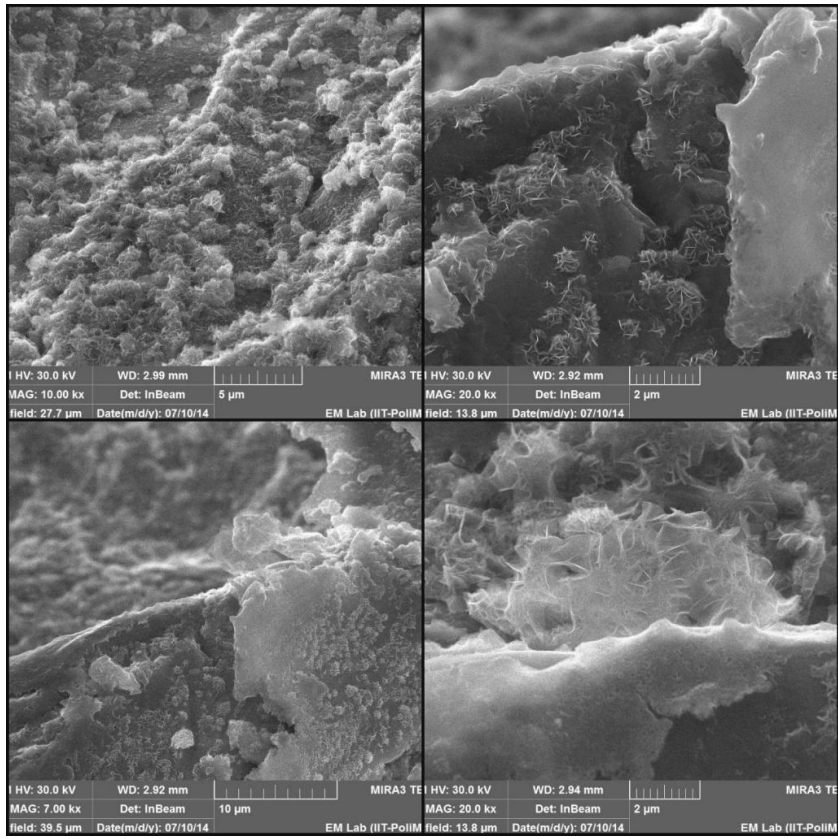
Fig. 63 - SEM images of C12P_7 sample with different magnification.
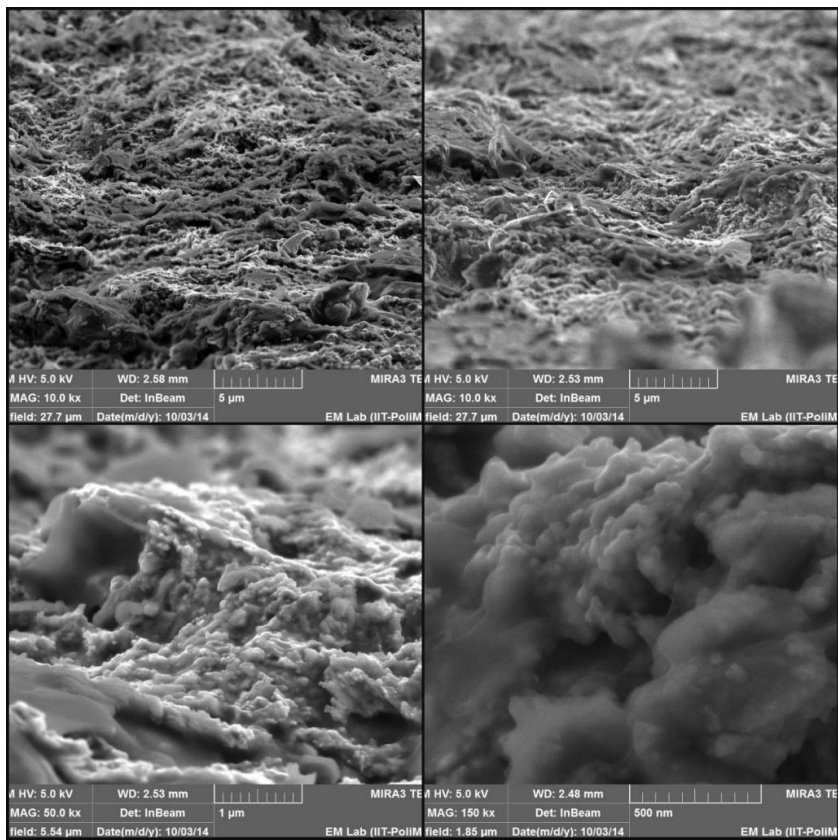
Fig. 64 - SEM images of PA12 sample with different magnification.
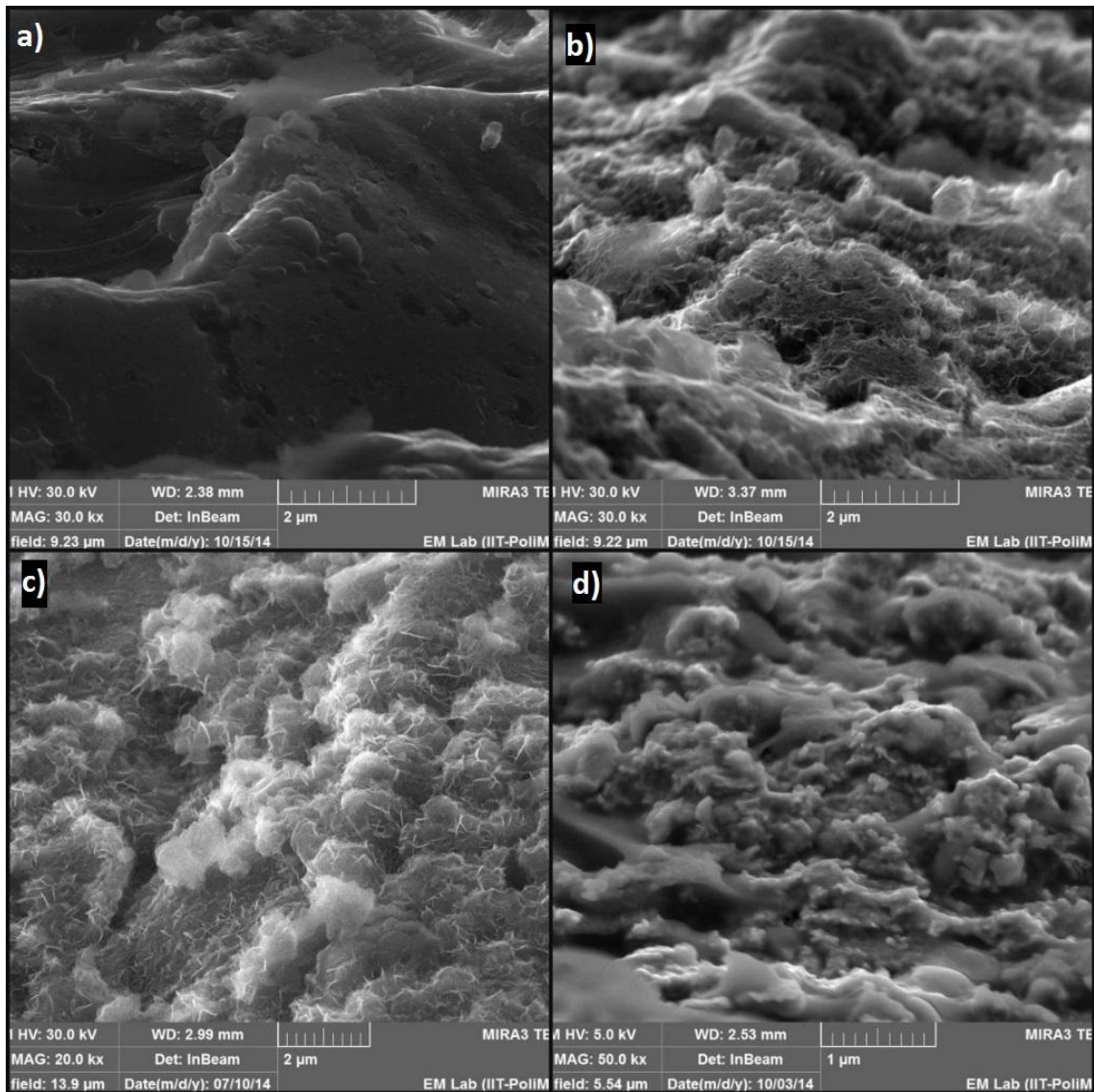
Fig. 65 - SEM images of a) bare sandlasted substrate, b) 6 min etched substrate, c) C12P_7 sample and d) PA12 sample.

4.6 BOUNCING

The characterization of superhydrophobic surfaces was usually restricted to equilibrium contact angle measurements. However, it has been recently reported that the value of the measured contact angle strongly depends on the way the droplet was deposited on the surface. Moreover, the drops do not only reduce their contact angle, but also increase their contact angle hysteresis, the contact line appears to be strongly pinned on the substrate, any self-cleaning properties are thus definitely lost.[44]

Bouncing experiments were performed in order to understand the behavior of the coating under a drop impact, but no further deepened studies were done. A water

drop with volume 5µl exits from a syringe needle from 20 mm height and impacts the surface. A rapid camera captures drop impacts on the surface that occurs in less than 1 s. Drop rebounds have been observed only on highly hydrophobic surfaces, while on the others samples drops splash and stick on the surface.

Tab. 12 - Drop rebounds.

SAMPLE	ϑ_{avg} (°)	DROP REBOUNDS
C4P_7	145	2
C12P_5	164	7
C12P_7	175	13
C18P_8	176	8
PA12	158	11

Fig. 66 shows the image sequences representing time evolution of water drop rebound on C12P_7.
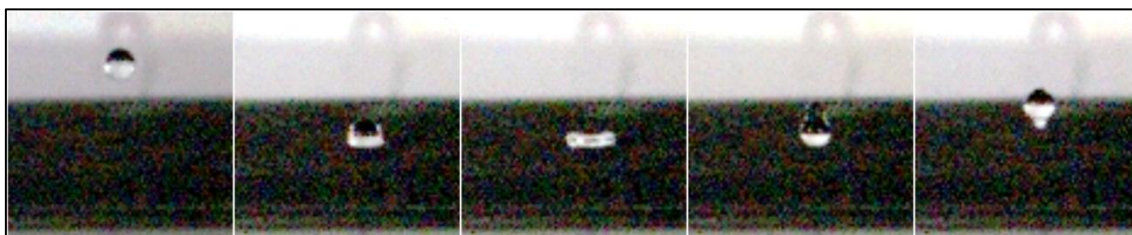
Fig. 66 - Drop impacting on superhydrophobic surface of C12P_7 sample.

4.7 EIS

EIS measurements were carried out with a conventional three-electrode cell at room temperature (25 °C). The electrolyte was 1 M H_2SO_4 solution. A platinum (Pt) electrode and a silver/silver chloride (Ag/AgCl) electrode were used as counter electrode and reference electrode, respectively. The working electrode was the sample with an exposed area of 0.237 cm^2. Electrochemical measurements were performed after 45 min of immersion time in the electrolyte. Impedance spectra were obtained in the frequency range of 10 kHz – 10 mHz with perturbation amplitude of 10 mV. The charge transfer resistance corresponds to the corrosion reaction at metal substrate/solution interface, whose value was a measure of electron transfer across the surface and was

proportional to corrosion rate.[45] In Nyquist plot, the diameter of the high frequency capacitive loop can be considered as the charge transfer resistance. The smaller the charge transfer resistance, the faster the corrosion rate.[46] The presence of a semicircle in the Nyquist plot indicates that the corrosion was under charge transfer control.
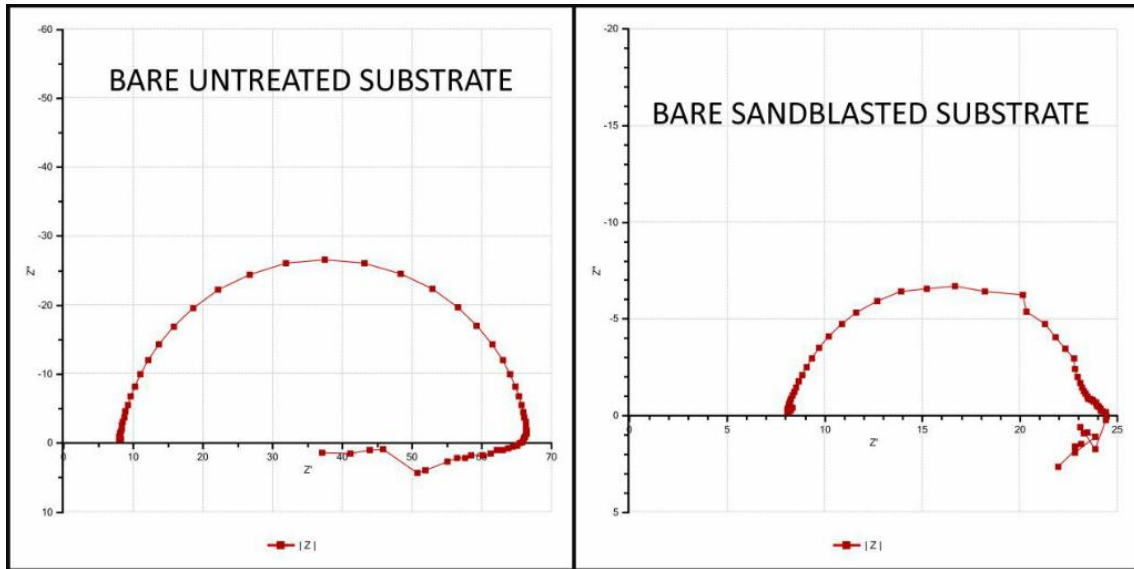
Fig. 67 - Nyquist plot of bare substrates.

Comparing EIS spectra of untreated and sandblasted bare substrate in Fig. 67, it can be said that sandblasting process decreases the protection against corrosion but in both cases corrosion was under charge transfer control.
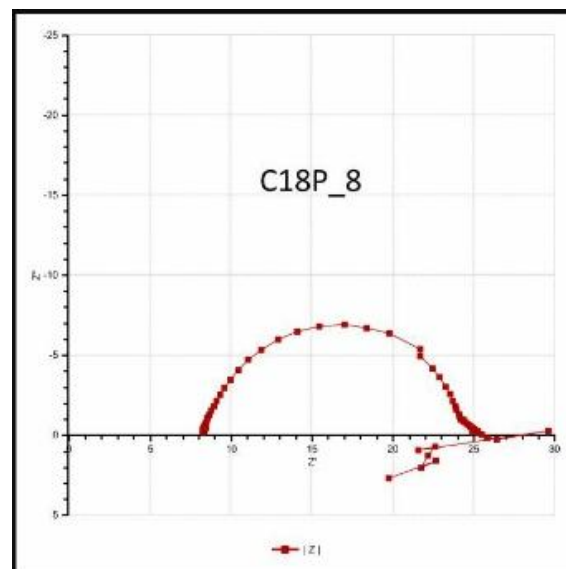
Fig. 68 - Nyquist plot of C18P_8 sample.

Fig. 68 shows EIS spectrum of octadecyl phosphonic acid coated sample. Only in the case of C18P_8 a typical trend was recorded, meaning the sample was under charge transfer control. Comparing with the behavior of bare sandblasted substrate (Fig. 67) it didn't show any improvement in corrosion protection. C4P_7 and C12P_7 spectra(not reported here) were very atypical: impedance values scatter without any order, with change in the order of 10^8. This can be interpreted as the film coating on the substrate was inhomogeneous, showing only in some moments a corrosion protection.
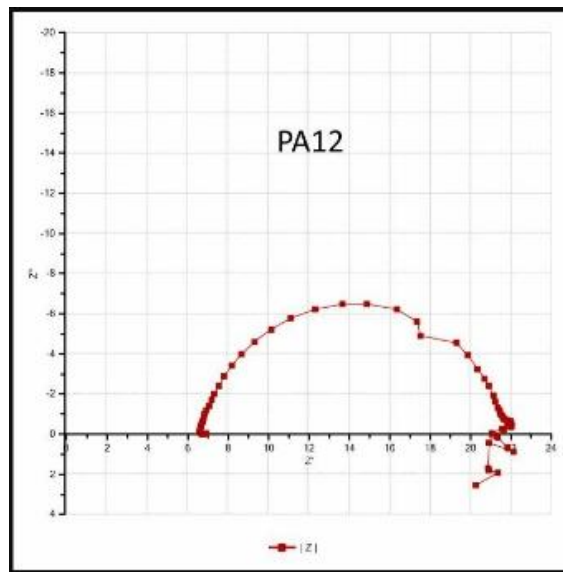
Fig. 69 - Nyquist plot of PA12 sample.

As in the case of alkyl phosphonic acid coatings, also for esterified polyacrylate some problems were found. Only PA12 was under charge transfer control (see Fig. 69), whose impedance was comparable with the bare substrate one. So the coating can produce no improvement in corrosion protection. For PA4 and PA18 an inhomogeneous coating can be supposed.
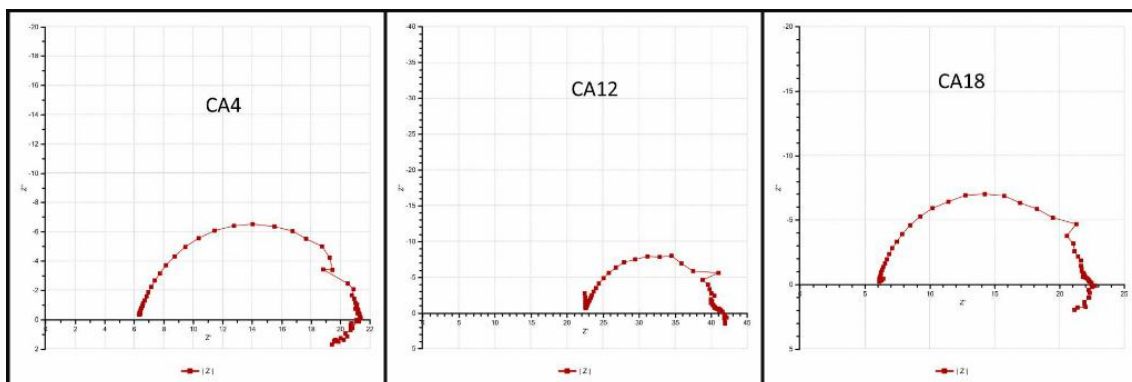
Fig. 70 - Nyquist plot of CAn samples.

79

In Fig. 70 were reported EIS spectra of carboxyl acid coated samples. The typical semicircular Nyquist plot was obtained for all of them, with the same charge transfer resistance of bare substrate. The coatings had no effect on corrosion protection.

5 DISCUSSION

5.1 Sandblasting

First of all it has to be noted the role of sandblasting: looking at Tab. 5 it can be seen that sandblasting treatment of the bare substrate slightly lowers contact angles, both ϑ_{avg} and ϑ_{max}. At the same time it greatly reduces standard deviation with respect to the untreated substrate (one half) and significantly decreases the range among the maximum and minimum contact angle ($\Delta_{untreated}=39°$, $\Delta_{sandblasted}=22°$). We can reasonably suppose that it was obtained a more homogeneous morphology of the substrate surface with the sandblasting treatment.

On the other side the roughness values, reported in Tab. 3, slightly increases after sandblasting treatment (see Fig. 71).
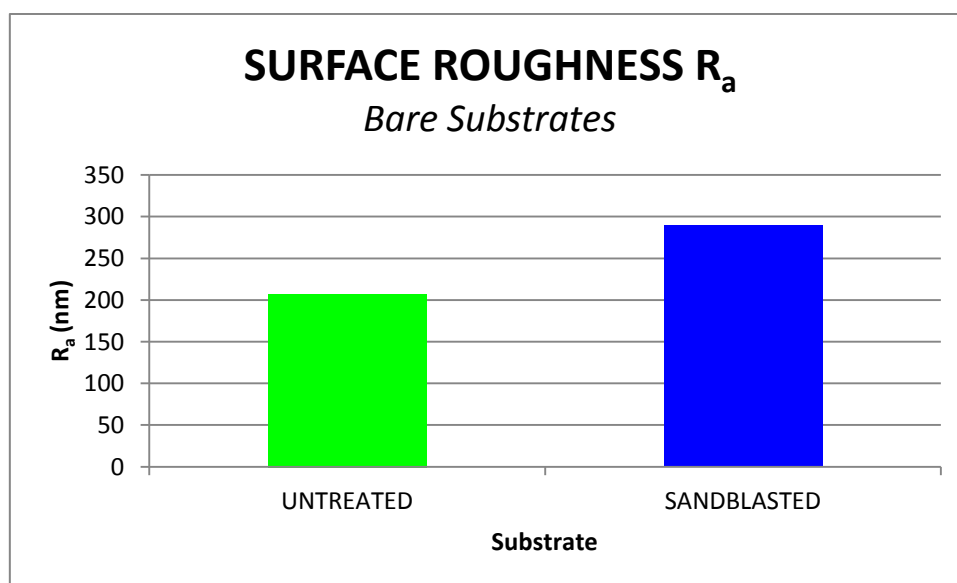
Fig. 71 - Surface roughness of bare untreated (green) and sandblasted (blue) substrate.

It appears straightforward that the morphology changes due to the sandblasting has some implications in coating homogeneity as suggested by the data collected in Tab. 6: sandblasting significantly increases the contact angles and greatly reduces their standard deviation leading to the conclusion that a more homogeneous coating was obtained on sandblasted substrate with respect to the untreated one.

The contact angles are reported graphically in Fig. 72 for each type of phosphonic acid coating: clearly we can observe an improvement of hydrophobicity on sandblasted substrate. About the alkyl chain influence, we observe that the contact angles increase with the alkyl chain length and they have closer values when applied on sandblasted surfaces. The roughness appears one relevant physical parameter.
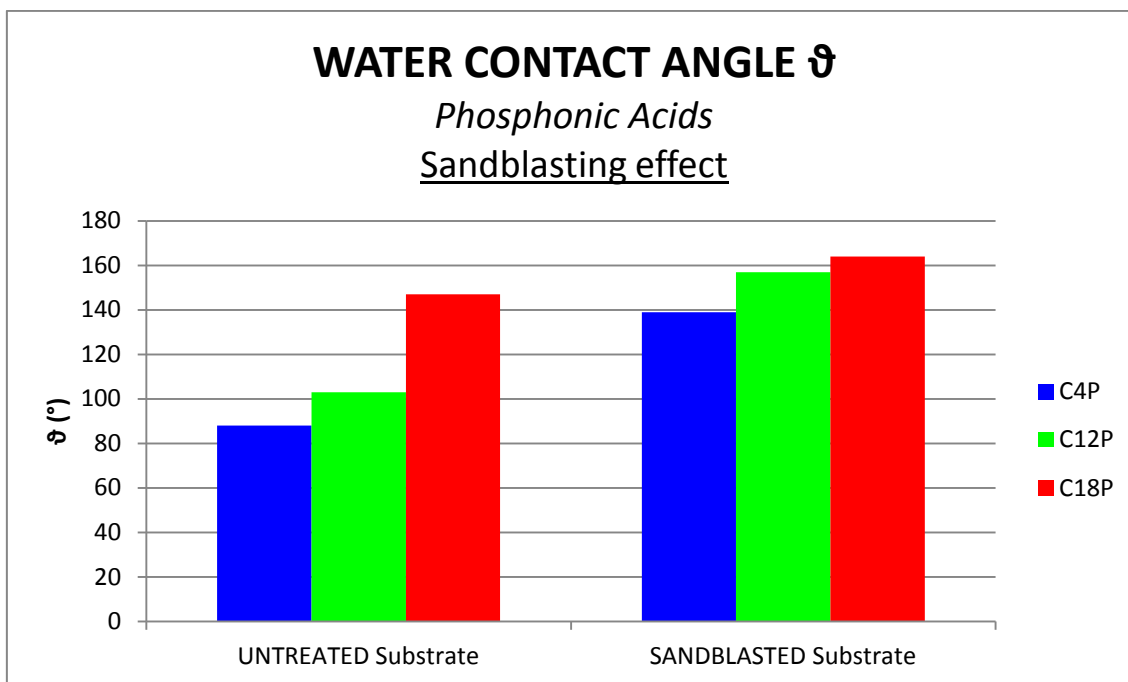
WATER CONTACT ANGLE ϑ
Phosphonic Acids
Sandblasting effect

The observations agree with a scenario where a uniform roughness, compulsory for the hydrophobic behavior, is created. Going deeper in the analysis, the contact angles of C4 and C12 alkyl chain phosphonic acid increased with a larger increment than the C18 one when the substrate is sandblasted. The last has the same standard deviation obtained without sandblasting treatment of the substrate. The angle however remains the highest among those reported.

Due to the fact that a long chain might assume a cloud conformation, not ordered, very different from a SAM assembly, and then create many very small hills and valleys over the blasted surface, we can suppose that a micro- nano-roughness has been formed due to the organic layer over a macro-roughness of the sandblasted steel. The SEM microphotographies, Fig. 62 and Fig. 63, sustain our hypothesis. Observing the images b) and c) of Fig. 65 we get a further confirmation at the same enlargement.

Analyzing more in details the data of Tab. 3, bare sandblasted substrate has higher roughness than bare untreated substrate (Fig. 71). But it is important to highlight that in the case of untreated substrate, the amplitude roughness parameters decrease with almost all the coatings (see Fig. 73). It occurs probably due to the coating material in the valleys. On the other side, starting from sandblasted substrate the application of the coating increased the roughness (see Fig. 74).
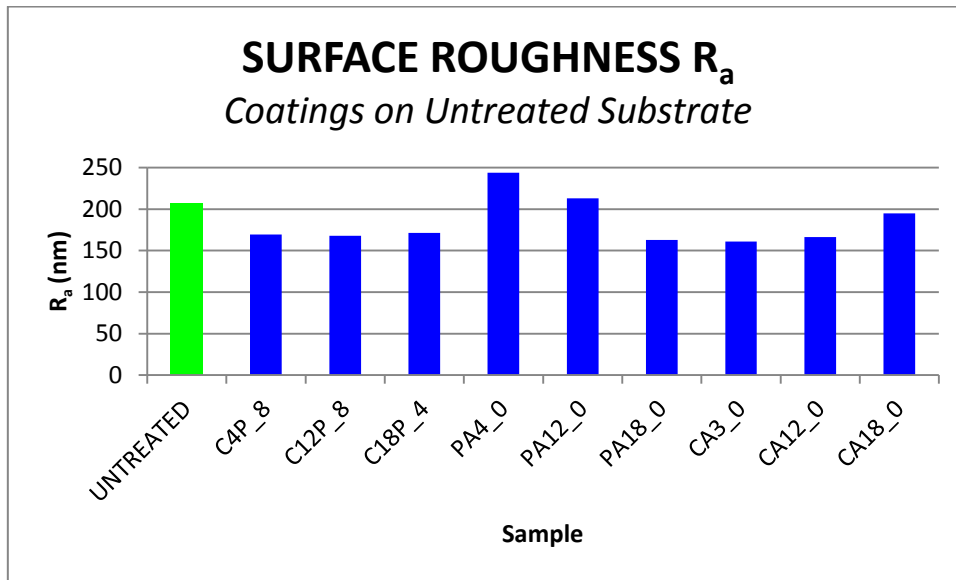
Fig. 73 - Comparison of surface roughness of coatings on untreated substrate.
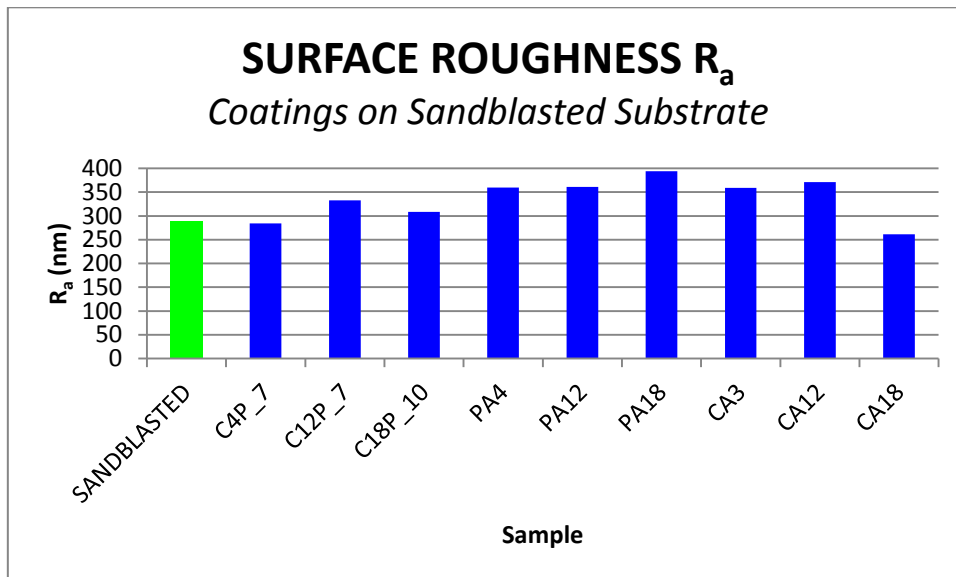
Fig. 74 - Comparison of surface roughness of coatings on sandblasted substrate.

5.2 Etching time

A very important question in this type of analysis is the amount of active sites onto the substrate and the kind of those. The amount is directly linked to the etching time. Looking at the data in Tab. 7, graphically reported in Fig. 75, we can evaluate the etching time influence. A light increase of the contact angle is observed with the etching time. We suppose that the higher the number of available active sites, created by a prolonged etching reaction, the higher is the number of anchored SAMs. This was true for C12P coatings, where contact angle increased with the etching time. The decreasing of the C18 derivative could be explained by the bending of the alkyl chain due to its excessive length (cloud conformation).

5.3 Thermal treatment

Comparing Tab. 7 and Tab. 8 post thermal treatment effect can be evaluated: it positively influenced hydrophobic properties of the coating, enhancing chemical bond with the substrate and allowing an optimization in the re-organization of alkyl chain.[47,48] All contact angles were improved, independently of the coating type or the etching time selected, but in particular post thermal treatment highly increased contact angles for C18P coating (see Fig. 75).

The thermal treatment seems do not greatly affects the contact angles at the same etching time: only a slight increase is observed for the thermally treated samples. The behavior of the only C18 alkyl chain derivative, not thermally treated, shows a totally different trend and we suppose something is gone wrong during experimental evaluation. (We reported the data hoping someone has some right cause).
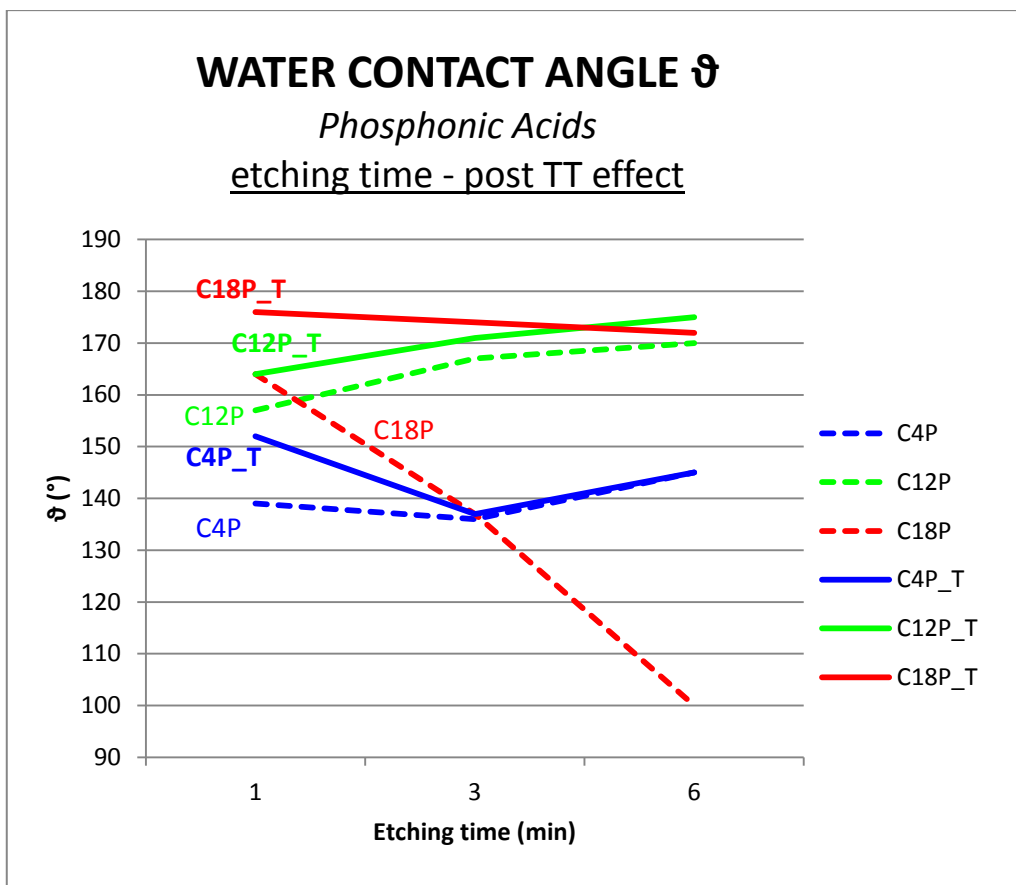
Fig. 75 - Comprehension of etching time and post thermal treatment effects on contact angle.

5.4 Chain length

Since the deposition parameters have been set for all the coating types, it is possible to compare the coating effect on the wettability grade: observing Tab. 8 and Fig. 75, longer alkyl chains produced higher contact angle values, with no significant difference between C12 and C18, in presence of the post thermal treatment. Without thermal treatment this trend can be confirmed at high etching time excluding the anomalous data of C18P. The rate of increasing the contact angles seems to depend mainly on the chain length:

C18(treated)>C12 (both treated and untreated) > C4 (both treated and untreated)

5.5 Structure of organic molecules

The studies on alkyl carboxylic acids and partially esterified polyacrylates reported in Tab. 9 and Tab. 10, respectively, indicate very low contact angles with carboxylic functional group and, on the contrary, some controversial data that necessitate to be discussed for polyacrylate coatings.

For the first series our opinion is that the deposition procedure has to be optimized in order to enhance the chemical bond strength between carboxyl head group and the activated surface, most likely just increasing deposition time. Indeed a different bond strength is supposed between carboxylic and phosphonic acid with phosphorous group more negative than carboxyl group. This means that a different adsorption procedure has to be followed. Also the qualitative kind of active adsorption sites would be examined.

It is different the case of partially esterified polyacrylates: they have been synthesized in laboratory and a better control in the esterification grade was the great challenge. Here very different wettability properties were obtained between the coatings: PA12 showed superhydrophobic behavior, while PA4 was slightly hydrophobic and PA18 has a very low contact angle with respect the bare substrate. Certainly the study of the optimization of the esterification grade is a key point for further analysis, since it influences the molecule adhesion on the substrate: the higher the number of anchoring groups (lower esterification grade) the easier anchorage to the substrate and also the backbone is outstretched on the surface, covering a larger area. Another important parameter to be take into account during the synthesis is the regioselectivity of the esterification, but it requires a complete control of the reaction.

5.6 Adhesion force

Tab. 4 shows the data of the adhesion force of the coatings: the values were almost the same for the analyzed samples, but the trend revealed higher adhesion forces for coatings on untreated substrates than on sandblasted ones (see Fig. 76 and Fig. 77). Phosphonic acids on sandblasted substrates had poorer adhesion than on untreated substrate (Fig. 76), while regarding carboxylic acids the trend seems to be the opposite (Fig. 77).

ADHESION FORCE F
Phosphonic Acids
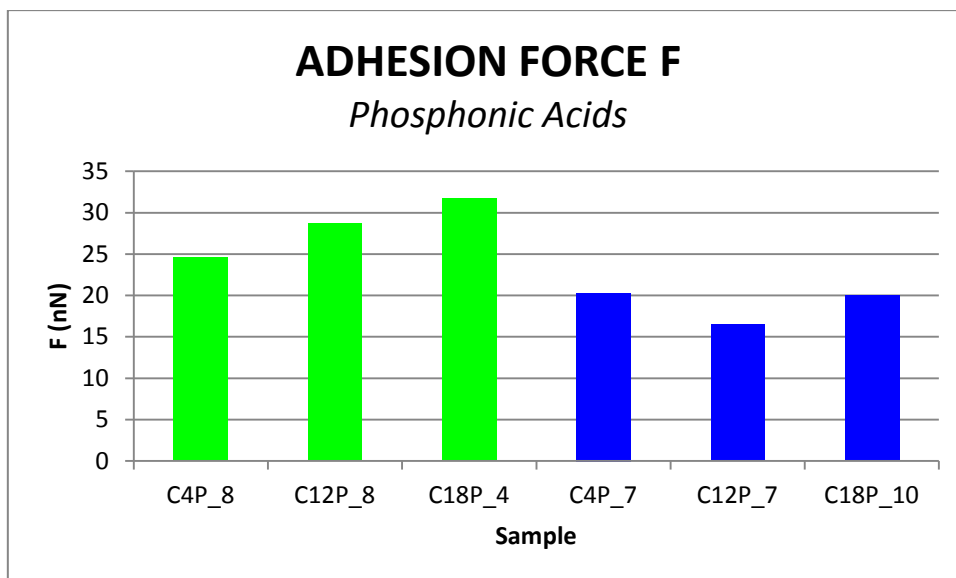
Fig. 76 - Adhesion force of phosphonic acids on untreated (green) and sandblasted (blue) substrate.

ADHESION FORCE F
Carboxylic Acids
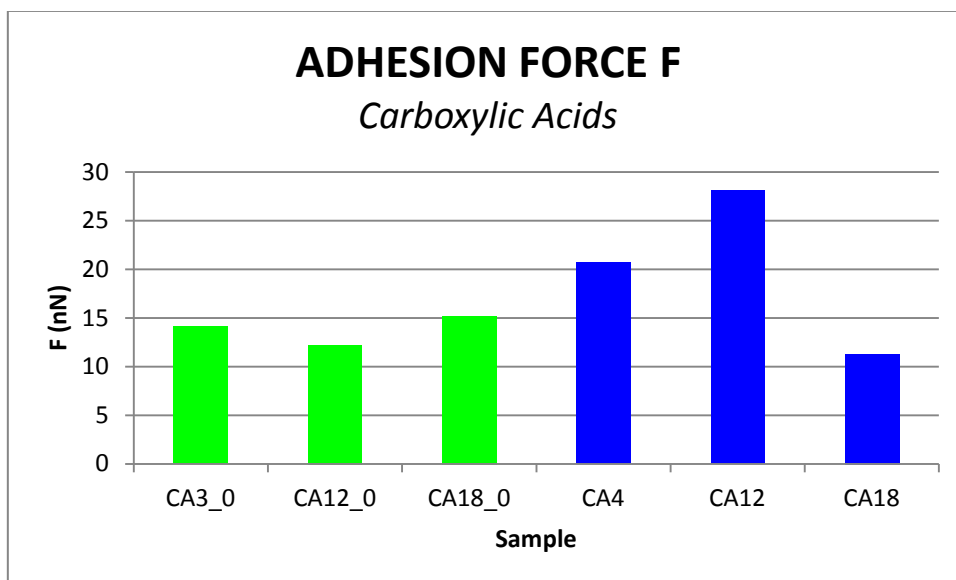
Fig. 77 - Adhesion force of carboxylic acids on untreated (green) and sandblasted (blue) substrate.

Among the carboxylic acid derivatives the C18 only has an opposite behavior. As already noted the long alkyl chain, probably with a bundle conformations, hinders the functional group causing disturbance on the adhesion.

It is difficult to explain the different behavior of phosphonic derivates and carboxylic ones; probably it concerns the work of adhesion that depends on the polarity of group.

5.7 Surface tension

We have seen before that sandblasting treatment mainly influences coating homogeneity, but the wettability properties of coated surfaces, strongly depends on

the physical properties of coating: e.g. the lower the surface tension, the lower the wettability (or greater is the hydrophobic behavior of the coated surface). In Tab. 11 we report the surface tension values of all the samples. The samples that reached superhydrophobicity had surface tension lower than 2 mN/m or about. Some observation can be drawn from the analysis of the data reported in Tab. 11. The sample C18P_7 cannot be considered as previously mentioned. The most relevant observation relate to C18P_X samples and specifically to the low surface tension for the thermally treated samples C18P_8-10. The low values probably indicate that the long chain can rearrange into a different conformations responsible of the lowering of the surface tension.

The C12P_X series show low tension of each components in comparison of the high values of the other samples. This observation let us to suppose that the optimum chain length probably is > 4 and < 18.

In Fig. 78 were reported surface tension of the sample coated with C12P. Looking at the blue bars, the higher the etching time the higher the surface tension. This trend was confirmed also observing the green bars in Fig. 79. A possible explanation is the following: long etching time increases the density of active sites providing higher adsorption of the SAM molecules, but at the same time due to their steric hindrance many active sites remain free. These still available active sites increases surface tension when the deposed drop can spread over the coating film covering coated and uncoated area.

SURFACE TENSION γ_s

Dodecyl Phosphonic Acids C12P
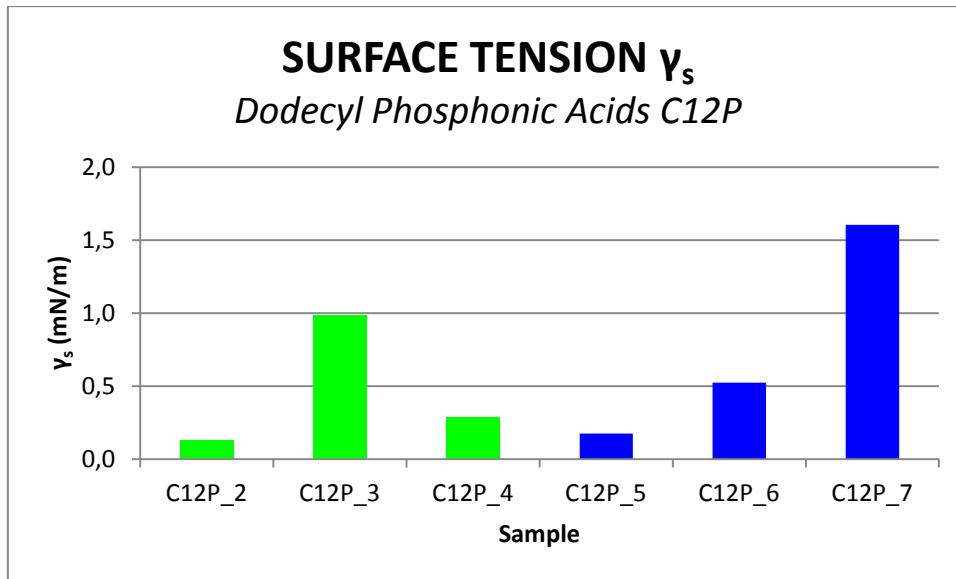
Fig. 78 - Surface tension of C12P caoting without (green) and with post thermal treatment (blue).

SURFACE TENSION γ_s

Octadecyl Phosphonic Acids C18P
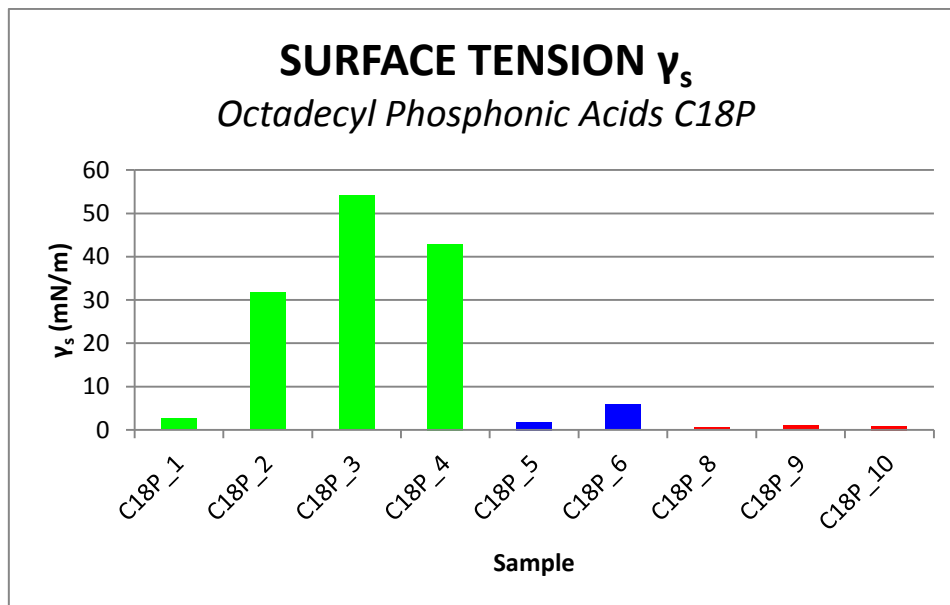
Fig. 79 - Surface tension of C18P coating on untreated (green) and sandblasting substrate without (blue) and with post thermal treatment (red).

Surface tension of partially esterified polyacrylates are reported in Fig. 80, where the bar of PA12 cannot be seen because of the graph scale since it has a value of only 0.097 mN/m.
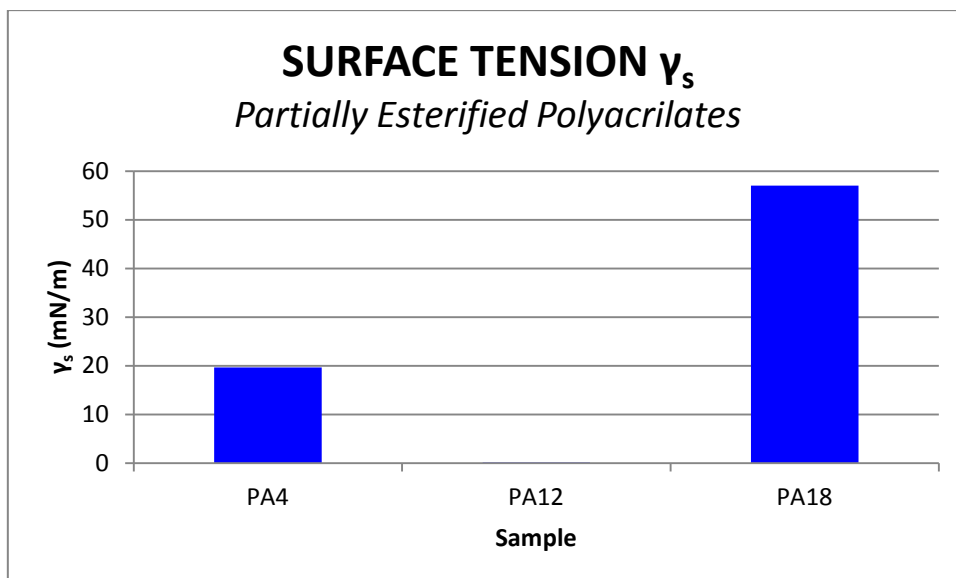
Fig. 80 - Surface tension of partially esterified polyacrylic coatings.

Carboxylic acids surface tensions were presented in Fig. 81. The higher the chain length the higher the contact angle (Tab. 9) the lower the surface tension.
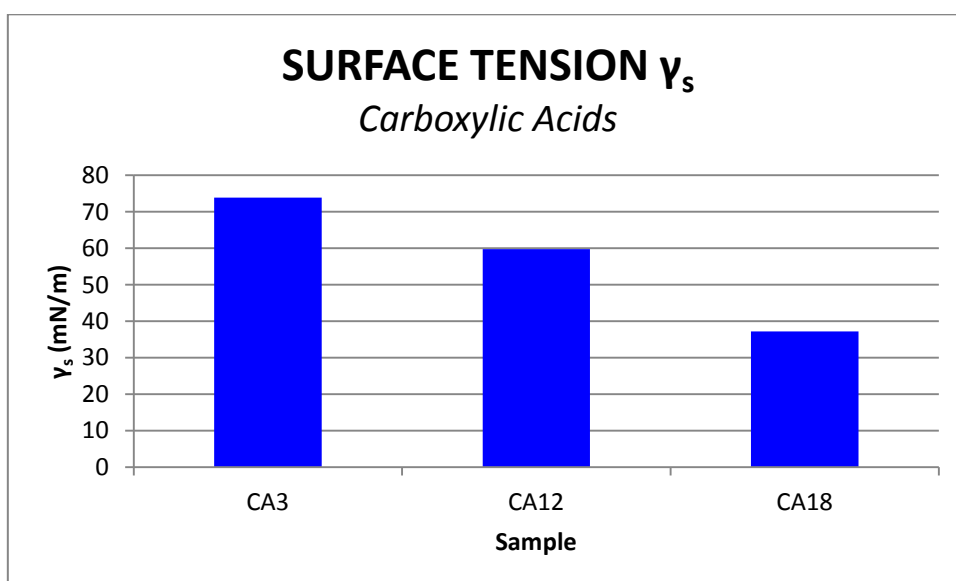
Fig. 81 - Surface tension of carboxylic acid coatings.

5.8 Thickness and composition

GDOES analysis has been done to survey film coating thickness and chemical composition. Both C12P_7 and CA12 samples were coated by self-assembled monolayer dodecyl phosphonic acid and dodecyl carboxylic acid, respectively. So should be expected a nanometric thickness, but it has been found 1.5 μm thickness for C12P_7 (see Fig. 55) and 0.3 μm thickness for CA12 (see Fig. 56). It can be explained by

the anchoring mode: theoretically it has been assumed a bidentate mode, but actually in the case of phosphonic acid other anchoring mechanisms were proposed and observed in previous studies: the linkage of organophosphorous coupling molecules to oxide surfaces involves the formation of M-O-P bonds by heterocondensation of surface hydroxyl groups (-OH) with P-OH groups and by complexation of the phosphoryl oxygen to the surface metal atoms. Hydrogen bonds between surface hydroxyl groups and residual P-OH and P=O groups may also be involved.[49] The bonding mode of organophosphorous coupling molecules likely depends on the nature of both the coupling molecule and the inorganic surface, and on the conditions of the surface modification.

Moreover looking at Fig. 55, it is clear that more than one layer have been deposited on the surface. Indeed the GDOES curve for carbon and phosphorous are characterized by two peaks. These appear at the same depth for the two elements.
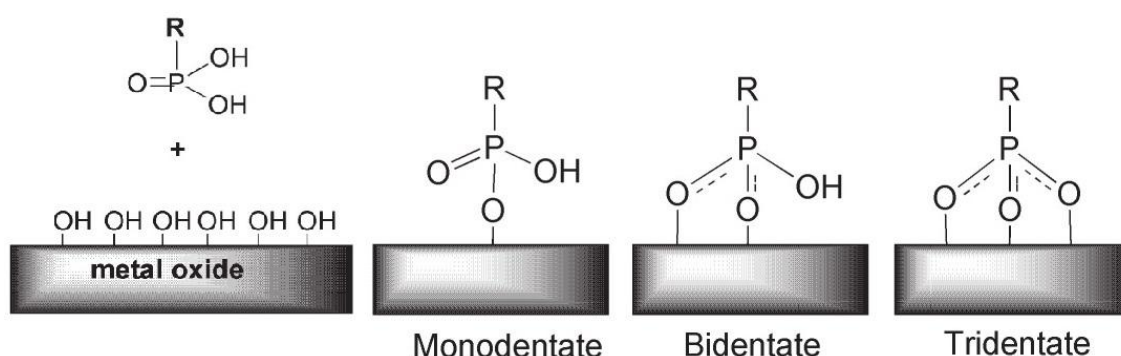
Fig. 82 - Different bonding modes of a phosphonate unit to a metal oxide surface.

For PA12 (see Fig. 57) the film was made by a polymer that did not self-assembly on the substrate, and the bonds and polymer configuration were rather unpredictable.

SEM images confirmed that coating application successfully occurred. Fig. 65 shows the different morphology of bare substrate, etched substrate, C12P and PA12 coatings with comparable magnification. As it can be seen they were very different: etching role can now be understood more in detail (see also Fig. 62), showing that it increased significantly the porosity of the surface (it has been not possible to measure the roughness at AFM) allowing a better anchorage of the molecules. The coated

substrates were very different with respect to the bare substrate, with C12P_7 sample showing a homogeneous crystalline film completely coating the substrate (see Fig. 63). Also for PA12 sample the surface is homogeneously coated, but it look more like a wax than a crystalline structure.

6 CONCLUSIONS AND OUTLOOKS

The aim of this thesis work is to study the properties of organic coatings applied onto mild carbon steel surfaces. Specifically the deposition parameters have been investigated in order to understand how and which of them are relevant for the achievement of hydrophobic/superhydrophobic state. Since hydrophobicity strongly depends on roughness and surface tension, two types of substrates and three types of coatings have been selected, one of which had never been proposed before in literature regarding this topic: it is a comb polymer constituted by a polyacrylate backbone with free carboxyl groups and carboxyl groups esterified with alkyl chain. For each of them three different versions have been used, in order to survey the chain length effect on hydrophobicity. The work consisted in two main parts: the synthesis of organic molecules and the optimization of the deposition parameters of phosphonic acid SAMs, analyzing the substrate onto which they anchor, the etching time and the post thermal treatment. Then we applied the results also to the carboxylic acids and polyacrylates deposition.

The synthesis of phosphonic acids did not show any problems, but regarding the polyacrylates troubles were found in the control of esterification grade and the regioselectivity.

Sandblasting treatment produces higher surface roughness of the substrate, enhancing the coating homogeneity and increasing the contact angles. Thus sandblasting can have good effects in the final purpose of lower the wettability.

Etching time is a key parameter in substrate pretreatment: it allows the formation of active sites required for the anchoring of the organic molecules. From the experimental data we can say that the higher the etching time the higher the surface activation.

Post thermal treatment is not compulsory for the phosphonic acids, but it is found a positive effect on the stabilization of the film coating, improving slightly the hydrophobicity in all the presented cases.

Chain length affects wettability properties: in general the higher the chain length the higher the hydrophobicity. But this is not always true since longer chain can assume a cloud conformation, producing coating inhomogeneity and increasing surface tension.

Thickness of the film coatings is not the expected ones: despite phosphonic acids and carboxyl acids are SAMs, they did not self-assembly onto the substrate forming a monolayer but also other bonds between organic molecules can occur.

Adhesion force is comparable for every type of coatings, showing slightly higher values when deposition occurs on untreated substrate.

Molecular structure greatly influences all the surface properties, in particular surface tension. From their structure depends the order of assembly onto the surface.

Comparing the final results we can say that phosphonic acids are the most reliable organic molecules since they produce very good results, but polyacrylates give promising results since they have wide possibility of improvement better controlling the esterification grade and the regioselectivity. Carboxylic acids require adjustment in deposition parameters to find great improvement with respect to the obtained results during this work.

REFERENCES

1.   Marmur A. The lotus effect: Superhydrophobicity and metastability. *Langmuir* 2004;20(9):3517-3519.

2.   Lam CNC, Wu R, Li D, Hair ML, Neumann a. W. Study of the advancing and receding contact angles: Liquid sorption as a cause of contact angle hysteresis. *Adv. Colloid Interface Sci.* 2002;96(1-3):169-191.

3.   Bartell FE, Shepard JW. The Effect of Surface Roughness on Apparent Contact Angles and on Contact Angle Hysteresis. I. The system Paraffin–Water–Air. *J. Phys. Chem.* 1953;57(2):211-215. doi:10.1021/j150503a017.

4.   Johnson RE, Dettre RH. Contact Angle Hysteresis. In: *Contact Angle, Wettability, and Adhesion*.Vol 43. Advances in Chemistry. AMERICAN CHEMICAL SOCIETY; 1964:112-135 SE - 7. doi:doi:10.1021/ba-1964-0043.ch007.

5.   Eick J., Good R., Neumann A. Thermodynamics of contact angles. II. Rough solid surfaces. *J. Colloid Interface Sci.* 1975;53(2):235-248. doi:10.1016/0021-9797(75)90010-7.

6.   Oliver JP, Huh C, Mason SG. An experimental study of some effects of solid surface roughness on wetting. *Colloids and Surfaces* 1980;1(1):79-104. doi:10.1016/0166-6622(80)80039-4.

7.   Oliver JF, Mason SG. Liquid spreading on rough metal surfaces. *J. Mater. Sci.* 1980;15(2):431-437. doi:10.1007/BF02396792.

8.   Johnson RE, Dettre RH. Contact Angle Hysteresis. III. Study of an Idealized Heterogeneous Surface. *J. Phys. Chem.* 1964;68(7):1744-1750. doi:10.1021/j100789a012.

9.   Dettre RH, Johnson RE. Contact Angle Hysteresis. IV. Contact Angle Measurements on Heterogeneous Surfaces1. *J. Phys. Chem.* 1965;69(5):1507-1515. doi:10.1021/j100889a012.

10.   Liu Y, Lotero E, Goodwin JG. Effect of carbon chain length on esterification of carboxylic acids with methanol using acid catalysis. *J. Catal.* 2006;243(2):221-228. doi:10.1016/j.jcat.2006.07.013.

11.   Neumann A., Good R. Thermodynamics of contact angles. I. Heterogeneous solid surfaces. *J. Colloid Interface Sci.* 1972;38(2):341-358. doi:10.1016/0021-9797(72)90251-2.

12.   Schwartz LW, Garoff S. Contact angle hysteresis on heterogeneous surfaces. *Langmuir* 1985;1(2):219-230. doi:10.1021/la00062a007.

13.   Marmur A. Contact Angle Hysteresis on Heterogeneous Smooth Surfaces. *J. Colloid Interface Sci.* 1994;168(1):40-46. doi:10.1006/jcis.1994.1391.

14.   Decker EL, Garoff S. Using Vibrational Noise To Probe Energy Barriers Producing Contact Angle Hysteresis. *Langmuir* 1996;12(8):2100-2110. doi:10.1021/la951021n.

15.   Decker EL, Garoff S. Contact Line Structure and Dynamics on Surfaces with Contact Angle Hysteresis. *Langmuir* 1997;13(23):6321-6332. doi:10.1021/la970528q.

16.   Brandon S, Marmur A. Simulation of Contact Angle Hysteresis on Chemically Heterogeneous Surfaces. 1996;355:351-355.

17.   Timmons C., Zisman W. The effect of liquid structure on contact angle hysteresis. *J. Colloid Interface Sci.* 1966;22(2):165-171. doi:10.1016/0021-9797(66)90080-4.

18.   Fadeev AY, McCarthy TJ. Binary Monolayer Mixtures: Modification of Nanopores in Silicon-Supported Tris(trimethylsiloxy)silyl Monolayers. *Langmuir* 1999;15(21):7238-7243. doi:10.1021/la9903806.

19.   Chen W, McCarthy TJ. Layer-by-Layer Deposition: A Tool for Polymer Surface Modification. *Macromolecules* 1997;30(1):78-86. doi:10.1021/ma961096d.

20.   Fadeev AY, McCarthy TJ. Trialkylsilane Monolayers Covalently Attached to Silicon Surfaces: Wettability Studies Indicating that Molecular Topography Contributes to Contact Angle Hysteresis. *Langmuir* 1999;15(11):3759-3766. doi:10.1021/la981486o.

21.   Youngblood JP, McCarthy TJ. Ultrahydrophobic Polymer Surfaces Prepared by Simultaneous Ablation of Polypropylene and Sputtering of Poly(tetrafluoroethylene) Using Radio Frequency Plasma. *Macromolecules* 1999;32(20):6800-6806. doi:10.1021/ma9903456.

22.   Sedev RV, Petrov JG, Neumann a. W. Effect of Swelling of a Polymer Surface on Advancing and Receding Contact Angles. *J. Colloid Interface Sci.* 1996;180(1):36-42. doi:10.1006/jcis.1996.0271.

23.   Sedev RV, Budziak CJ, Petrov JG, Neumann AW. Dynamic Contact Angles at Low Velocities. *J. Colloid Interface Sci.* 1993;159(2):392-399. doi:10.1006/jcis.1993.1338.

24.   Meziane D, Hardouin J, Elias A, Gu E, Lecouvey M. Microwave Michaelis – Becker Synthesis of Diethyl Phosphonates , Tetraethyl Diphosphonates , and Their Total or Partial Dealkylation. 2009;20(6):369-377. doi:10.1002/hc.

25.   Ghassamipour S, Sardarian AR. Friedländer synthesis of poly-substituted quinolines in the presence of dodecylphosphonic acid (DPA) as a highly efficient, recyclable and novel catalyst in aqueous media and solvent-free conditions. *Tetrahedron Lett.* 2009;50(5):514-519. doi:10.1016/j.tetlet.2008.09.097.

26.   Maege I, Jaehne E, Henke A, et al. Self-assembling adhesion promoters for corrosion resistant metal polymer interfaces. *Prog. Org. Coatings* 1997;34(1-4):1-12.

27.   Socrates G. Infrared Characteristic Group Frequencies: Tables and Charts, Second Edition (Socrates, George). *J. Chem. Educ.* 1995;72(4):A93. doi:10.1021/ed072pA93.5.

28.   Dodecyl Phosphonic Acid properties. Available at:
        http://www.chemspider.com/Chemical-Structure.71152.html. Accessed October 29,
        2014.

29.   C18P. Available at:
        http://www.sigmaaldrich.com/catalog/product/aldrich/715166?lang=it&region=IT.
        Accessed November 17, 2014.

30.   Fischer esterification. Available at: http://www.organic-
        chemistry.org/namedreactions/fischer-esterification.shtm. Accessed October 29, 2014.

31.   Press C, ed. *Handbook of Chemistry and Physics*. 2008th ed.

32.   Van Alsten JG. Self-assembled monolayers on engineering metals: Structure,
        derivatization, and utility. *Langmuir* 1999;15(22):7605-7614.

33.   Buraschi R, Danzi S, Di Dio L, Gesualdi A, Realini P. Metodi di caratterizzazione di film
        sottili anticorrosivi. 2013.

34.   Lim MS, Smiley KJ, Gawalt ES. Thermally driven stability of octadecylphosphonic acid
        thin films grown on SS316L. *Scanning* 2010;32(5):304-311. doi:10.1002/sca.20192.

35.   Raman A, Gawalt ES. Self-assembled monolayers of alkanoic acids on the native oxide
        surface of SS316L by solution deposition. *Langmuir* 2007;23(5):2284-2288.

36.   PART 3 . Atomic Force Microscopy. :1-131.

37.   Pierce E, Carmona FJ, Amirfazli a. Understanding of sliding and contact angle results in
        tilted plate experiments. *Colloids Surfaces A Physicochem. Eng. Asp.* 2008;323(1-3):73-
        82. doi:10.1016/j.colsurfa.2007.09.032.

38.   Antonini C, Villa F, Bernagozzi I, Amirfazli a., Marengo M. Drop rebound after impact:
        The role of the receding contact angle. *Langmuir* 2013;29(52):16045-16050.

39.   Del Rìo OI, Neumann AW. Axisymmetric Drop Shape Analysis : Computational Methods
        for the Measurement of Interfacial Properties from the Shape and Dimensions of
        Pendant and Sessile Drops. 1997;147(196):136-147.

40.   Extrand CW, Moon SI. Contact angles of liquid drops on super hydrophobic surfaces:
        understanding the role of flattening of drops by gravity. *Langmuir* 2010;26(22):17090-9.
        doi:10.1021/la102566c.

41.   Owens DK, Wendt RC. Estimation of the surface free energy of polymers. *J. Appl. Polym.
        Sci.* 1969;13(8):1741-1747. doi:10.1002/app.1969.070130815.

42.   Xiaoxue Zhang, Wang L, Levänen E. Superhydrophobic surfaces for reduction of
        bacterial adhesion. *RCS Adv.* 2013;3(30):1-53. doi:10.1039/c3ra40497h.

43.   Zhao Q, Liu Y, Abel EW. Effect of temperature on the surface free energy of amorphous
        carbon films. *J. Colloid Interface Sci.* 2004;280(1):174-83.
        doi:10.1016/j.jcis.2004.07.004.

44.   Bartolo D, Bouamrirene F, Verneuil É, Buguin a, Silberzan P, Moulinet S. Bouncing or sticky droplets: Impalement transitions on superhydrophobic micropatterned surfaces. *Europhys. Lett.* 2006;74(2):299-305. doi:10.1209/epl/i2005-10522-3.

45.   Alagta A, Felhösi I, Bertoti I, Kálmán E. Corrosion protection properties of hydroxamic acid self-assembled monolayer on carbon steel. *Corros. Sci.* 2008;50(6):1644-1649. doi:10.1016/j.corsci.2008.02.008.

46.   Liu X, Chen S, Ma H, Liu G, Shen L. Protection of iron corrosion by stearic acid and stearic imidazoline self-assembled monolayers. *Appl. Surf. Sci.* 2006;253(2):814-820. doi:10.1016/j.apsusc.2006.01.038.

47.   Danahy MP, Avaltroni MJ, Midwood KS, Schwarzbauer JE, Schwartz J. Self-assembled Monolayers of α,ω-Diphosphonic Acids on Ti Enable Complete or Spatially Controlled Surface Derivatization. *Langmuir* 2004;20:5333-5337.

48.   Gawalt ES, Avaltroni MJ, Koch N, Schwartz J. Self-Assembly and Bonding of Alkanephosphonic Acids on the Native Oxide Surface of Titanium. *Langmuir* 2001;17:5736-5738.

49.   Mutin PH, Guerrero G, Vioux A. Hybrid materials from organophosphorus coupling molecules. *J. Mater. Chem.* 2005;15(35-36):3761. doi:10.1039/b505422b.